

PL-TR-96-2314

REGIONAL DISCRIMINATION STUDIES: PHASE II

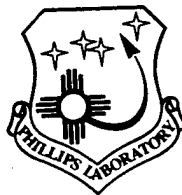
**Jessie Bonner
Chris Hayward
Eugene Herrin
G. G. Sorrell**

**Southern Methodist University
Dallas, TX 75275**

October 1996

Scientific Report No. 2

APPROVED FOR PUBLIC RELEASE; DISTRIBUTION UNLIMITED



**PHILLIPS LABORATORY
Directorate of Geophysics
AIR FORCE MATERIEL COMMAND
HANSCOM AFB, MA 01731-3010**

DTIC QUALITY INSPECTED 3

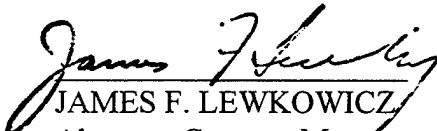
19970421 055


SPONSORED BY
Advanced Research Projects Agency (DoD)
Nuclear Monitoring Research Office
ARPA ORDER No. 0325

MONITORED BY
Phillips Laboratory
CONTRACT No. F19628-95-C-0184

The views and conclusions contained in this document are those of the authors and should not be interpreted as representing the official policies, either express or implied, of the Air Force or U.S. Government.

This technical report has been reviewed and is approved for publication.


JAMES F. LEWKOWICZ
Alternate Contract Manager
Earth Sciences Division


JAMES F. LEWKOWICZ
Director
Earth Sciences Division

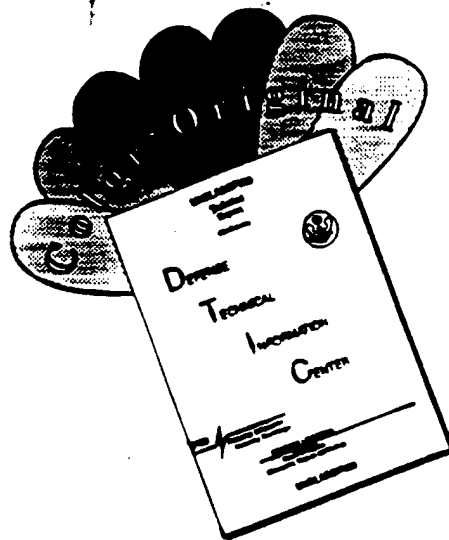
This report has been reviewed by the ESD Public Affairs Office (PA) and is releasable to the National Technical Information Service (NTIS).

Qualified requestors may obtain copies from the Defense Technical Information Center. All others should apply to the National Technical Information Service.

If your address has changed, or you wish to be removed from the mailing list, or if the addressee is no longer employed by your organization, please notify PL/IM, 29 Randolph Road, Hanscom AFB, MA 01731-3010. This will assist us in maintaining a current mailing list.

Do not return copies of this report unless contractual obligations or notices on a specific document requires that it be returned.

DISCLAIMER NOTICE



THIS DOCUMENT IS BEST QUALITY AVAILABLE. THE COPY FURNISHED TO DTIC CONTAINED A SIGNIFICANT NUMBER OF COLOR PAGES WHICH DO NOT REPRODUCE LEGIBLY ON BLACK AND WHITE MICROFICHE.

REPORT DOCUMENTATION PAGE			Form Approved OMB No. 0704-0188	
Public reporting burden for this collection of information is estimated to average 1 hour per response, including the time for reviewing instructions, searching existing data sources, gathering and maintaining the data needed, and completing and reviewing the collection of information. Send comments regarding this burden estimate or any other aspect of this collection of information, including suggestions for reducing this burden, to Washington Headquarters Services, Directorate for Information Operations and Reports, 1215 Jefferson Davis Highway, Suite 1204, Arlington, VA 22202-4302, and to the Office of Management and Budget, Paperwork Reduction Project (0704-0188), Washington, DC 20503.				
1. AGENCY USE ONLY (Leave blank)	2. REPORT DATE October 1996	3. REPORT TYPE AND DATES COVERED Scientific #2		
4. TITLE AND SUBTITLE Regional Discrimination Studies Phase II		5. FUNDING NUMBERS PE 62301F PR NM95 TA GM WU AD Contract F19628-95-C-0184		
6. AUTHOR(S) Jessie Bonner, Chris Hayward, Eugene Herrin, G.G. Sorrell				
7. PERFORMING ORGANIZATION NAME(S) AND ADDRESS(ES) Southern Methodist University Dallas, TX 75275-0395		8. PERFORMING ORGANIZATION REPORT NUMBER		
9. SPONSORING / MONITORING AGENCY NAME(S) AND ADDRESS(ES) Phillips Laboratory 29 Randolph Road Hanscom AFB, MA 01731-3010 Contract Manager: Delaine Reiter, GPE		10. SPONSORING / MONITORING AGENCY REPORT NUMBER PL-TR-96-2314		
11. SUPPLEMENTARY NOTES				
12a. DISTRIBUTION / AVAILABILITY STATEMENT Approved for public release; distribution unlimited		12b. DISTRIBUTION CODE		
13. ABSTRACT (Maximum 200 words) This report consists of four parts and an appendix. Part 1, "Seismo-Acoustic Studies at TXAR", is by Eugene Herrin and G.G. Sorrells. Part 2, "Inversion of Surface Waves for Shallow Velocity Structure in the Fort Worth Basin," is by Jessie Bonner. Part 3, "A Preliminary Investigation of the Use of Acoustic and Seismo-Acoustic Observations to Identify Vented Explosive Seismic Sources", is by G.G. Sorrells and Eugene Herrin. Part 4 consists of the Acknowledgments called for by the contract. Appendix 1 "Preliminary Report" Characteristics of the Broadband Acoustic Sensors Installed in the SMU Lajitas GSE Array," is by Chris Hayward.				
14. SUBJECT TERMS Seismo-acoustic studies Shallow Velocity Structure Characteristic of Broadband Acoustical Sensors			15. NUMBER OF PAGES 112	
			16. PRICE CODE	
17. SECURITY CLASSIFICATION OF REPORT Unclassified	18. SECURITY CLASSIFICATION OF THIS PAGE Unclassified	19. SECURITY CLASSIFICATION OF ABSTRACT Unclassified	20. LIMITATION OF ABSTRACT SAR	

CONTENTS

1. SEISMO-ACOUSTIC STUDIES AT TXAR	1
1.1 INTRODUCTION	1
1.2 DISCUSSION	2
1.2.1.CTBT Monitoring Goals	2
1.2.2 Objective	2
1.2.3 Research Accomplished	2
1.3 CONCLUSIONS	17
2. INVERSION OF SURFACE WAVES FOR SHALLOW VELOCITY STRUCTURE IN THE FORT WORTH BASIN	20
2.1 EXECUTIVE SUMMARY	20
2.2 INTRODUCTION	20
2.2.1 Fort Worth Basin	20
2.2.2 Chemical Lime Quarry and Data Acquisition	22
2.2.3 Short Period Love and Rayleigh Wave Discussion	25
2.2.4 Inversion Fundamentals	28
2.3 RESULTS TO DATE	31
2.3.1 Obtaining A Priori Information	31
2.3.2 Inversion Results	33

CONTENTS

2.4 CONCLUDING REMARKS	36
2.5 REFERENCES	41
3. A PRELIMINARY INVESTIGATION OF THE USE OF ACOUSTIC AND SEISMO-ACOUSTIC OBSERVATIONS TO IDENTIFY VENTED EXPLOSIVE SEISMIC SOURCES	43
3.1 INTRODUCTION	43
3.2 SEISMIC DETECTION OF ACOUSTIC WAVES	46
3.2.1 Seismo-Acoustic Transfer function	46
3.2.1.1 <u>The Thomson Hollow Experiment</u>	47
3.2.1.2 <u>The TXAR Experiments</u>	49
3.2.2 Seismo-Aoustic Correlation Detection of Short Period Acoustic Signals at TXAR	56
3.2.3 Seismo-Acoustic Identification of Vented Near Regional Explosions	57
3.3 SUMMARY AND CONCLUSIONS	61
3.4. ACKNOWLEDGEMENTS	62
3.5 REFERENCES	63
4. ACKNOWLEDGEMENTS	64
4.1 PREVIOUS CONTRACTS AND PUBLICATIONS	64

CONTENTS

4.1.1 Previous Contracts and Reports	64
4.1.1.1 ARPA Contract # MDA 972-88-K-0001	64
4.1.1.2 ARPA Contract # MDA 972-89-C-0054	66
4.1.1.3 Contract # 19628-93-C-0057	67
4.1.2 Publications	68
4.1.2.1 Special Reports, Papers, and Posters	68
4.1.2.1 Publications	70
APPENDIX 1. PRELIMINARY REPORT: CHARACTERISTICS OF THE BROADBAND ACOUSTICAL SENSORS INSTALLED IN THE SMU LAJITAS GSE PROTOTYPE ARRAY	72

1. SEISMO-ACOUSTIC STUDIES AT TXAR¹

Eugene Herrin and G. G. Sorrells

with contributions from

Jessie Bonner, Valeriu Burlacu, Nancy Cunningham, Paul Golden, Chris
Hayward, Jack Swanson, Karl Thomason and Ileana Tibuleac

1.1 INTRODUCTION

Data from the TXAR array showed that infrasonic signals from explosions caused ground motion that was detected on the seismic sensors (seismo-acoustic signals). Experiments recording acoustic and seismo-acoustic signals from quarry blasts in Central Texas confirmed a theoretical transfer function between the two types of signals in the band of interest (0.5 - 5.0 Hz). Four infrasonic stations were established at TXAR using porous hose arrays and inexpensive, low-frequency acoustic sensors collocated in boreholes with the seismometers. A number of different designs of the hose arrays were tested in order to maximize the acoustic signal-to-noise ratios. Acoustic and seismo-acoustic signals have been detected from a large number of mining explosions at regional distances from TXAR. As many as 75% of the regional signals detected at TXAR are now thought to result from commercial explosions, so that identification of these events is an essential part of routine analysis. Detection of acoustic and seismo-acoustic signals from both surface and underground explosions has been used as a positive discriminant that allows the construction of a ground-truth data base to be used in testing purely seismic discriminants.

¹ Herrin, Eugene, G. G. Sorrells, et al., 1996, Seismo-acoustic studies at TXAR: Proceedings [poster], 18th Annual Seismic Research Symposium, 4-6 September 1996, Annapolis, MD, Sponsored by Phillips Laboratory, AFOSR, and AFTAC.

1.2. DISCUSSION

1.2.1 CTBT Monitoring Goals

CTBT monitoring goals are to detect, locate, and identify:

1. Evasively conducted nuclear tests, down to a few kilotons, worldwide, in all environments,
2. With enhanced coverage in regions of interest.

Meeting this challenge with high confidence will require enhancements in:

1. Monitoring sensors and network coverage,
2. Regional characterization and calibration,
3. Data processing,
4. On-site inspection.

1.2.2 Objective

The detection of seismic, acoustic and seismo-acoustic signals from both surface and underground mining explosions at regional distances from TXAR provides positive identification of the source. Using these observations we are building a ground-truth data base that can be used to test purely seismic discriminants. This same approach can be used at seismic arrays to be constructed in areas of particular interest for CTBT monitoring.

1.2.3 Research Accomplished

During GSETT2 a large number of teleseismic and regional signals were detected at the Lajitas, Texas, station (now TXAR) and reported to the National Data Center. Figure 1 shows the number of teleseisms detected during the test period sorted by day of week and hour of day. There is no clear pattern of occurrences. On the other hand, the number of regional events similarly sorted reveals a clear pattern of activity that peaks during the daylight hours of working days as shown in Figure 2. We estimate that up to 75% of the regional detections at TXAR are from commercial explosions up to m_b 3.5. Under a CTBT, commercial explosions of larger than about m_b 2.5 to

3.0 must be identified using data from arrays located in areas of particular interest.

Investigations at the Lajitas station and experiments carried out in Central Texas using quarry blasts have confirmed that low-frequency (0.5 to 5 Hz) acoustic signals can be detected at regional distances from commercial explosions on both acoustic and seismic arrays. The acoustic wave causes ground motion that is recorded by the seismic systems (seismo-acoustic signals). Detection of seismic, acoustic and seismo-acoustic signals at TXAR with appropriate arrival times, azimuths and phase velocities clearly identifies the source as an explosion. Figure 3 shows the location of the seismic elements in the TXAR array. Acoustic pipe arrays were collocated with seismic stations TX01, TX02, TX03 and TX09. Inexpensive acoustic sensors were placed in the boreholes that house the seismometers and electronic systems. One of these sensors is shown in Figure 4.

Figure 5 shows the acoustic signal recorded at TXAR for an m_b 2.0 surface explosion in the Micare coal mining district of northern Mexico after band pass filtering (upper figure) and beaming to the appropriate azimuth and velocity (lower figure). The amplitude is about 4 μ bars. Figure 6 shows the seismo-acoustic signal from this explosion as recorded by the 9-element seismic array with the array beam (upper figure) and the result of application of an adaptive, pure-state filter to the signal (lower figure). These recordings clearly identify the event as an explosion.

Figure 7 shows the acoustic signal from an underground m_b 3.0, explosion in the same mining district after band pass filtering (upper figure) and beaming to the appropriate azimuth and velocity (lower figure). The amplitude is approximately 0.7 μ bars 0-P. The presence of an acoustic signal indicates the event as an explosion. Figure 8 shows the seismo-acoustic signal from this underground explosion as recorded by the 9-element seismic array with the array beam (upper figure) and the result of application of an adaptive, pure-state filter to the signal (lower figure). This event is clearly identified as an explosion. Collateral information leads us to conclude that the event is a vented, underground explosion with

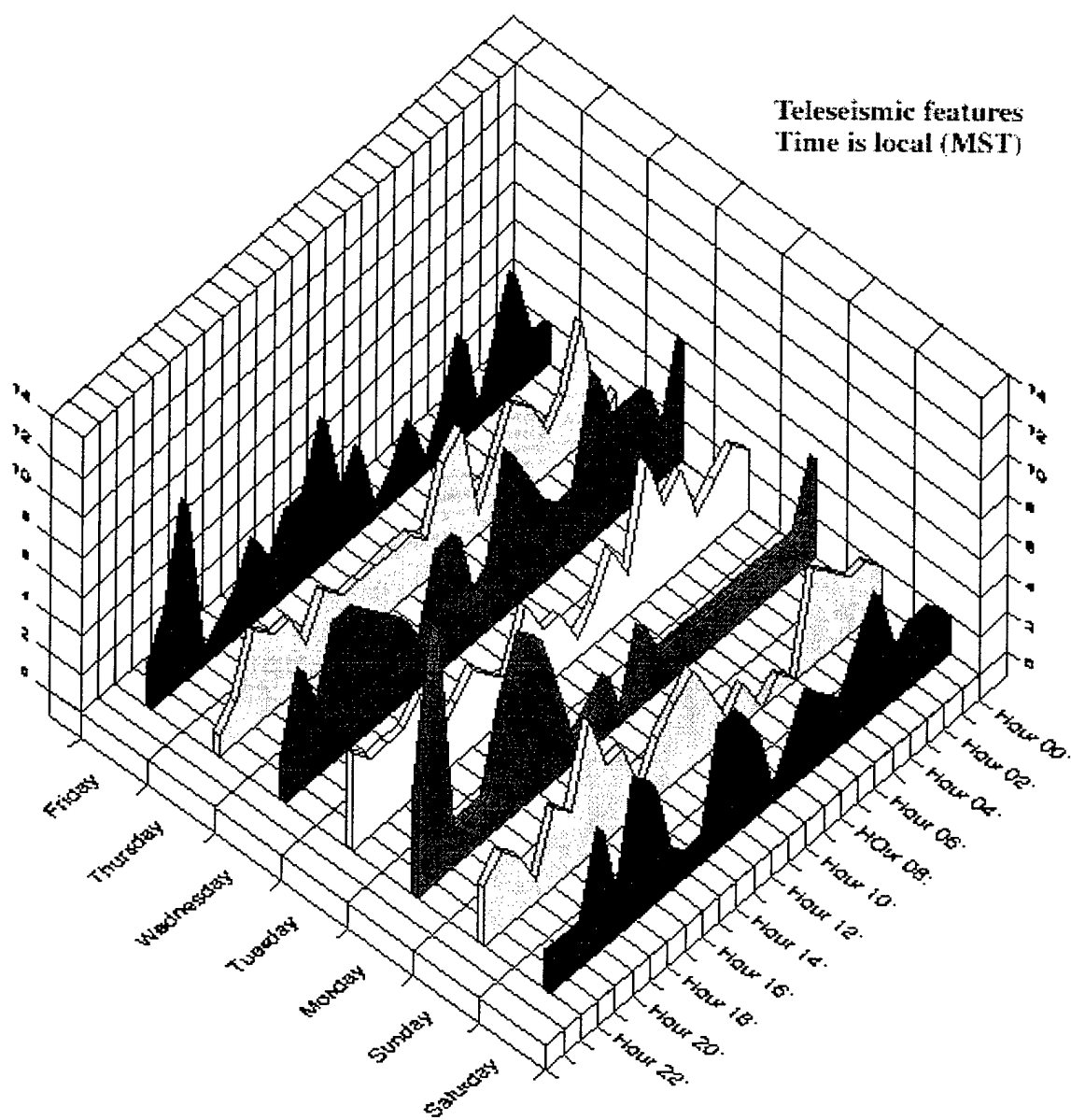


Figure 1. Number of teleseisms detected and sorted by day and hour.

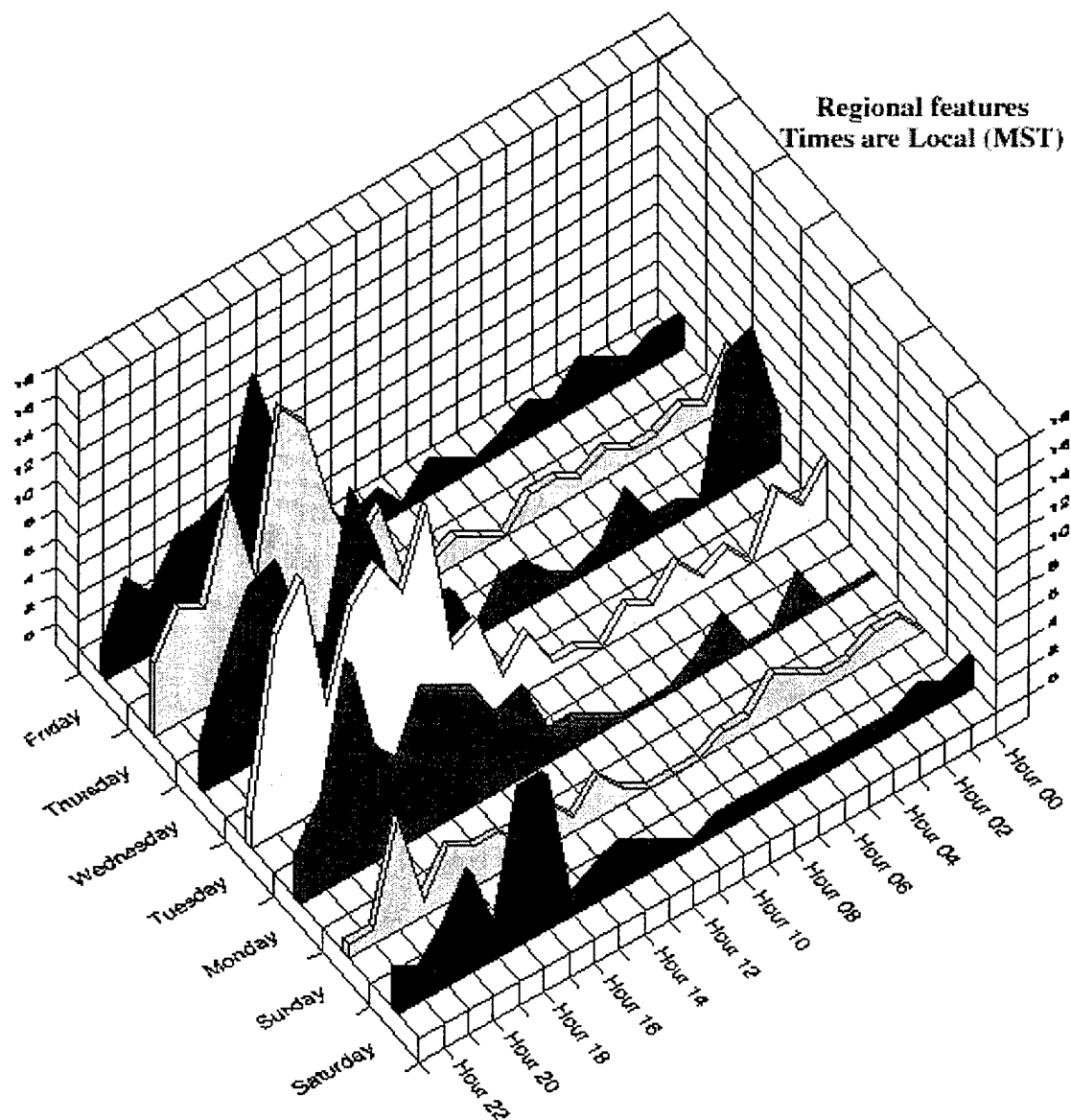


Figure 2. Pattern of regional events during GSETT-2.

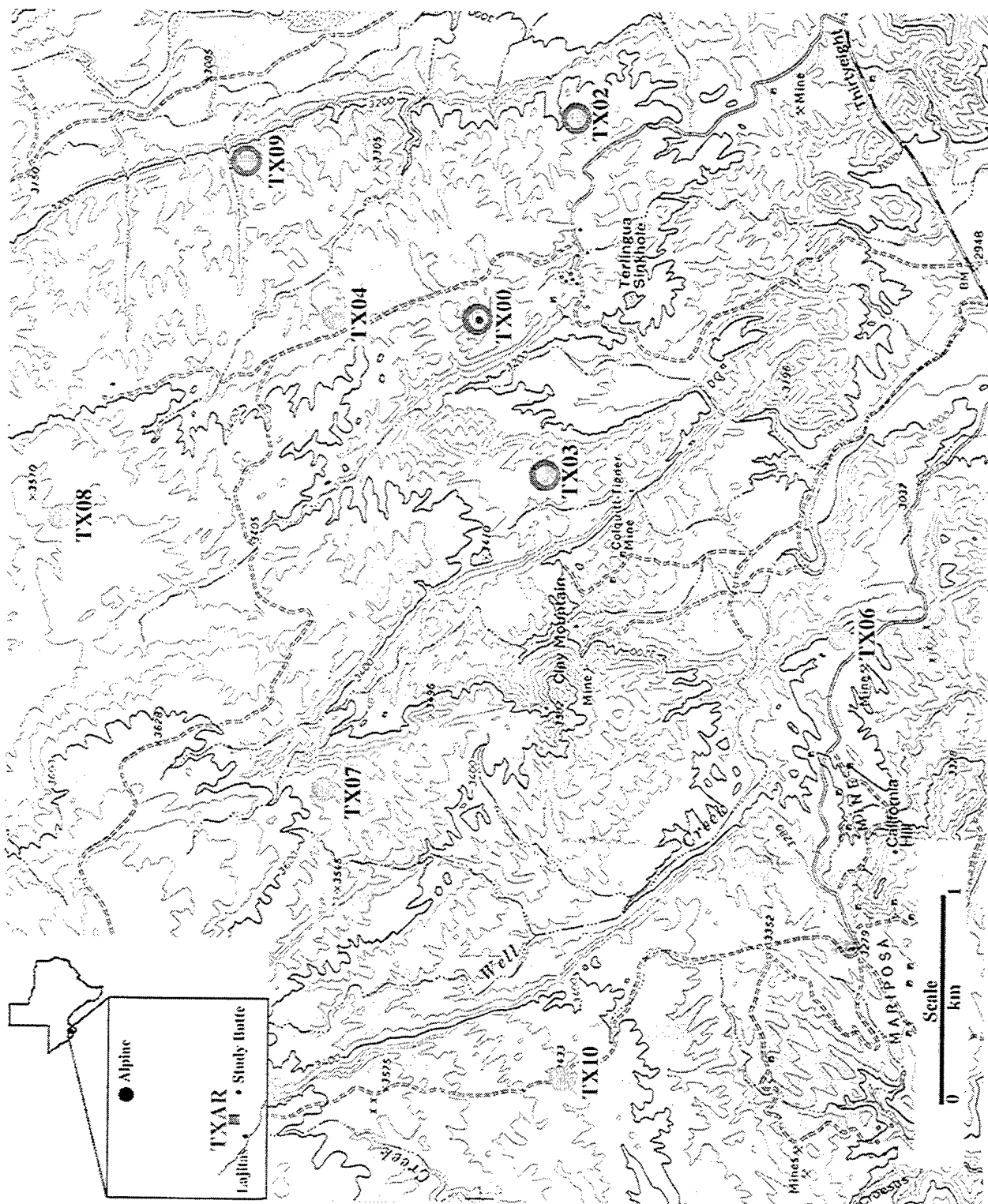


Figure 3. TXAR site location map. Acoustic sensors are located at TX00, TX02, TX03, and TX09.

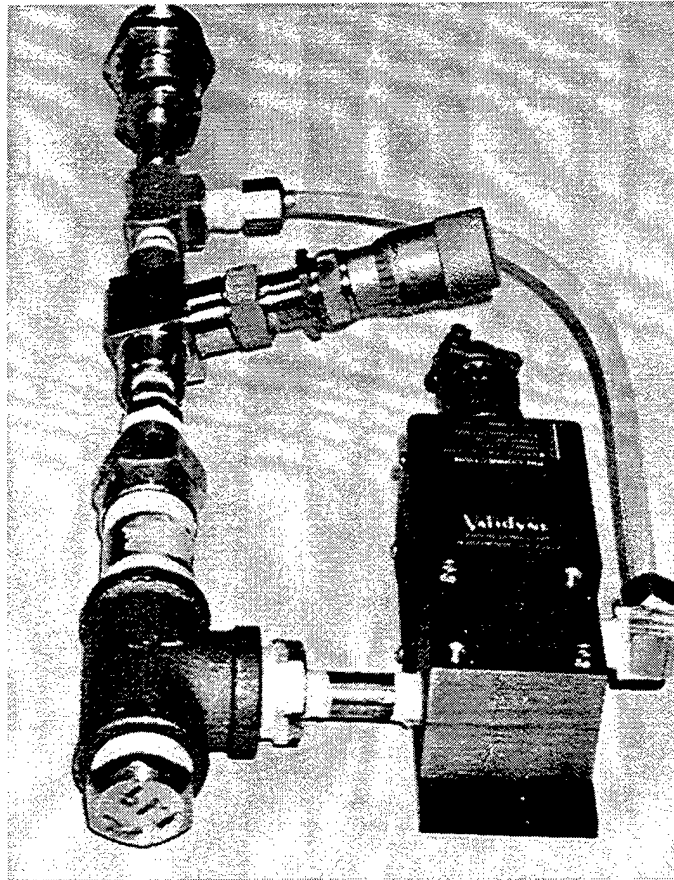
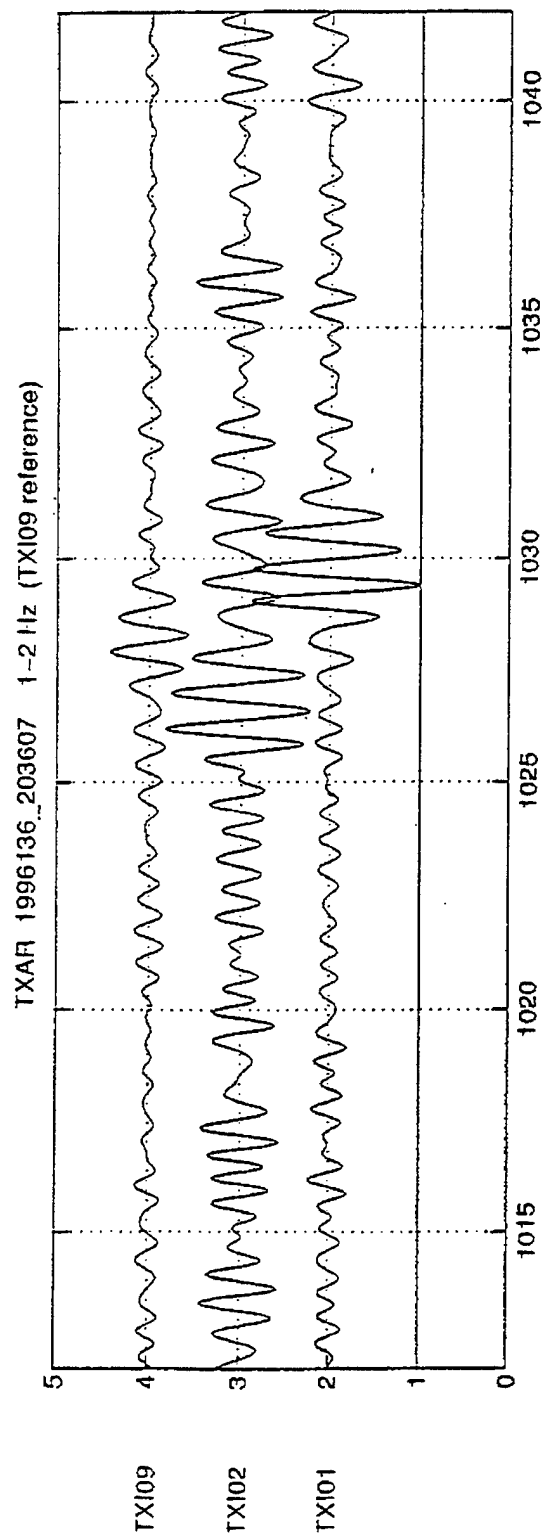


Figure 4. Validyne acoustical sensor.



8

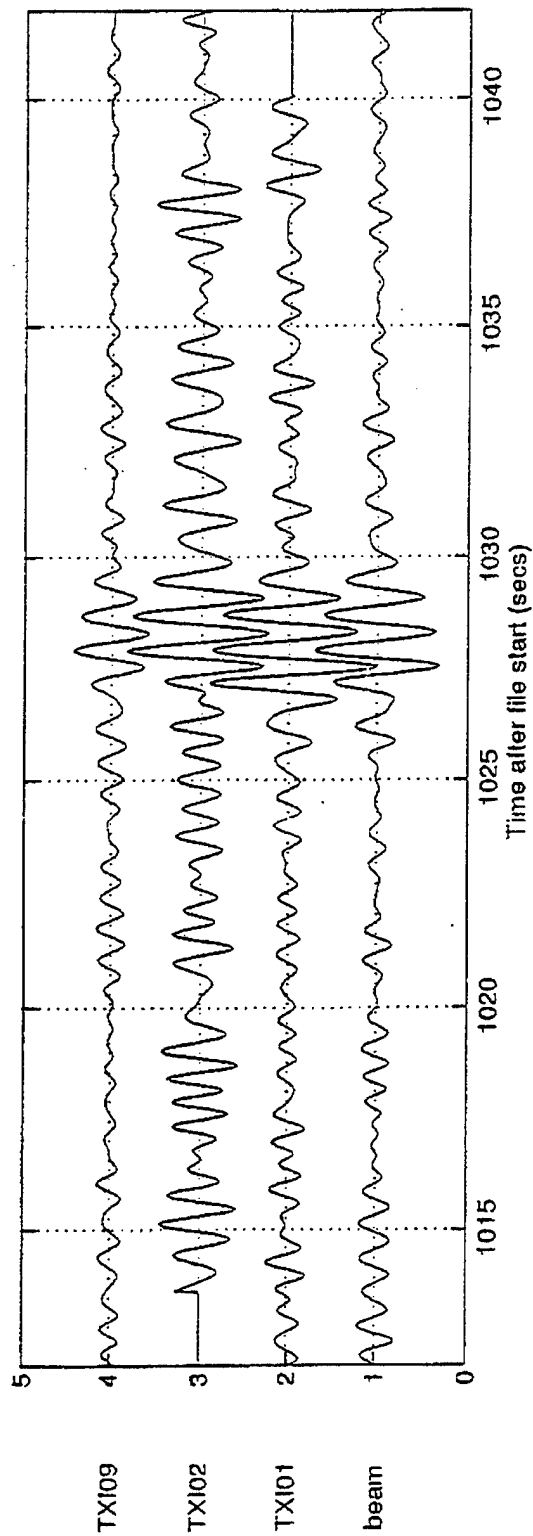


Figure 5. TXAR Acoustical signal from mb 2.0 surface mining explosion.

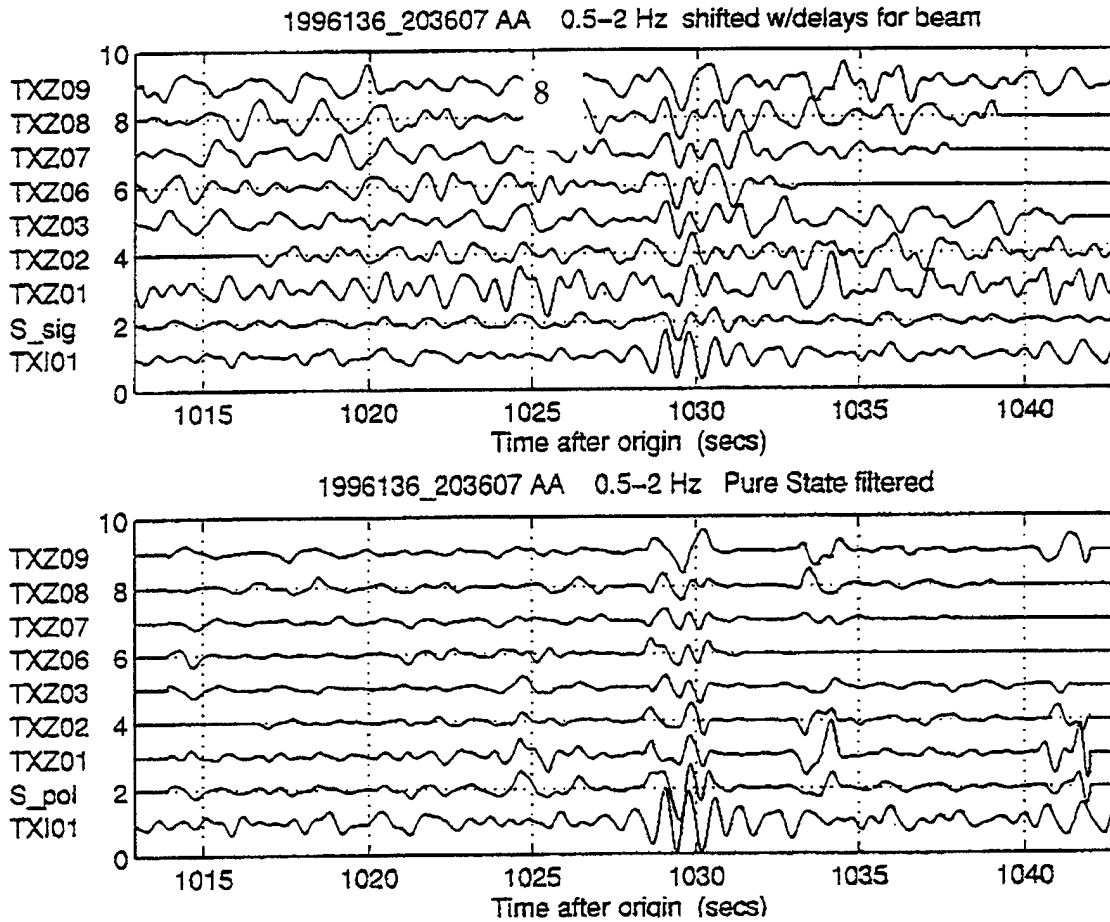


Figure 6. Seismo-acoustic signals from the surface mining explosion as recorded by the seismic array.

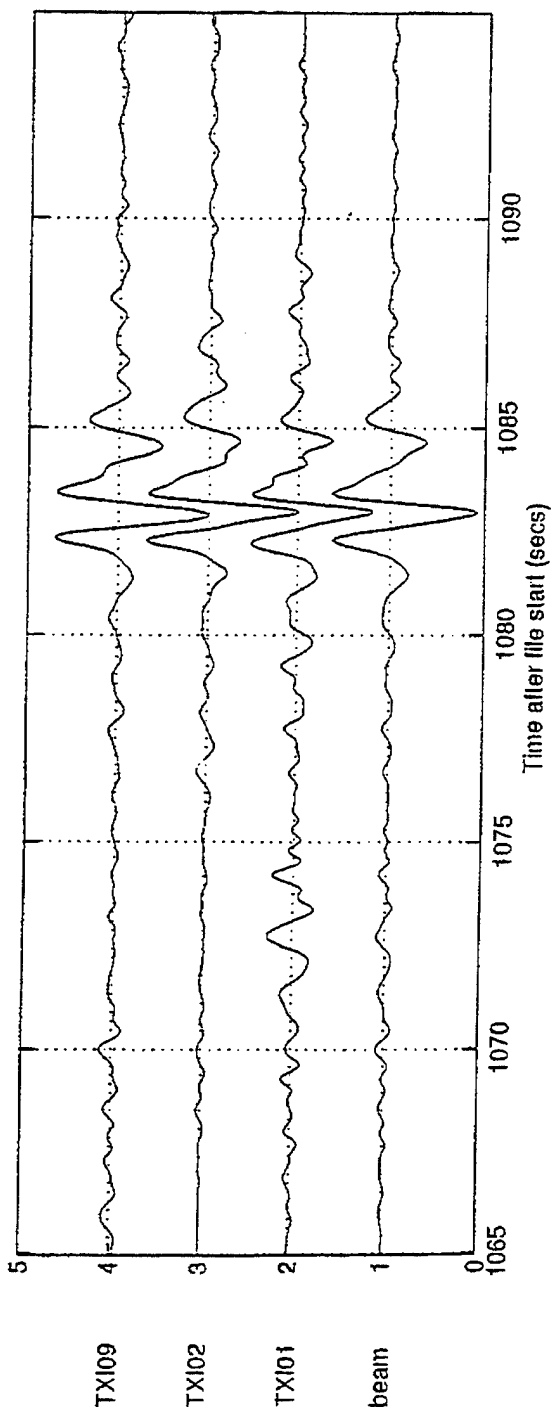
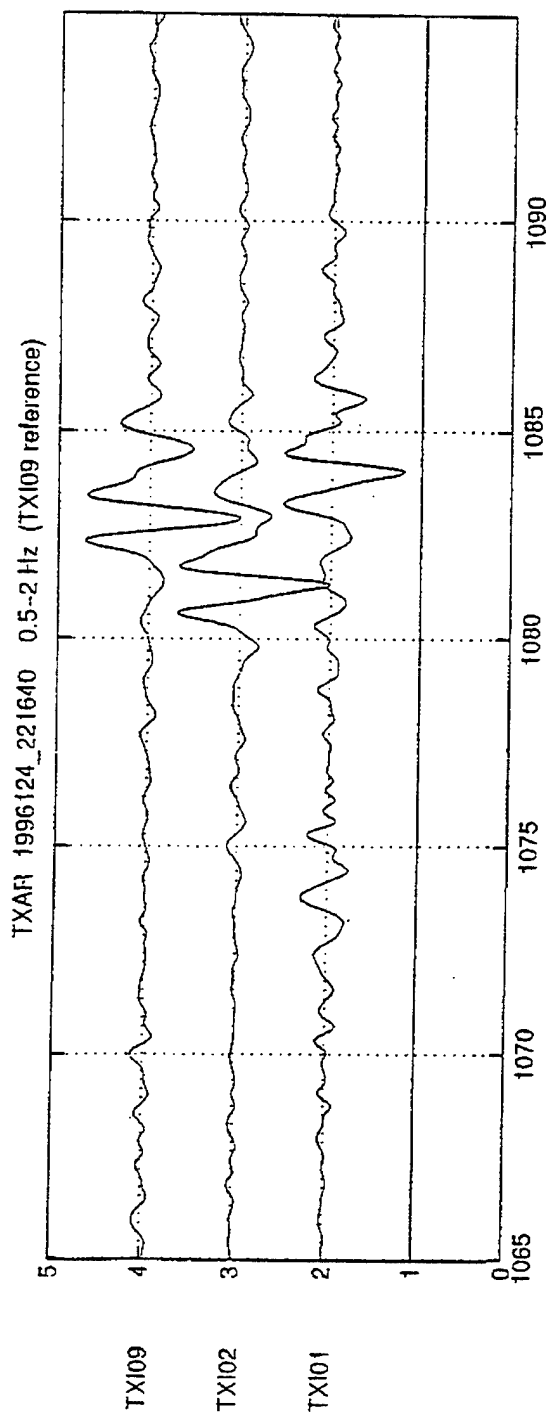


Figure 7. TXAR Acoustical signal from a suspected underground explosion in the MICARE mining district.

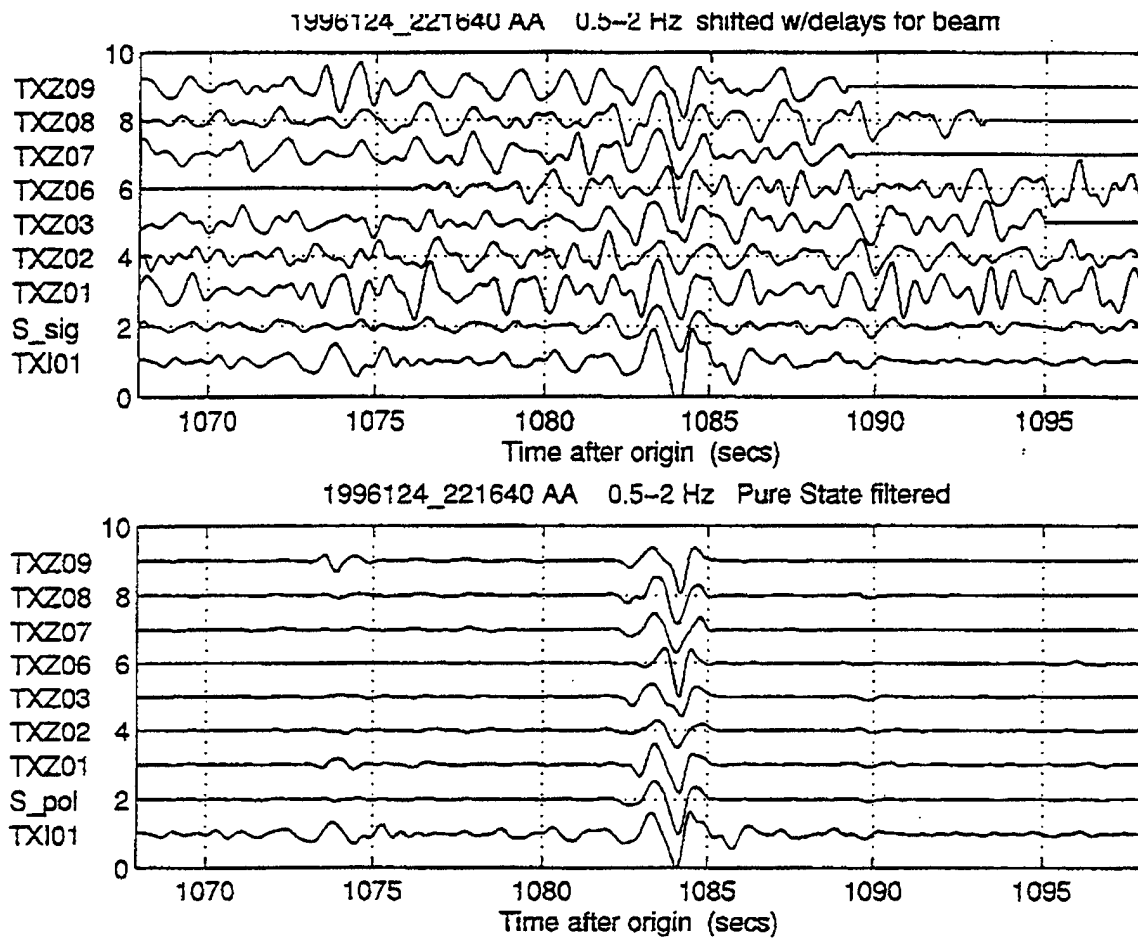


Figure 8. Seismo-acoustic signal from the suspected underground explosion as recorded by the seismic array.

small, if any, delays in the firing sequence. A number of events from mining districts in Mexico and the Western United States have been positively identified by the detection of associated seismic, acoustic and seismo-acoustic signals. These identified events then become, along with earthquake aftershock sequences, part of a ground-truth data base that can be used to test seismic discriminants.

In order to increase the detection capability of the 4-element acoustic array at TXAR, we have been experimenting with changes in the geometry of the porous-hose arrays connected to the infrasonic sensors. One simple change in the hose array led to a 10 dB reduction in the acoustic background noise in the 0.5 to 5.0 Hz band. The collocation of the acoustic and seismic sensors makes possible the estimation of the transfer function of the acoustic array for signals of interest.

Figure 9 is a diagram showing as blocks the acoustic array and seismo-acoustic response functions. The latter function depends upon the seismometer response, which is well known, and the earth response to the acoustic signal for which we have an experimentally verified theoretical model. Deconvolution of these two effects provides an estimate of the acoustic signal that can be used, along with the acoustic sensor output, to calculate the array transfer function. Figure 10 shows the amplitude and phase response of the pipe array at TX09. The linear trend in the phase response corresponds to the pure signal delay in the pipes.

Figure 11 shows the balanced zonal winds at 30 deg N. latitude. The darker colors indicate that the zonal winds are blowing from east to west, and the lighter colors indicate that the zonal winds are blowing from west to east. Because the winds blow from east to west in the spring and summer, and reverse from west to east in the fall and winter, this should result in a seasonal bias on the detection of infrasonic signals at TXAR.

Figure 12 is a Landsat image of an area in northern Mexico showing the MICARE mining district. Figure 13 is a map of northern Mexico and Southern U. S. region showing the TXAR array site in southwest Texas and locations of MICARE mining events.

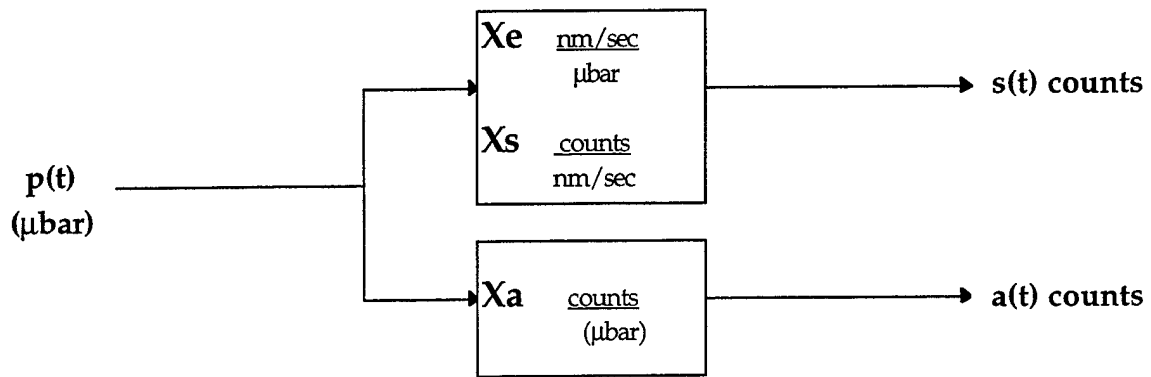


Figure 9. Block diagrams of acoustic array and seismo-acoustic response functions.

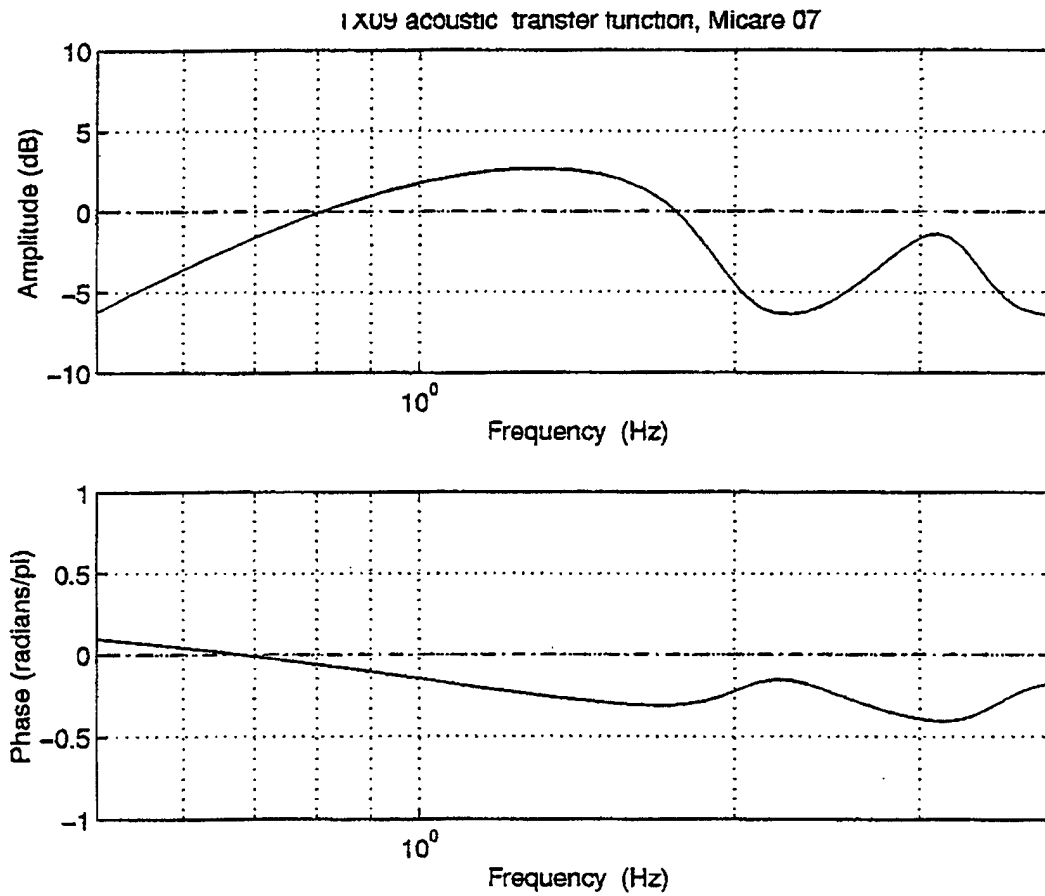


Figure 10. Amplitude and phase response of one element of the pipe array.

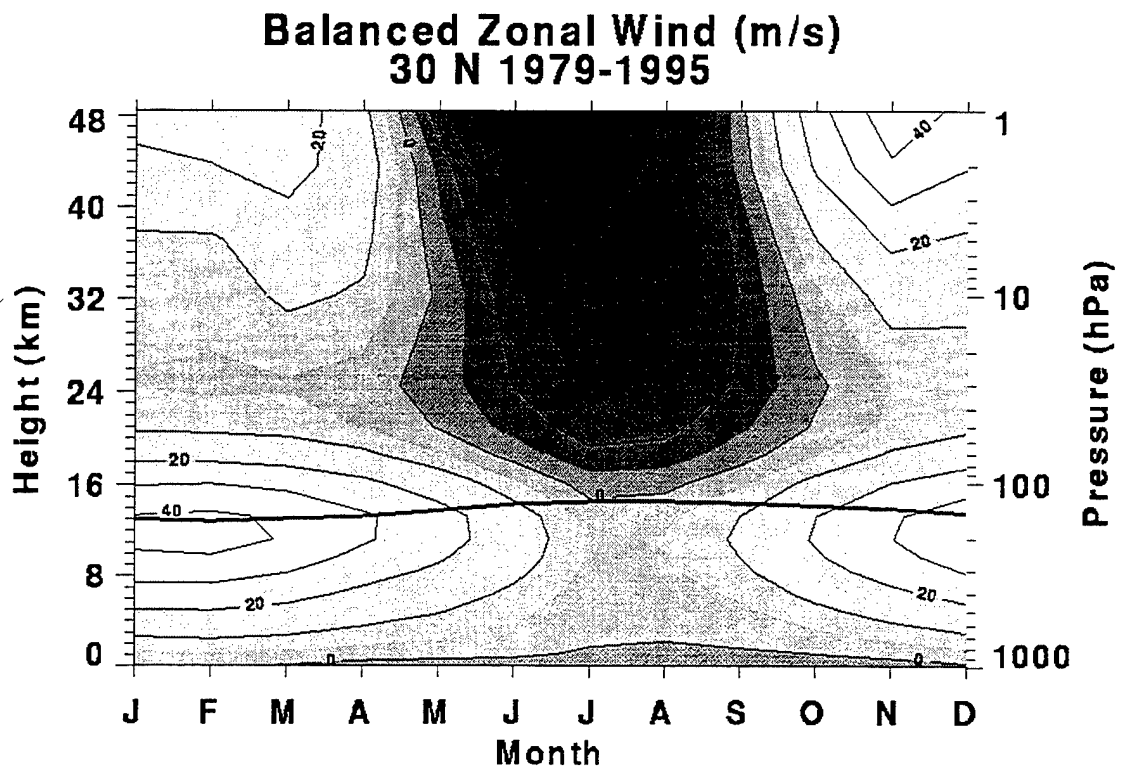


Figure 11. Balanced zonal winds at N 30 degrees latitude.

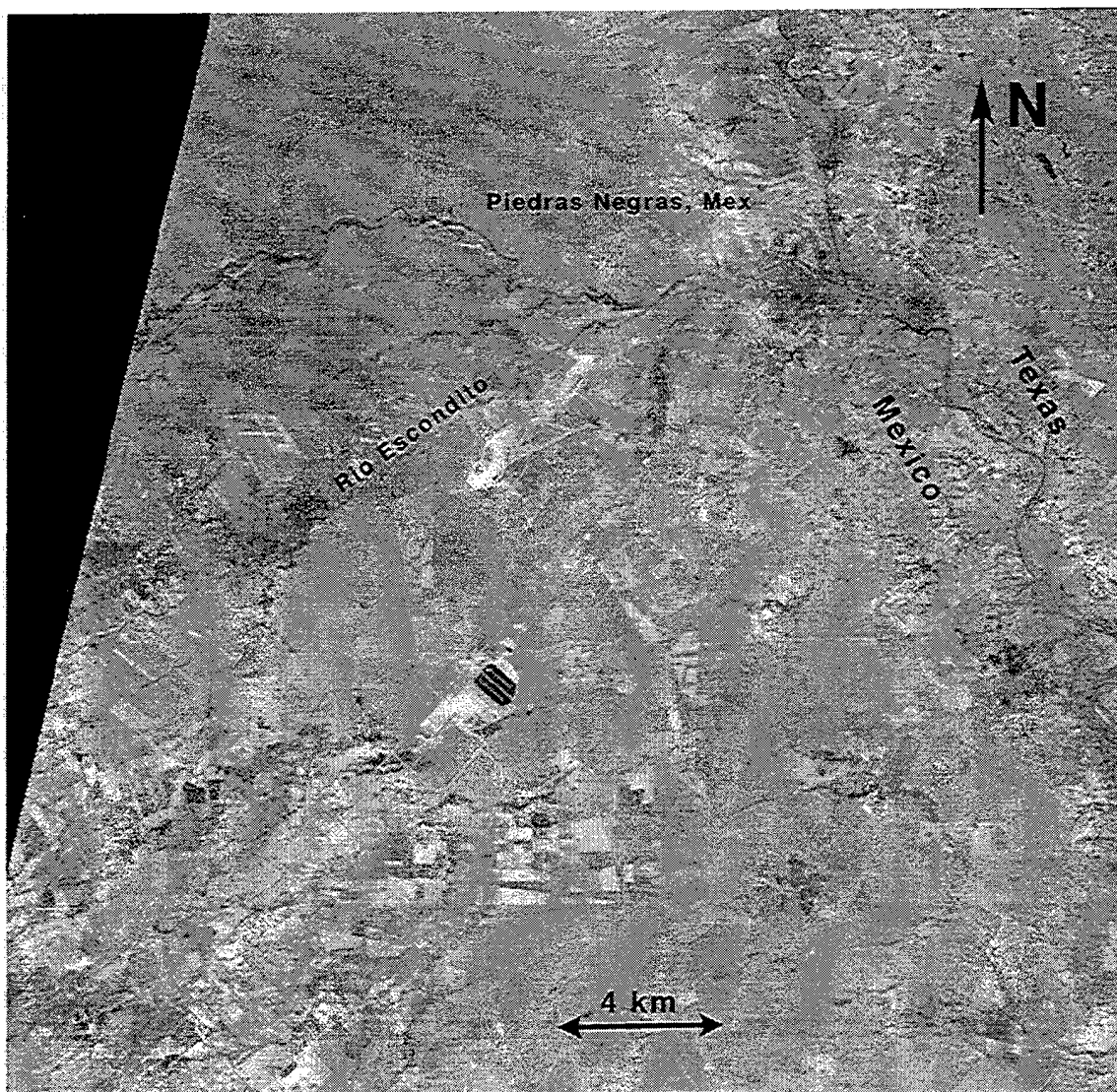


Figure 12. Landsat image of MICARE mining district in Northern Mexico.

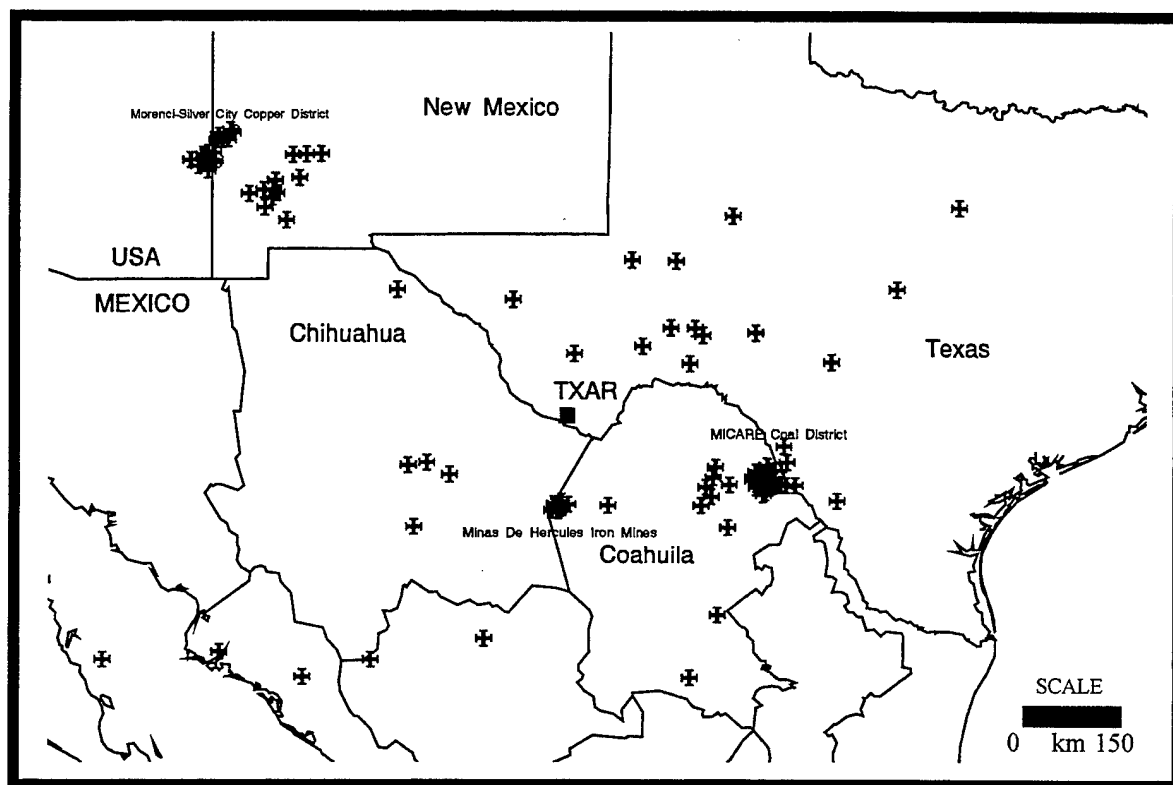


Figure 13. Map of northern Mexico and Texas showing TXAR and location of MICARE mining events.

Figure 14 shows the AR3 Spectral discriminant applied to an explosion from a coal mine in northern Mexico. The discriminant clearly indicates that the source is a "ripple fired" mining explosion. Figure 15 shows the AR3 spectral discriminant applied to an event in the vicinity of a coal mine in northern Mexico. The discriminant classifies this event as an outlier, neither explosion-like or earthquake-like.

1.3 CONCLUSIONS

The use of seismic, acoustic and seismo-acoustic detections has been clearly established as a means of positively identifying surface and vented underground explosions. These identified events then become part of a ground-truth data base. This procedure can be used at collocated seismic and acoustic arrays that detect explosions of m_b 2.5 or larger from regional sources.

Detection of acoustic signals allows the identification of clusters of similar seismic signals from explosions.

Under light wind conditions the acoustic detection threshold is a few tenths of a microbar.

Under moderate wind conditions the seismo-acoustic detection threshold is about a microbar.

Acoustic signals from explosions in Coahuila, Mexico, with seismic magnitudes above about 2.5 are detectable during months with a favorable zonal stratospheric wind direction.

We expect to detect acoustic signals from explosions in New Mexico and Arizona this winter when the zonal stratospheric winds are from the west.

Work now in progress includes:

1. Pipe array design studies
2. Evolution of the use of the pure-state filter
3. Seismo-acoustic detector algorithms
4. Development of a ground-truth data base for TXAR.

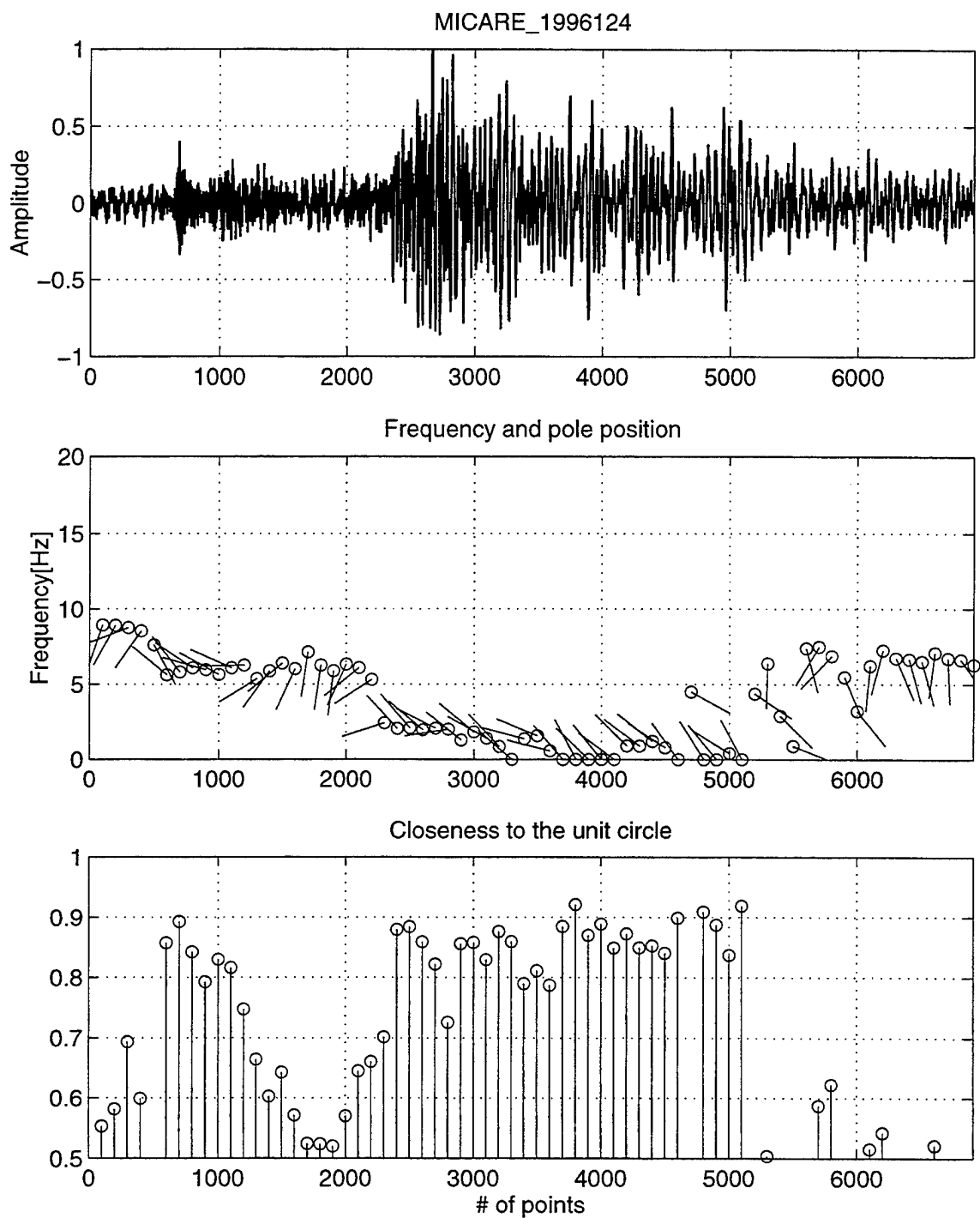


Figure 14. AR3 discriminant applied to an explosion in the MICARE district.

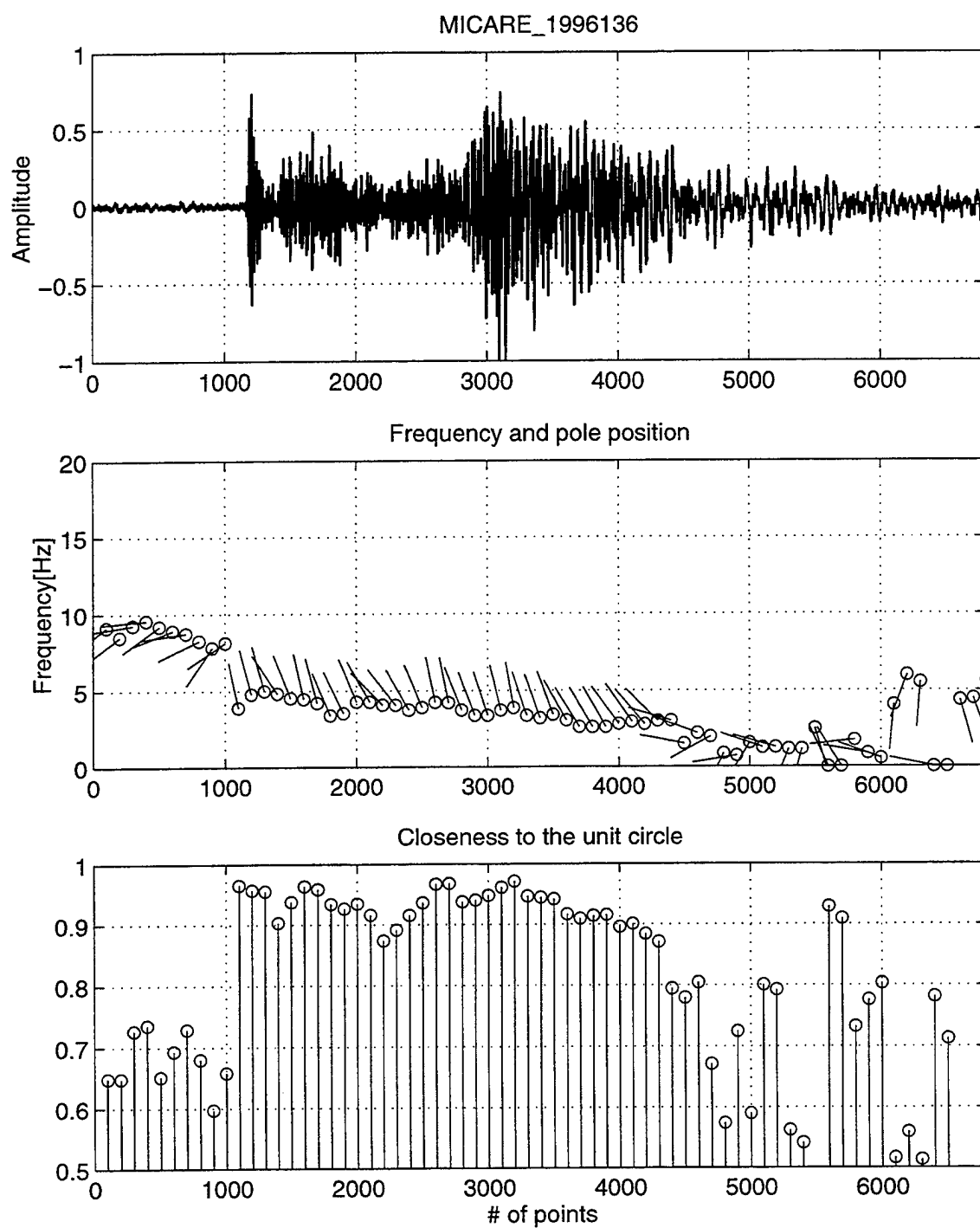


Figure 15. AR3 discriminant applied to an event in the MICARE district.

2. INVERSION OF SURFACE WAVES FOR SHALLOW VELOCITY STRUCTURE IN THE FORT WORTH BASIN

Jessie L. Bonner

2.1 EXECUTIVE SUMMARY

Short-period Love and Rayleigh (Rg) waves are guided surface waves that are generated efficiently by chemical explosions at quarries. One such quarry, operated by Chemical Lime, 40 km west of Waco, Texas, was the source for an intensive surface wave study to determine the radiation patterns for Love and Rg waves generated by ripple-fired explosions (Bonner et al., 1996). This same quarry was also the source for a seismo-acoustic experiment conducted to determine the coupling of acoustic waves in the ground (The Thompson Hollow Experiment, see Section 3 of this report). As a result of these study, surface-wave dispersion curves were generated for eight different propagation paths inside the Fort Worth basin. The purpose of this research is to invert these group-velocity dispersion curves for both Love and Rayleigh waves in order to determine shallow, shear-wave, velocity structure (< 2 km) for the Fort Worth basin. Such velocity structure is important for successful application of seismic source discriminants.

2.2 INTRODUCTION

2.2.1 Fort Worth Basin

As the proto-continents of Africa and South America advanced further toward and eventually collided with the North American craton during the Carboniferous, major thrust faults developed and folding along the Appalachian-Ouachita trend began. Several deep, foreland basins formed in front of these advancing thrust sheets, and sediment that was shed off these thrust sheets filled the basins. Some of these Paleozoic foreland basins contain up to or in excess of 16 km of synorogenic sediment, and this entire thickness is predominantly composed of flysch deposited during the Mississippian and Pennsylvanian (Viele and Thomas, 1989). The Fort Worth basin, located in north-central Texas, is one of these foreland basins (Figure 16).

The Fort Worth basin was at one time one of the most active provinces for drilling in the United States, appearing consistently on the list of top 10 most

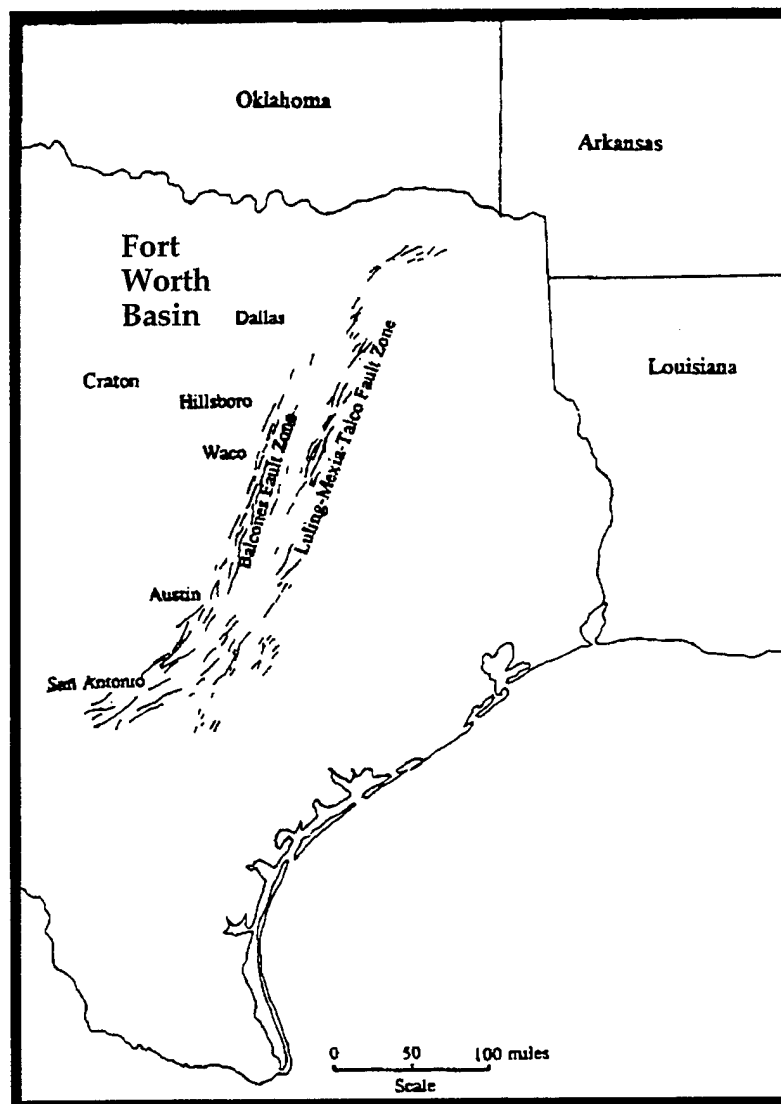


Figure 16. Approximate outline of the Fort Worth foreland basin, North-Central Texas (modified from Rinard, 1994).

active provinces up to 1980. In fact, for a six year period (1974-1980), 25% of all wells drilled as new field wildcats resulted in some sort of productive completion, a figure significantly higher than the average for the United States (see Rapaport and Grender, 1986). Obviously, falling petroleum prices have taken its toll on the basin, as production has dropped off substantially. Even so, any geophysical information obtained during this downtime could prove substantial for future plays within the basin. The stratigraphic columns for the Central Texas region and the Fort Worth basin are shown in Figure 17

The basin is filled with poorly-consolidated, low-density sediment, as noted by the pronounced gravity anomaly seen on a Bouguer gravity map (Figure 18). The thousands of feet of basin fill are largely comprised of sands and shales in turbidite sequences which were deposited synorogenically. Gravity lows reach a minimum of -85 mGals in the northern sections of the Fort Worth basin.

2.2.2 Chemical Lime Quarry and Data Acquisition

Chemical Lime (Chemlime) operates a quarry 40 km west of Waco, Texas, that extracts lime from the Edwards formation, a Cretaceous rudistid reef complex, for road and agricultural purposes. Chemlime's quarry, located within the southern confines of the Fort Worth basin, casts material into the pit by detonating 3-4 tons of ammonium nitrate explosives several times per week (Figure 19). These blasts were the source for a detailed study of the radiation patterns for Love and Rayleigh waves generated by surface explosions. Seismograms from blasts on June 28, July 12, and July 17, 1994, were recorded on eight Sprengnether 6000 three-component, 2-Hz geophones connected to Reflection Technologies (REFTEK) DAS 72-0A systems. A Teledyne Geotech PDAS 100 system, placed at the quarry, recorded the origin time of each event using GPS hardware. Ten sites were selected to surround the quarry at a distance of approximately 10 km. At this distance, higher modes have separated from fundamental mode surface waves enough to allow adequate processing. Each site was selected based upon geology and site accessibility, such that all sites have several feet of well-defined soil to allow seismometer burial of 1-2 m, with the exception of B1, which was located in the rocky soils

STRATIGRAPHIC COLUMN					
CENTRAL TEXAS-FORT WORTH BASIN					
SYSTEM	SERIES	CENTRAL TEXAS		FORT WORTH BASIN	
CRETACEOUS (LOWER)	COMANCHE	WASHITA GROUP			
		FREDERICKSBURG	EDWARDS PALUXY	FREDERICKSBURG	GOODLAND PALUXY
		TRINITY	GLENN ROSE	TRINITY	GLENN ROSE
TRIASSIC	UPPER	CHISLE SANTA ROSA TIDWAS			
PERMIAN	OCHOA				
	GUADALUPE	WHITEHORN	YAMILL		
			YATES		
			SEVEN RIVERS		
			QUEEN		
	LEONARD	FEASE RIVER	SAN ANDRES		
			SAN ANGELO		
			TUBB BULL WAGON VALE ARROYO		
	WOLF CAMP	CLEAR FORK			
		WICHITA	LUEDERS BELLE PLAINE ADMIRAL PUTMAN MORAN	VALERA COLEMAN JUNCTION SEWICK ROTHMAN-INEK STOCKWETTER TARNHILL SADDLE CREEK FLOWER CODE SAND	
		ALBANY			
PENNSYLVANIAN	CISCO	THRIFTY	CRYSTAL FALLS WEECHENRIDGE KING	THRIFTY	WEECHENRIDGE KING
		GRAHAM	GUNBRIGHT SHASTKA BUNGER	GRAHAM	GUNBRIGHT SHASTKA BUNGER
	CANYON	CADDO CREEK	HOME CREEK	CADDO CREEK	HOME CREEK COLUMBIA CREEK
		BRAD	RANGER	BRAD	RANGER PLACID
		GRAPOND	WINCHELL ADAMS BRANCH	GRAPOND	WINCHELL CEDAR TOWN ADAMS BRANCH
		WHITT	PALO PINTO CROSCUT ME	WHITT	PALO PINTO CROSCUT ME
	STRAWN	LOVE CAMP	CAFFE UPPER FRY LOWER CAFFE LOWER FRY	LOVE CAMP	CAFFE MORRIS
		MILLSAP LAKE	GOEN JENNINGS GARDNER GRAY ODON	MILLSAP LAKE	BRINDSTONE CREEK LAZY BEND
	ATOCA	BEND	KIMA LE RASBERRY SUNSHINE CADDO	BEND	NAYVILLE PARKS CADDO- POOL CADDO PRESIDENT BIG EALINE ATOCA LAETICE
MISSISSIPPIAN	MORROW		MARBLE FALLS		MORROW MARBLE FALLS
	CHESTER		DUFFER		CORRYN
	MERAMEC	BARNETT	BARNETT MISSISSIPPIAN LINE	BARNETT	BARNETT LIME BARNETT SHALE
	OSAGE	CHAPPEL	CHAPPEL	CHAPPEL	CHAPPEL LIME
ORDOVICIAN				VIOLA	VIOLA
				IMPSON	IMPSON (UNDIVIDED)
	CANADIAN	ELLENBURGER	UPPER ELLENBURGER	ELLENBURGER	HONEYCUTT ODONIAN TANYARD
	OZARKIAN	ELLENBURGER	LOWER ELLENBURGER		WILBERNE RILEY HICKORY
CAMBRIAN	UPPER		WILBERNE RILEY HICKORY		
PRECAMBRIAN			GRANITE WASH		

Figure 17. Stratigraphic column for Central Texas and the Fort Worth basin (from Martin, 1982).

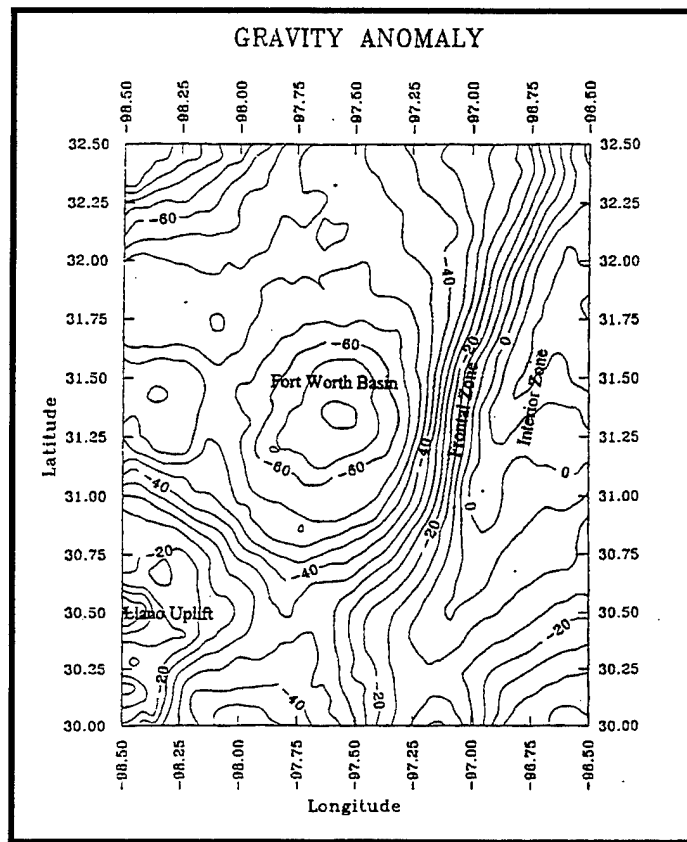


Figure 18. Bouguer gravity map of the Fort Worth basin and associated structural features of central Texas (Rinard, 1994).



Figure 19. The June 28, 1994, Chemlime quarry blast.

of the Edwards formation. Field logistics and accessibility resulted in a skewed network (Figure 20) with the seismograms ranging from 9.2 km (B7, B8, Figure 20) to 12.85 km (B10, Figure 20) from the quarry. At each site, the recorder was set to detect the quarry blast signals using a STA/LTA trigger. Disk failure at two sites (B6 and B4, Figure 20) reduced the active network to eight sites. Lack of triggering caused additional failures on the dates of the blasts, resulting in seven stations recording the June 28, and July 17, explosions, while only six recorded the July 12, blast. The data were transferred to a workstation and corrected for the instrument response.

2.2.3 Short-period Love and Rayleigh Wave Discussion

As a result of this study, eight different propagation paths for short-period Love and Rayleigh (Rg) waves were sampled. The group velocities of Love and Rg are controlled mainly by variations in the velocity structure of the upper few kilometers of the crust along their propagation paths. Rg waves on short-period seismograms are prominent at epicentral distances of 5 to 200 km along propagation paths characterized by smooth-terrain and by low-velocity surface sediments or weathered rock. The same is true for Love waves, except short-period, Love waves are usually observed out to 400 km (Delitsyne et al, 1996). The range of distances of propagation and depth of penetration make Rg waves appropriate for the study of facies changes in sedimentary basins (Kocaoglu and Long, 1993). Since, in general, velocity increases with depth, a situation arises known as dispersion in which the longer period surface waves penetrate deeper into the crust than short-period surface waves, thus having greater group velocities. The multiple filter technique (MFT) is shown to be a fast, efficient method of analyzing these dispersed signals. (Dziewonski et al, 1969). The MFT applies narrow band Gaussian filters to the dispersed wave train to determine group velocity as a function of period. When the MFT results are combined with the phase match filtering technique (Figures 21 and 22), a method for extracting a particular mode or arrival from a complex surface wave train (Herrin and Goforth, 1977), the dispersion curves for different propagation paths can be studied without interference from other parts of the waveform. The dispersion curves for the Love and Rg waves recorded from the June 28 blast

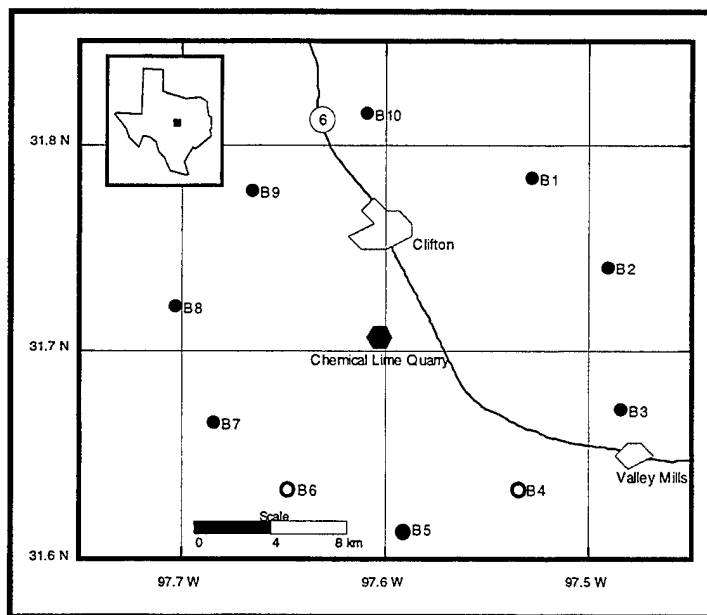


Figure 20. Portable network of seismometers monitoring blasting operations at Chemlime

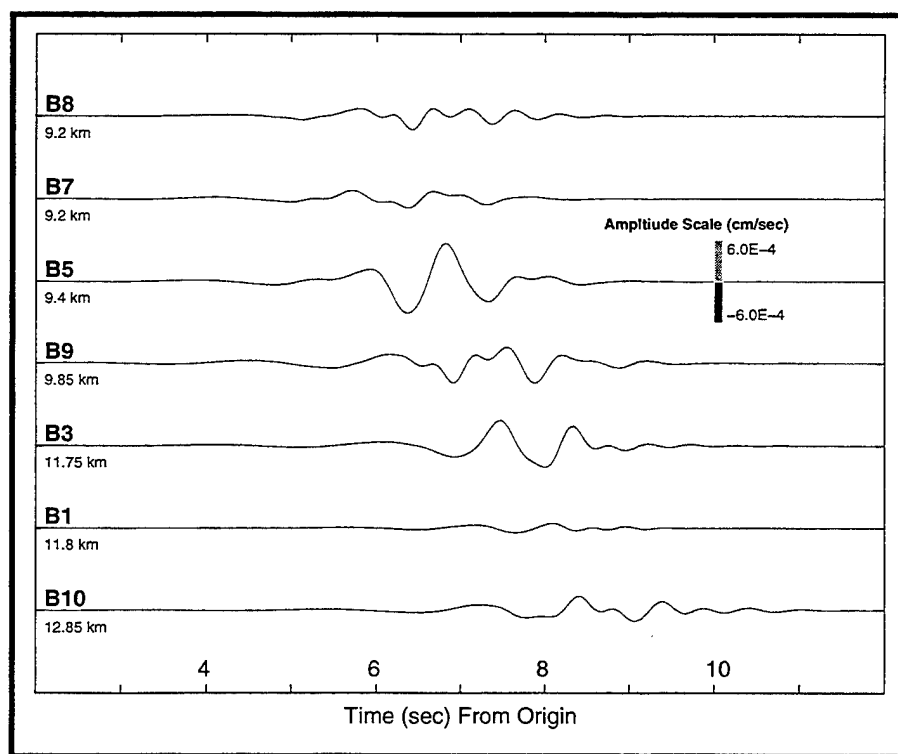


Figure 21. PMF extracted Love waves for the June 28, 1994, Chemlime explosion.

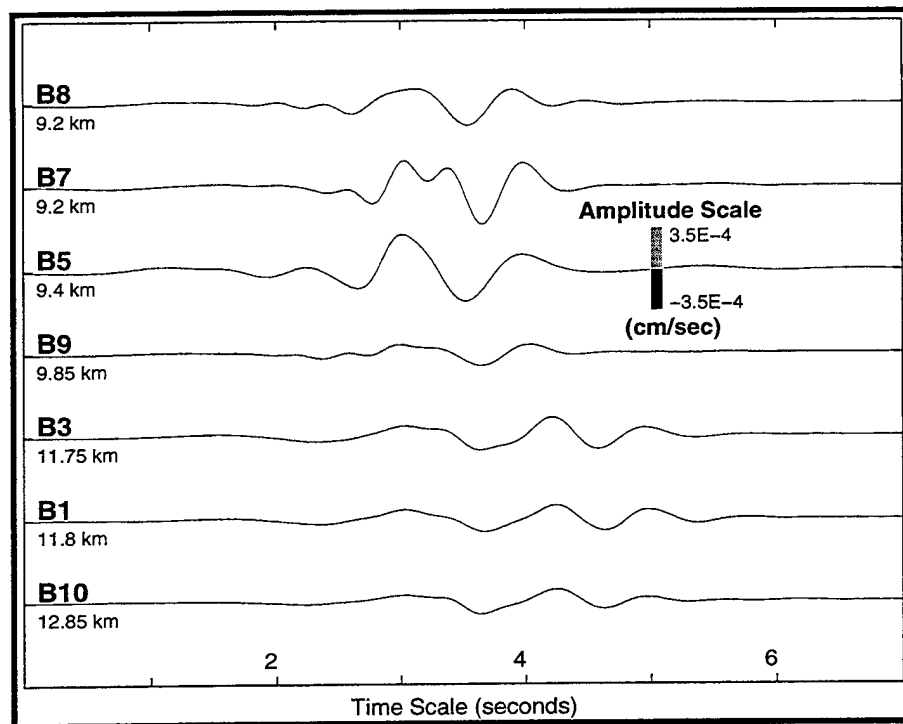


Figure 22. PMF extracted Rg for the June 28, 1994, Chemline explosion aligned to the most prominent pulse .

are shown in Figure 23. Given these dispersion curves, the near term objectives of this study are:

1. Invert both short-period Rayleigh and Love waves from Central Texas quarry blasts to determine the upper-crustal, velocity structure.
2. Determine if the highly-fractured, loosely-consolidated rocks comprising the upper crust of Central Texas are transversely anisotropic.

2.2.3 Inversion Fundamentals

According to Panza (1981), two different approaches for surface wave inversions are used; the first is the "linearized inversion" of Backus and Gilbert, (1968, 1970) and second, trial-and-error techniques similar to the Monte Carlo random search (Keilis-Borok and Yanovskaya, 1967). Backus and Gilbert's method is essentially based on the iterative procedure of referring the Earth model by small disturbances of an initial a priori known Earth structure. This structure consists of physical properties that fall into two classes; properties that can be described as discrete parameters and those that are described by continuous functions. The research presented in this proposal considers the former, assuming numerical values for different parameters within the Earth. The earth will be assumed to consist of several discrete layers that can be represented by parameters such as density (ρ), P (α) and S (β) wave velocity, and attenuation (Q). The data used to determine these parameters will be the group velocity curves shown in Figure 23.

The method of inversion used in this proposal will be similar to the problem described below. Consider the linear equation:

$$A\underline{x}=\underline{b}$$

where A is the data kernel, \underline{x} is a vector that contains the parameters being estimated, and \underline{b} is the vector of the data (group-velocity dispersion in this case). This equation applies not only to this research, but also to most discrete inverse theory. Inversion is generally an iterative technique where this equation can be worked backwards based on the estimated model parameters that yield predicted data. With this in mind, we must have some program to calculate the theoretical dispersion for the model parameters, thus we use

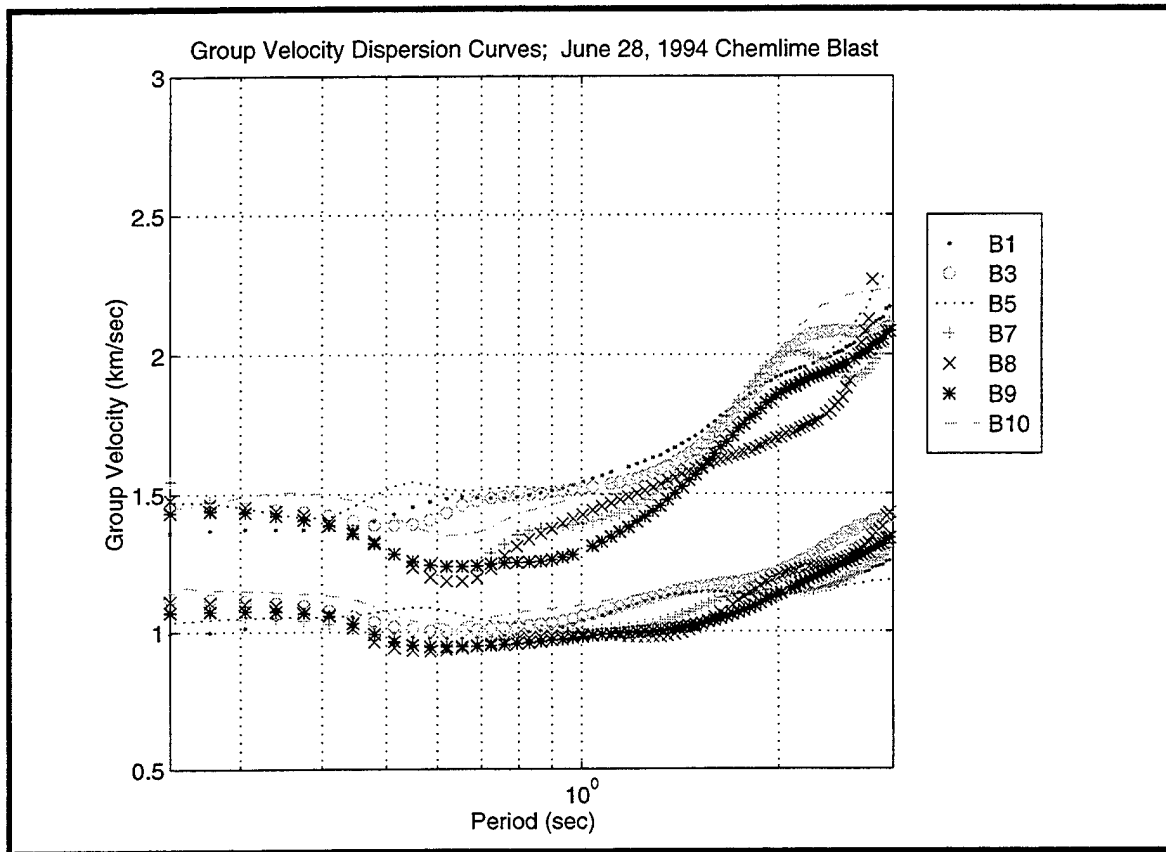


Figure 23. Group velocity data for Love and Rg waves recorded from the June 28, 1994, Chemlime explosion.

programs by Robert Herrman at St. Louis University. The frequently used least squares solution is a technique to pick model parameters that force the predicted data to be as close as possible to the observed data. The error e for each observation can be defined as:

$$e = \underline{b} \text{ (observed)} - \underline{b} \text{ (theoretical)}.$$

The line that has the smallest sum squared error is the best fit line, for this technique is commonly used to derive a best fit line to a series of points. For this proposal, a non-linear problem is solved by approximating it as a linear problem. Checking the observed data with the predicted can be achieved by slightly perturbing the model, and this perturbation is accomplished using a partial derivative approach to determine the relationship between parameters.

Determining these partial derivatives is not trivial, and will be discussed further. The numerical partial derivative computation used in this study is implemented by a set of computer programs written by Robert Herrmann and his associates at St. Louis University (1987). This program requires partial derivatives with respect to layer parameters, and computes the phase velocity values for a given mode, wave type, and frequency. When group velocities are computed, the phase velocities c are computed at two periods $(1 \pm h) T$ rather than at the single period T (the value of h used for initial results presented in this study is 0.001). The partial of the group velocity U with respect to a layer velocity v is then:

$$\frac{\partial U}{\partial v} = \frac{U}{c} \frac{\partial c}{\partial v} + \frac{U^2}{c^2} \left[\frac{T}{c} \frac{\partial c}{\partial t} \frac{\partial c}{\partial v} - T \frac{\partial}{t} \frac{\partial c}{\partial v} \right]$$

In this expression, the parameter v can take on the values for P and/or S wave velocities and the subscript o represents the value of the parameter in the purely elastic model.

2.3 RESULTS TO DATE

2.3.1 Obtaining A Priori Information

Borehole data for the study area was obtained at Geomap and includes electrical resistivity and spontaneous potential logs for numerous wells located within the study area. For the initial results of this proposal, only the Love and Rg dispersion curves for station B9's recording of the June 28, 1994, blast were considered. Further research will include all data in an attempt to determine facies changes and other depositional structures within the shallow crust. But, before this can be accomplished, more detailed a priori knowledge, including VSP profiles, will be compiled to limit the non-uniqueness in the models.

Due to the lateral variations in seismic velocity structure along the propagation path, the observed dispersion curve represents the weighted average of the dispersion properties along the path. Thus, determining which borehole information to use was done by considering the well closest to the middle of the propagation path. In the case of B9, this well is the Reichert #1 wildcat drilled in Bosque County, Texas, approximately 8 miles north of Valley Mills, Texas. A summary of the well is given in Figure 24. At this location, the Cretaceous cover consists of approximately 500 feet of sands, shales, and marls, underlain unconformably with the flysch deposits of the Pennsylvanian Cisco, Canyon, Strawn, and Atokan groups (Figure 17). At approximately 2 km depth, the first competent limestones are encountered, which include the Marble Falls and Ellenberger formations.

Since no velocity information is available for these wells presently, the initial model for the velocity inversion was estimated considering published compressional and shear wave velocities for similar rocks at equivalent pressures. This is by no means the correct procedure to approach this problem, and as soon as interval velocity information is obtained (assuming that it will be), the initial model will be constrained much more adequately for this problem. The starting model for the velocity inversion is shown in Table 1. The velocities presented are in accordance with published values compiled in Sheriff and Geldart (1995) for similar lithologies.

Using well log information and borehole velocity data is similar to work completed by Herrmann (1969) in a study of the Cincinnati arch. Craven (1992) used shallow refraction data to determine the thickness of layers as well as compressional and shear wave velocities for each layer. On the other hand, some researchers do not consider any a priori knowledge of the geologic structure. Kocaoglu and Long (1993) used a trial model with layers of constant thickness that had shear velocity increasing at a constant rate with depth. No assumptions about the subsurface geology were made, but the inversion results agreed with the known geologic structure.

Table 1. Initial Starting Model for Inversion

Z	α	β	ρ	Dominant Lithology
.05	2	1	2	K-shales
.05	2.5	1.25	2	K-limestones
.05	2.5	1.25	2	K-sands
.1	3	1.5	2.2	P -sands,shales
.1	3	1.5	2.2	P -sands,shales
.1	3	1.5	2.2	P -sands,shales
.1	3	1.5	2.2	P -sands,shales
.4	4.0	2	2.5	P -sands,shales
.4	4.0	2	2.5	P -sands,shales
.4	4.0	2	2.5	P -sands,shales
Ha	5.5	3	2.5	O -Ellenberger limestone

2.3.2 Inversion Results

Surface wave dispersion is influenced by several material properties, some of which have greater influence than others. Shear-wave velocity and thickness of the layers seem to have the greatest effect on surface wave dispersion (especially in the case of Love waves), followed closely by compressional wave velocity and bulk density. All four of these properties are the input of an inversion program developed by Herrmann (1987) that inverts surface-wave dispersion curves for shear velocity structure.

The attenuation of seismic waves also affects surface wave dispersion. A quality factor (Q) is a measure of the attenuation of shear and compressional

waves for layers in which waves travel. Q values for Central Texas rocks are unknown; therefore, no Q was used in the inversion scheme making these results non-causal. The neglect of Q could make a substantial difference in how the actual shear wave velocities compare with those presented in these results. A recent survey in the region could shed some light on this problem. Data from a linear array of six seismometers recording a Chemlime blast could give Q information for the upper crust as well as phase velocity information-- both data are needed to provide additional constraints on the inversions.

To recap the inversion procedure, Herrmann's programs compute the theoretical dispersion for the starting model. These theoretical dispersion values are then compared to the observed dispersion values at each period, and the residuals are computed. A non-causal inversion then finds a model that reduces the sum of the squares of the residuals. The non-linear process is iterated until satisfactory results, as measured in rms error between predicted and observed values, are achieved.

Love and Rayleigh waves were inverted separately. The Love-wave inversion for the propagation path between Chemlime and B9 is shown in Figure 25. The starting model for this inversion is from Table 1 and consisted of 10 layers over an Ellenberger half space. Thirty iterations were needed to minimize the error between the predicted and observed dispersion, for a damping factor, which limits how fast parameters can change, was set very low for this inversion (.01).

The resolving kernels are a measure of the resolving power of the data within each layer. The kernels associated with the layered model are found to be quite narrow in the upper 0.50 km. At depths greater than 0.50 km, the resolution kernels increase in width (lose resolving power) with increasing depth, and the maximum depth at which shear velocity can be estimated is approximately 2 km. This is consistent with the depth of penetration of short-period Love waves. With an average group velocity of 2.0 km/sec and a period of 2.0 seconds, the depth of penetration should be approximately 60 percent of wavelength, or 2.2 km (Kocaoglu and Long, 1993).

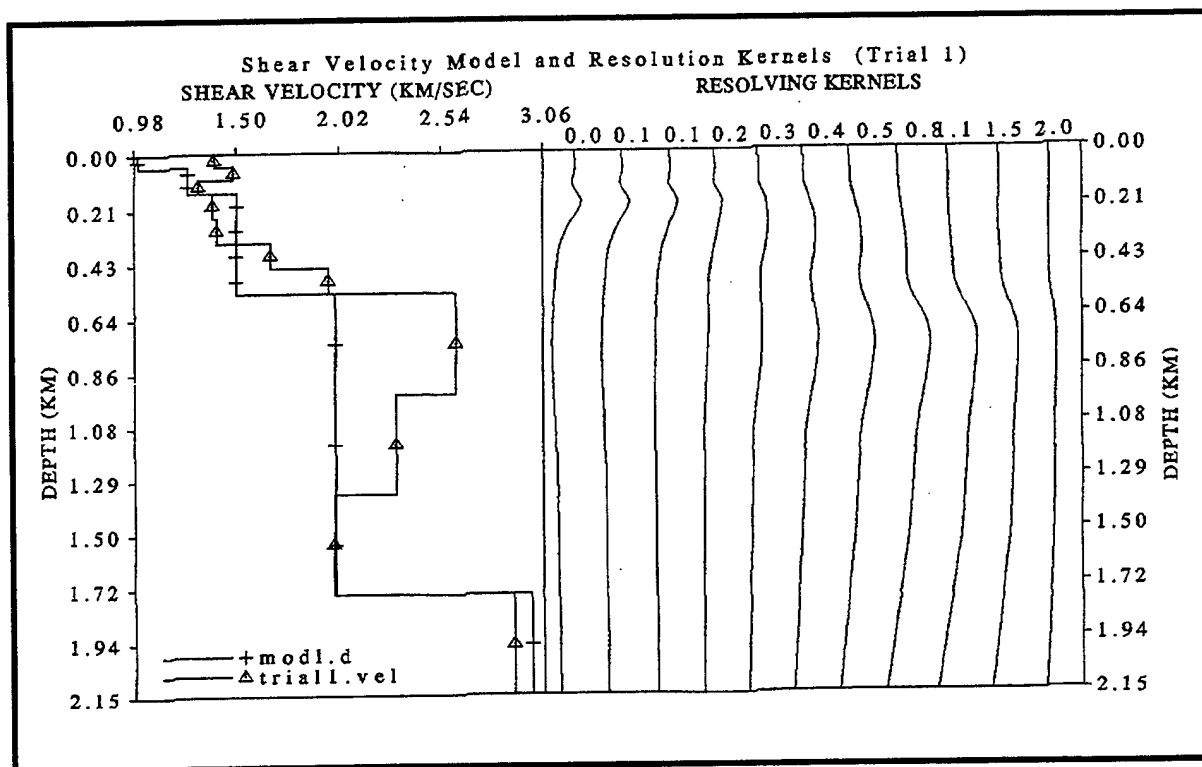


Figure 25. Love wave inversion for the propagation path between Chemline and B9. The initial model is shown here and in Table 1. Also shown are the resolving kernels (see text for discussion).

The dispersed signal is sampling rocks of both Paleozoic and Mesozoic ages. The velocity decrease at 0.10 km depth represents the transition between the Glen Rose limestone and the Cretaceous sands of the Trinity group. The shear wave velocities then increase slightly into the strata of the Pennsylvanian flysch deposits. A lithology change is probably not the reason for this increase, but rather, the change is most likely related to age differences between the two suites. On the other hand, the large velocity increase at 0.6 km depth can not be explained, and the validity of the inversion is in question. A shear velocity increase to 3.0 km/sec in the half space is expected due to the dense, dolomitic nature of the Ordovician Ellenberger formation. Several different starting models that included different layer thickness and different shear wave velocities were used in the Love wave inversion at B9. All of these models converge to a similar model (Figure 26) suggesting the low-velocity zone between 1.10 and 1.75 km depth is real.

Results for the Rayleigh wave inversions are shown in Figures 27 - 29. For the three different Rg inversions compiled using different starting models (Figure 28), the same general structure is obtained. The Cretaceous rocks have low-velocities (1.0 - 1.2 km/sec), and in one of the models, the Glen Rose limestone/Trinity sandstone transition might be resolved. Velocities increase into the Paleozoic rocks, and the hint of a low velocity zone (LVZ) is suggested by the Rg inversions that is similar in size and depth to the LVZ found from Love wave results.

All the inversions presented thus far consider constant Poisson's ratio with depth-- a value of 0.33 that corresponds to normal values found in sedimentary basins. Figure 29 shows the effect of changing this number (0.33; trial 5) to anomalously high values (> 0.45 ; trial 9) and low values (< 0.2 ; trial 8). The overall result is to vary the velocity structure produced by each model significantly. Obtaining interval velocities for the region will constrain the compressional velocities and somewhat alleviate this problem.

2.4 CONCLUDING REMARKS

The Love and Rayleigh wave inversions were treated as separate problems to determine if the upper crust in the Fort Worth basin is transversely

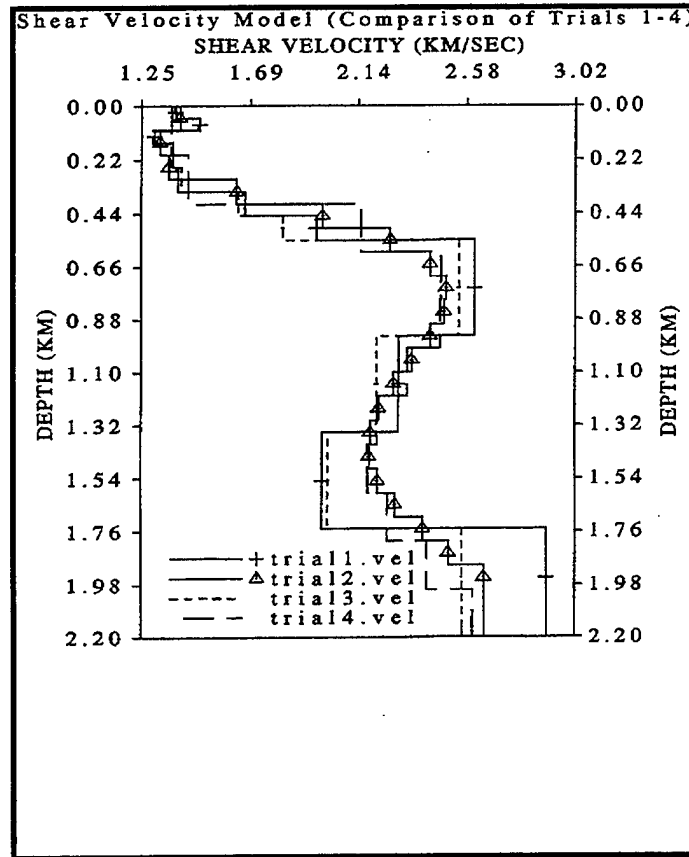


Figure 26. Combined results of four different Love wave inversions with different starting models.

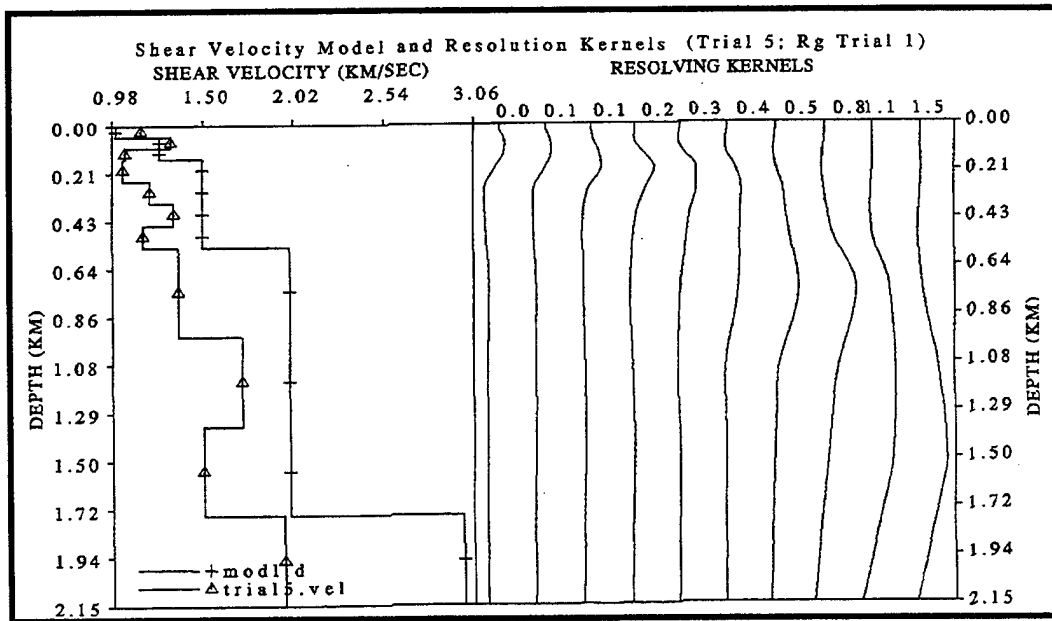


Figure 27. Rayleigh wave inversion for velocity structure. The initial model is shown here and in Table 1.

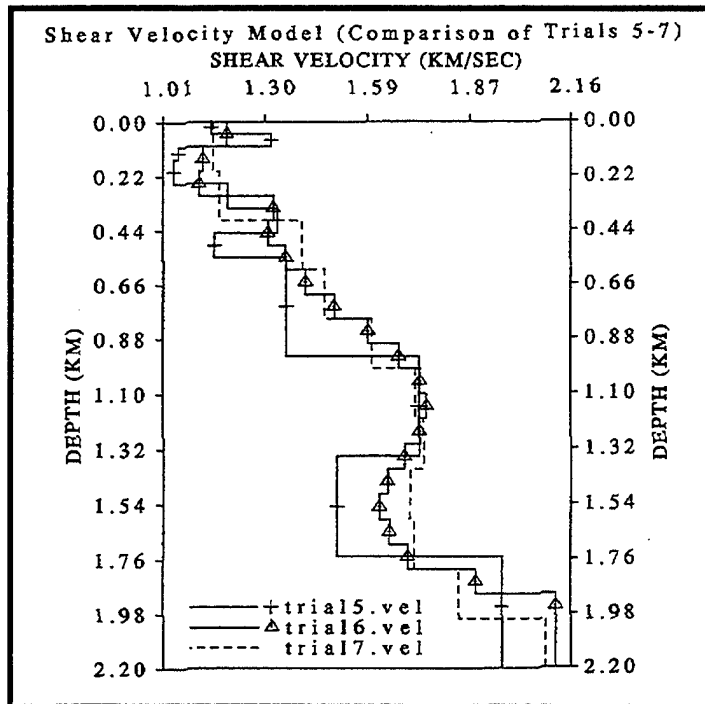


Figure 28. Combined results for three different Rayleigh wave inversions with different starting models.

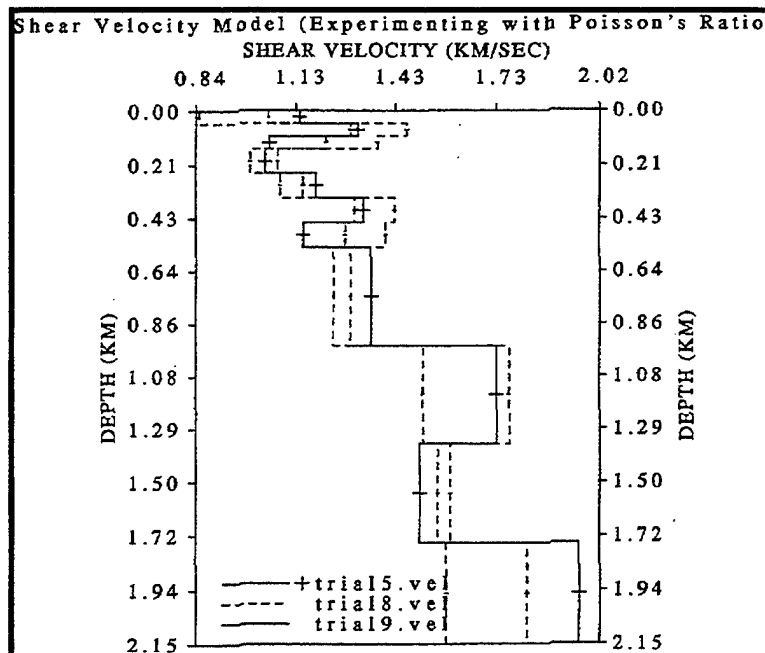


Figure 29. Rayleigh wave inversion that considers anomalous values for Poisson's ratio (see text for discussion).

anisotropic. The initial results are quite conclusive (Figure 30). Two different velocity structures are obtained through the separate inversion of the Rayleigh (P-SV) and Love (SH) waves that have traveled along the same path. This is not unexpected considering the highly- fractured nature of the rocks in the upper crust of central Texas and the total percentage of clays in the stratigraphic column. But the magnitude of this phenomenon is unexpected and raises doubts about the validity of the results. Further research will work to alleviate these doubts, as methods for inverting Love and Rayleigh waves simultaneously using code that considers transversely anisotropic media are employed. Further geophysical data from the basin will be sought to constrain the models more efficiently, and as a means of testing the final answer.

2.5 ACKNOWLEDGMENTS

I wish to thank Angela Maddox, Beth Rinard, Tom Goforth, and the Baylor University geophysical field class (Summer '94) for helping install the portable array of seismometers used in this study. Also, without the cooperation of Chemical Lime, especially Freeman Mullins and Robert "Squeaky" Shannon, this project would not have been possible. Finally, I wish to thank Dr. John Ferguson for helpful comments about the research and manuscript.

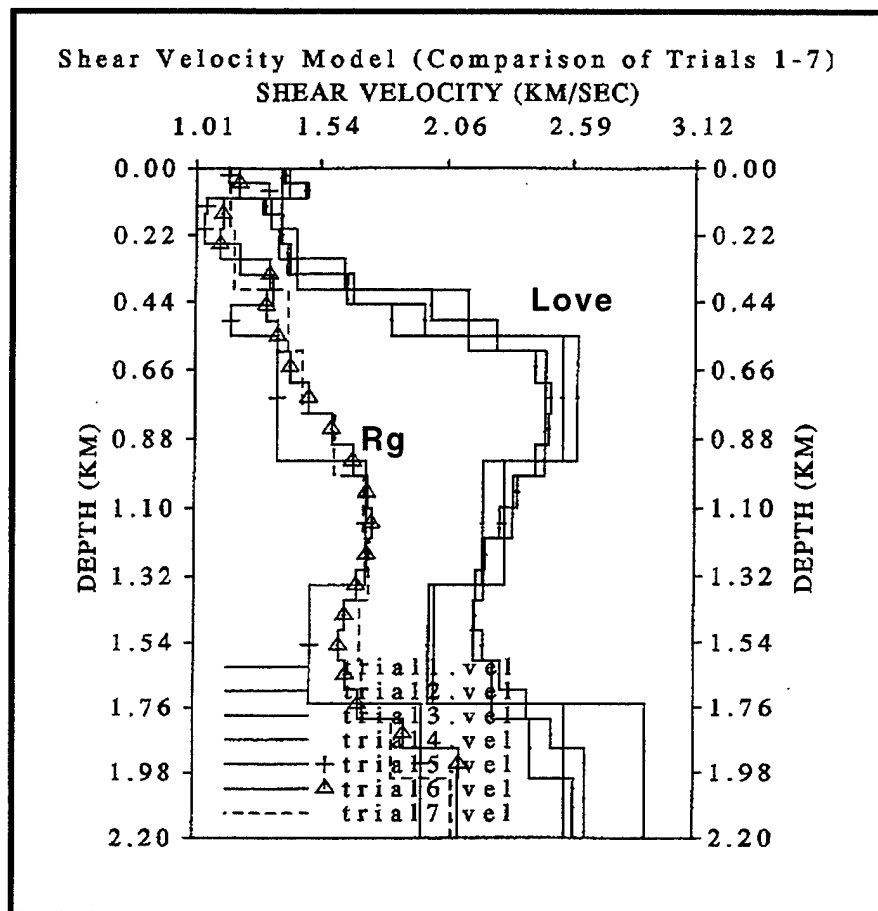


Figure 30. Combined results for all Love and Rayleigh (Rg) wave inversions for this research.

2.6 REFERENCES

- Backus, G.E., and Gilbert, J. F., 1968, The resolving power of gross earth data, *Geophys. J. Roy. Astron. Soc.*, 16, 169.
- Backus, G.E., and Gilbert, J.R., 1970, Uniqueness in the inversion of inaccurate gross Earth data, *Phil. Trans. Roy. Soc., A*, 266, 123.
- Bonner, J., Herrin, E., and Goforth, T., Azimuthal variations of Rg energy from quarry blasts in Central Texas, *Seis. Res. Let.*, 4, 43.
- Craven, M. 1992. Shear wave velocity determination using surface wave dispersion, M.S. Thesis, Southern Methodist University, Dallas, Tx, 215 p.
- Delitsyne, L. Meyer, R., and Burkholder, P., 1996, Generation of shear waves at quarries from near-regional data (abstract), *Seis. Res. Let.*, 67, no. 2, 29.
- Dziewonski, A., Bloch, S., and Landisman, M., 1969, A technique for the analysis of transient seismic signals, *Bull. Seis. Soc. Am.*, 59, 427-444.
- Herrin, E., and Goforth, T., 1977, Phase-matched filters: application to the study of Rayleigh waves, *Bull. Seis. Soc. Am.*, 67, 399-407.
- Herrmann, R.B., 1969, The structure of the Cincinnati arch as determined by short-period Rayleigh waves, *Bull. Seis. Soc. Am.*, 59, 399-407.
- Herrmann, R.B., 1987, Surface wave inversion, Vol IV., *Computer Programs in Seismology*.
- Keilis-Borok, V.I., and Yanoskaya, T.B., 1967, Inverse problems of seismology, *Geophys. J. Roy. Astron. Soc.*, 13, 223.

- Kocaoglu, A., and Long, L., 1993, Tomographic inversion of Rg wave group velocities for regional near-surface structure, *J. Geophys. Res.*, 98., p. 6579-6587.
- Martin, C.A., 1982, *Petroleum Geology of the Fort Worth Basin and Bend Arch Area*, Dallas Geological Society, Dallas, 441 p.
- Panza, G., 1981, Resolving power of seismic surface waves with respect to crust and upper mantle structural models, in Cassinis, R., ed., *The Solution of the Inverse Problem in Geophysical Interpretation*: New York, 381 p.
- Rapaport, L. A and G. C. Grender, 1986, Normalized measures of exploration performance in terms of basin sediment volumes: *Bull. AAPG*, 70 (12), 1777-1786.
- Rinard, B., 1994, *Geophysical study of the Ouachita trend in Central Texas*: M. S. Thesis, Baylor University, Waco, Texas.
- Sherrif, R., and Geldart, L., 1995, *Exploration Seismology*, Cambridge University Press:New York, 592 p.
- Viele, G.W., and Thomas, W.A., 1989, Tectonic synthesis of the Ouachita orogenic belt, in Hatcher, R.D., Jr., Thomas, W.A., and Viele, G.W., eds., *The Appalachian-Ouachita Orogen in the United States*: Boulder, CO, Geological Society of America, *The Geology of North America*, v. F-2, p. 695-727.

3. A PRELIMINARY INVESTIGATION OF THE USE OF ACOUSTIC AND SEISMO-ACOUSTIC OBSERVATIONS TO IDENTIFY VENTED EXPLOSIVE SEISMIC SOURCES

G. G. Sorrells and Eugene Herrin

3.1 INTRODUCTION

Current plans for the verification of a Comprehensive Test Ban Treaty call for the collocation of infrasonic and seismic monitoring systems at future IMS sites. While the collocation strategy has been proposed primarily for logistical purposes it may yield technical benefits, as well. Vented explosions such as quarry blasts, mining shots and other types of industrial explosions can account for a significant fraction of the low magnitude, near regional seismic activity observed in many locations. Consequently, positive identification of these sources could eliminate a large number of events from further consideration as possible underground nuclear explosions. In contrast to earthquakes and fully contained explosions, vented explosions will generate acoustic as well as seismic signals. Therefore, by using data from both the seismic and infrasonic systems at the IMS sites it may be possible to distinguish vented explosions from other seismic source types. The success of this approach will be determined by the capabilities of the available monitoring systems to detect the associated acoustic signal. The pressure amplitudes of these signals are expected to peak at frequencies greater than 1 hertz and to be of the order of a few μ bars or less at near regional distances from the source. Pressure transducers with system noise levels of a few tens of nanobars are commercially available at a reasonable price and have the potential to detect very weak infrasonic signals. However, this potential is rarely realizable without spatial filtering because the wind generated perturbations of the local atmospheric pressure field may be of the order of a few tens of μ bars. Pipe arrays (Daniels, 1951; Grover, 1971) are usually coupled to the pressure transducers to provide the spatial filtering necessary to that partially suppresses the wind generated noise. A well designed pipe array may reduce wind noise by as much as 20-40 db. Nevertheless, a large fraction of the wind noise may still be passed by the pipe array during periods of moderate to high surface wind speeds because the pressure amplitudes of the

wind generated noise tend to scale as the cube of the mean wind speed (Bedard et al, 1992). This latter point is illustrated by the results shown in Figure 31. The data shown in this figure are power spectral density estimates of infrasonic noise observed at the output of a pressure transducer coupled to a conventional short period pipe array. They are representative of calm and windy intervals at the TX01 site in the TXAR seismic array. Notice that despite the use of a pipe array the infrasonic background noise levels increase by as much as 40 db as the local micrometeorological state changes from calm to windy conditions. Thus, there is a clear need to identify and investigate alternative short period infrasonic signal detection systems which may be used to supplement pressure transducer/pipe array systems during adverse wind conditions.

Donn et al (1971) proposed the use of shallow buried short period vertical seismographs to obtain improved acoustic signal to noise ratios relative to those provided by conventional infrasonic monitoring systems during periods of moderate to high surface wind speeds. Their proposal was motivated by the simultaneous observation of infrasonic signals and large acoustically coupled Rayleigh waves following the Apollo 13 and 14 launches at Cape Kennedy and by the fact that wind-generated seismic noise can be strongly attenuated by placing the seismic observation point at moderately shallow depths. Since the observation of acoustically coupled Rayleigh waves will be confined to media whose seismic wave velocities are comparable to the local sound speed (Press and Ewing, 1951), they are not likely to be observed at future IMS sites. However, Sorrells (1971) has shown that infrasonic signals also generate acoustically coupled near field earth movements which are common to all geologic environments. In this document and in future reports the acoustically coupled near field earth motion will be referred to as the "seismo-acoustic" signal. It may be deduced from equation 24 of this reference that for acoustic wavelengths which are much larger than the seismic observation depth but much less than the thickness of the formation containing the observation point, the amplitude of the vertical velocity component of the seismo-acoustic signal should scale linearly with the pressure amplitude of the acoustic wave and that the scaling factor should be proportional to the product of the local sound speed and the formation compressibility. The formation compressibilities at seismically

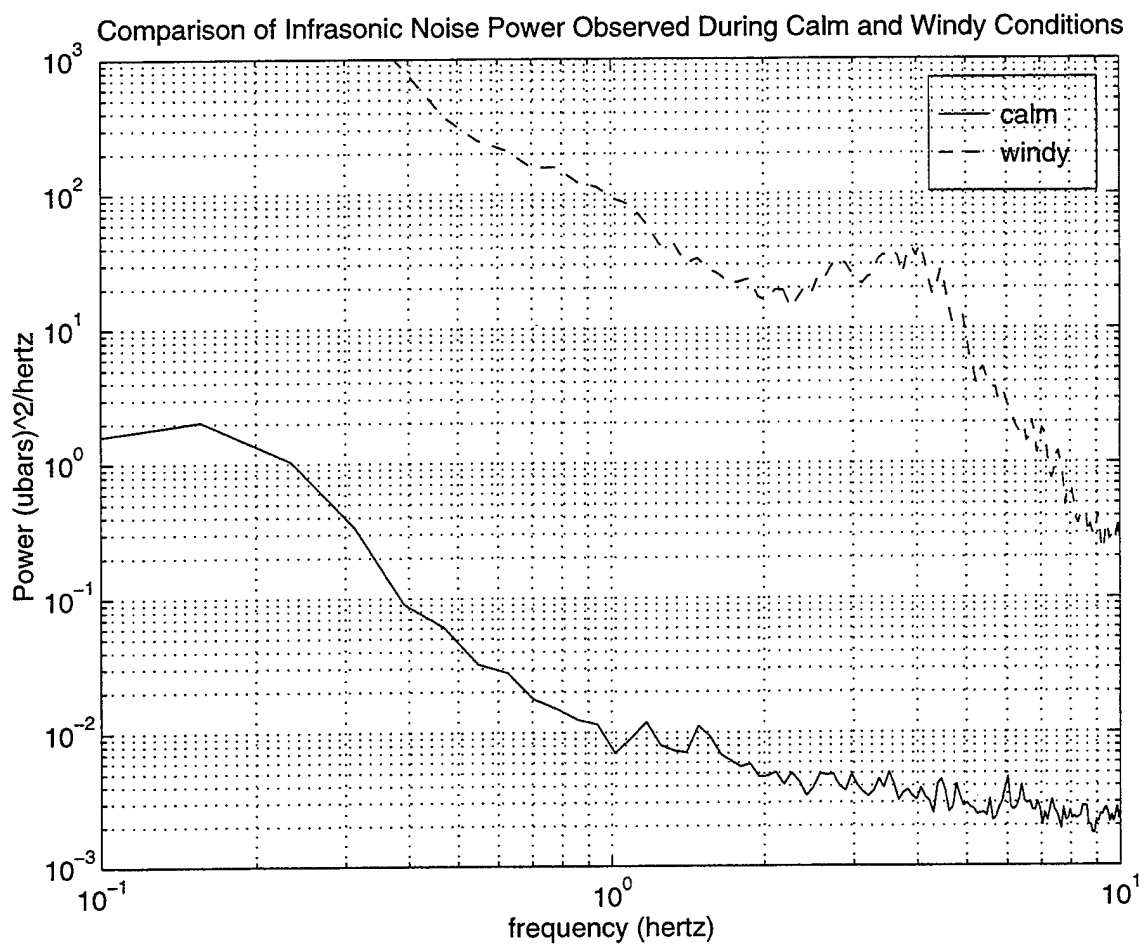


Figure 31. Power spectral density estimates of infrasonic background noise during calm and windy conditions.

"quiet" sites are expected to be of the order of 10^{-11} μ bars while the local sound speed is expected to about 340-350 m/sec. Therefore, an acoustic signal with a one μ bar pressure amplitude is predicted to generate a seismo-acoustic vertical velocity signal with an amplitude of about 3 nm/sec. at these types of sites. It is significant to note that the vertical component of the background noise levels at seismically "quiet" locations is typically of a similar magnitude or less at frequencies greater than about 1 hertz. For example, the rms noise threshold in the 1-4 hertz bandwidth at the TX01 site of the TXAR array during the calm and windy periods referenced above were found to be 1.5 and 2.9 nm/sec, respectively. Thus, on the basis of these arguments it may be inferred that acoustic signals with pressure amplitudes as low as one μ bar at frequencies greater than 1 hertz will generate seismo-acoustic signals that may be detectable at seismically "quiet" sites during both calm and windy local atmospheric conditions. Therefore, it should be possible to use seismo-acoustic observations to supplement infrasonic observations during adverse wind conditions to aid in the detection of short-period acoustic waves at future IMS sites. Studies to investigate this possibility and to evaluate the use of acoustic data to identify near regional vented explosions were initiated in the spring of 1995. The preliminary results of these studies are briefly summarized in the following paragraphs.

3.2 SEISMIC DETECTION OF ACOUSTIC WAVES

3.2.1 Seismo-Acoustic Transfer Functions

Suppose that a vertical seismograph system is located at a depth, z , beneath the surface of the earth. Assume that an infrasonic sensor system is located at the surface directly above the seismic observation point. Let $P(f)$ be the pressure spectrum of a plane acoustic wave referenced to the input of the infrasonic system. Let c be the horizontal phase velocity of the acoustic wave. Let $SA_3(f,z;c)$ be the spectrum of the vertical velocity component of the associated seismo-acoustic signal referenced to the input of the seismic system. It then follows from Sorrells and Goforth (1973) that,

$$SA_3(f,z;c) = \frac{1}{c} T_3(f/c,z) P(f) \quad (1)$$

where T_3 is defined to be the vertical velocity component of the seismo-acoustic transfer function.

3.2.1.1 The "Thompson Hollow" Experiment. A MATLAB code has been written to calculate the seismo-acoustic transfer function for a generic earth model consisting of multiple homogeneous, isotropic, perfectly elastic, horizontal layers. An initial test of the reliability of this model to accurately predict the seismo-acoustic transfer function observed in various geologic environments was undertaken at the "Thompson Hollow" site in central Texas. This site is located 9.75 km. west of the Chemical Lime Quarry in an area characterized by low topographic relief and "layer cake" stratigraphy. Blasts at the quarry typically occur on a semiweekly basis and thus it provides a convenient source of short period acoustic waves. An infrasonic sensor system and a short period vertical seismograph system were temporarily collocated at Thompson Hollow to record the acoustic and seismo-acoustic signals generated by blasts at the nearby quarry. The essential results of this experiment are summarized in Figures 32 and 33. The filtered waveform of an acoustic signal generated by a blast at the quarry is shown in the lower panel of Figure 32. The associated seismo-acoustic waveform is shown in the upper panel. It is important to observe that there is a phase difference of about 90° between the two waveforms. This difference can be fully explained by noting that the output of the seismograph system is proportional to particle velocity, while the output of the infrasonic system is proportional to pressure. It also implies that the "Thompson Hollow" seismo-acoustic response is to a first order, at least, perfectly elastic and that the acoustic pressures are acting on a surface that is approximately horizontal. The shallow seismic velocity structure beneath the site is approximated by the earth model shown in Figure 33a. The modulus of the associated seismo-acoustic transfer function for a zero observation depth and a nominal sound speed of 0.344 km/sec is shown in Figure 33b. The observed values of the transfer function in one octave bandwidths extending from one to eight hertz are also plotted as open circles in this figure. The relatively good agreement between the observed and predicted values of the seismo-acoustic transfer function indicates that a horizontally layered earth model with the properties shown in Figure 33a is a good approximation to the shallow seismic velocity

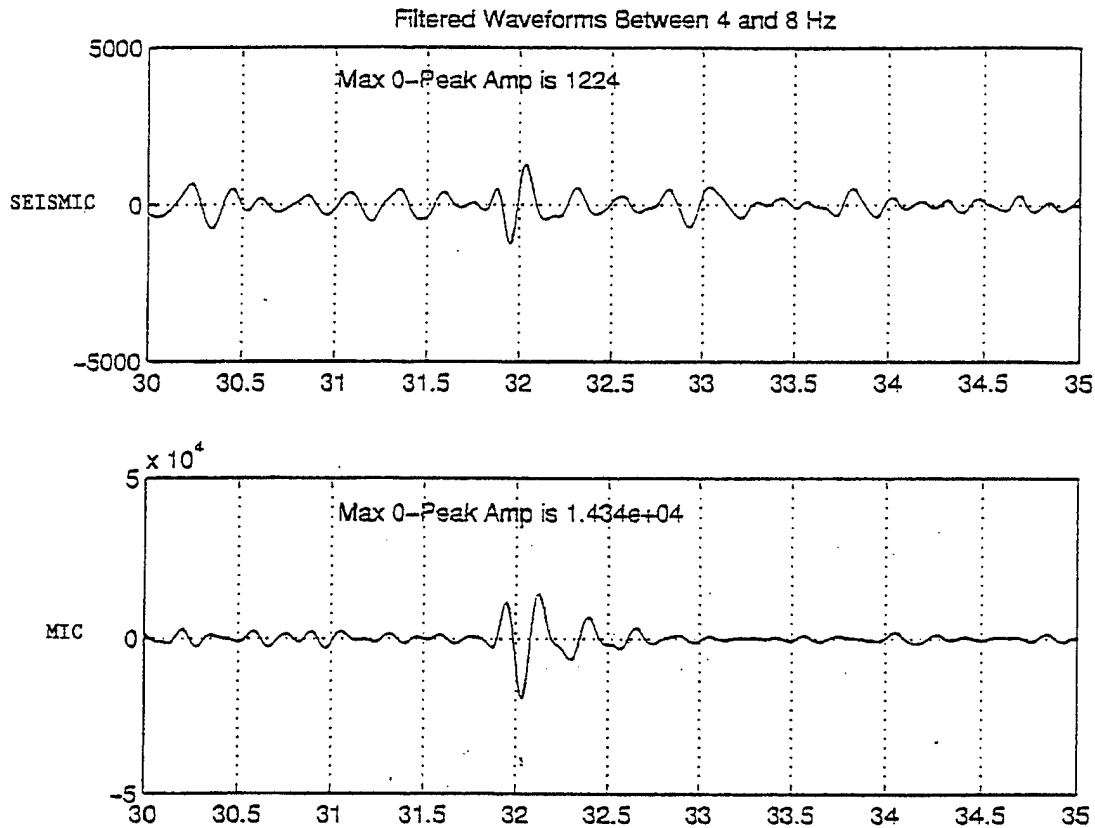


Figure 32. Filtered waveforms between 2 and 4 Hz. The lower panel shows the filtered waveform of an acoustic signal generated by a quarry blast. The upper panel shows the associated seismo-acoustic waveform.

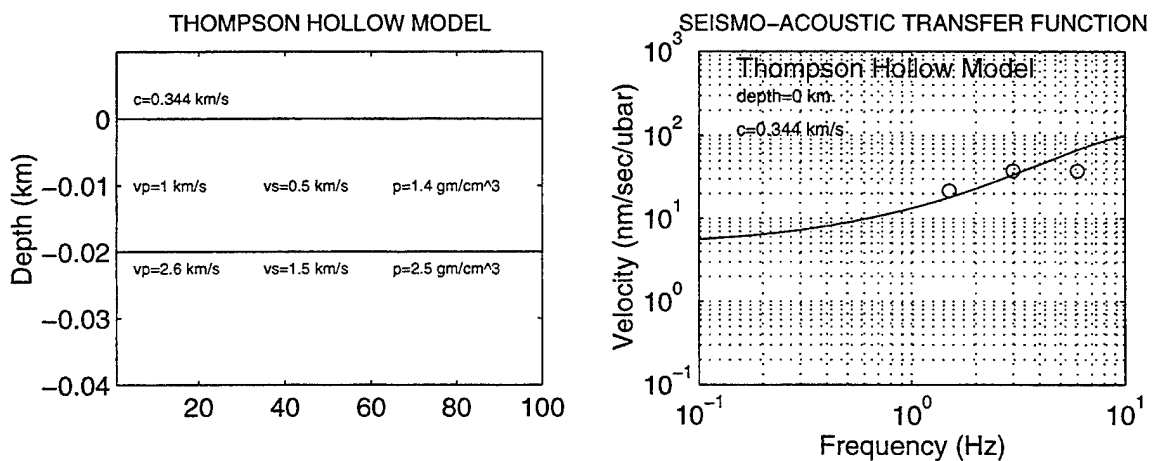


Figure 33. A) Shallow velocity structure model for Thompson Hollow. B) Seismo-acoustic transfer functions.

and density structure beneath the observation point. In summary, the results of the "Thompson Hollow" experiment demonstrated that the existing model can be used with confidence to predict seismo-acoustic transfer functions in areas characterized by low topographic relief and "layer cake" stratigraphy.

3.2.1.2 The TXAR Experiments. In the fall of 1995, a short period infrasonic sensor system was collocated with the TX01 short period vertical seismograph system in the TXAR array. The purpose of this installation was to acquire acoustic data to aid in the confirmation of apparent seismo-acoustic detections that had been previously reported at TXAR. It also provided the opportunity to test the reliability of the existing model to accurately predict the seismo-acoustic transfer function observed in a geologic environment that is significantly different from the "Thompson Hollow" site.

An example of an acoustic signal and its associated seismo-acoustic signal as recorded by the TXAR array is shown in the upper panel of Figure 34. In this figure, the seismic channels are identified by the *sz* prefix while the infrasonic channel is identified by the *aa* prefix. These data were recorded during a period of light surface winds at TXAR. The seismo-acoustic signal is partially obscured by the coda of a prior near regional event but a prominent acoustic signal is observed on the infrasonic channel. The seismic records of the seismo-acoustic signal are time aligned in the lower panel of Figure 39. The time shifts required to achieve this alignment were determined by passing the seismic channels through a matched filter whose impulse response was the time reverse of the acoustic signal then noting the arrival time of the maximum filter output. Analysis of the time shift data indicated that the horizontal phase velocity of the signal is 0.352 km/sec and that its azimuth is 294.°. The beam formed by summing the time aligned seismic channels is shown on the *beam2* channel. Notice that simple beamforming has resulted in a significant improvement in the seismo-acoustic signal to noise ratio. This result is surprising since the TXAR sensor spacing is large compared to acoustic wavelengths at frequencies greater than 1 hertz. It is also important to observe that the beamed seismo-acoustic waveform essentially replicates the acoustic waveform for at least 5 seconds. This result implies the absence of significant acoustic multi-pathing effects over the dimensions of the array.

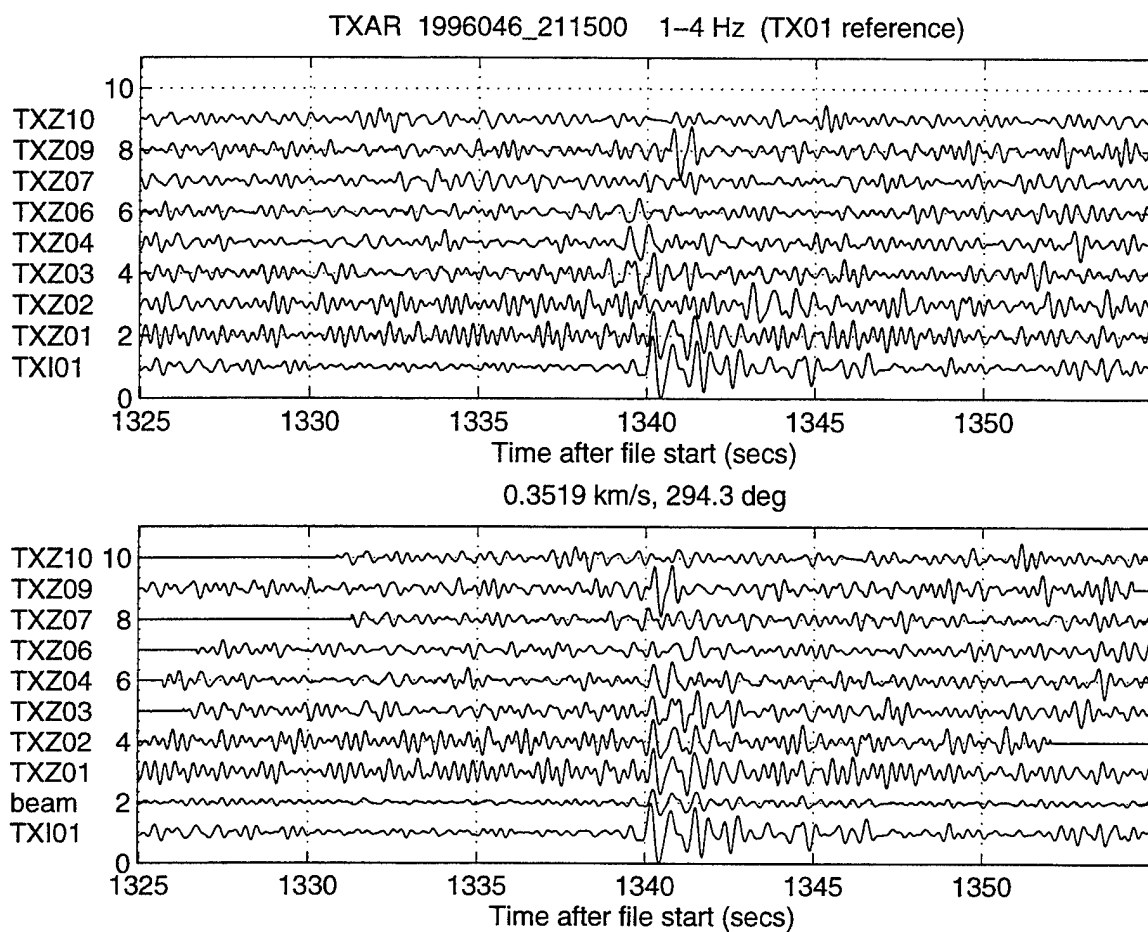


Figure 34. TXAR seismic traces. Upper panel shows acoustic signal (Channel aa01) and the seismo-acoustic signals on the other channels. Lower panel shows the aligned seismic records for the seismo-acoustic signal.

It also indicates that the TXAR seismo-acoustic transfer functions are sensibly constant in the 1-4 hertz band width. As shown in Figure 35, this result is consistent with predictions. The solid curve plotted in this figure is the modulus of the predicted TXAR seismo-acoustic transfer function for a sound speed of 0.352 km/sec and a nominal seismic observation depth of 0.007 km. Notice that at frequencies less than about 10 hertz, it asymptotically approaches a value of about 3 nm/sec/ μ bar. Therefore, at frequencies less than 10 hertz, the seismo-acoustic signal is expected to be a scaled replica of the acoustic signal with a scaling factor of about 3 nm/sec/ μ bar. While the experimental data validates the prediction of a shared common waveform, the experimental results shown in Figure 36 indicates that the model significantly overestimates the observed seismo-acoustic scaling factor. The acoustic and seismo-acoustic waveforms detected in the 1-4 hertz bandwidth at TX01 are shown individually in the upper and middle panels of Figure 37 and are overlain in the lower panel. To facilitate the estimation of the scaling factor, the acoustic signal waveform was filtered to match the nominal response of the short period seismograph system. It can be seen from this comparison that a generous estimate of the observed scale factor is about 0.7 nm/sec/ μ bar or about 10-12 dB less than the predicted value. The model of the shallow TXAR earth structure used for the calculation of the seismo-acoustic transfer function is shown in Figure 38. It is based upon the results of a shallow seismic refraction survey carried out in the immediate vicinity of TX01 and reported by Sandige-Bodoh (1989). In order to account for the discrepancy between the observed and predicted scaling factors the seismic velocities determined by this survey would have to been underestimated by as much as a factor of 2. The occurrence of a systematic error of this magnitude is extremely doubtful. It seems more likely that the discrepancy between the observed and predicted scaling factors indicates the existence of fundamental differences between the elastic properties of shallow TXAR earth structure and those characterizing the generic model currently used for the prediction of seismo-acoustic transfer functions. In this regard, it may be significant to note that the shallow structure at TXAR is characterized by pervasive vertical fracture sets that are dry to depths on the order of 1000 feet. This phenomenon may result in an anisotropic elastic response to surface applied pressure changes which is not accounted for by the existing model. Nevertheless, the results of the TXAR experiments have

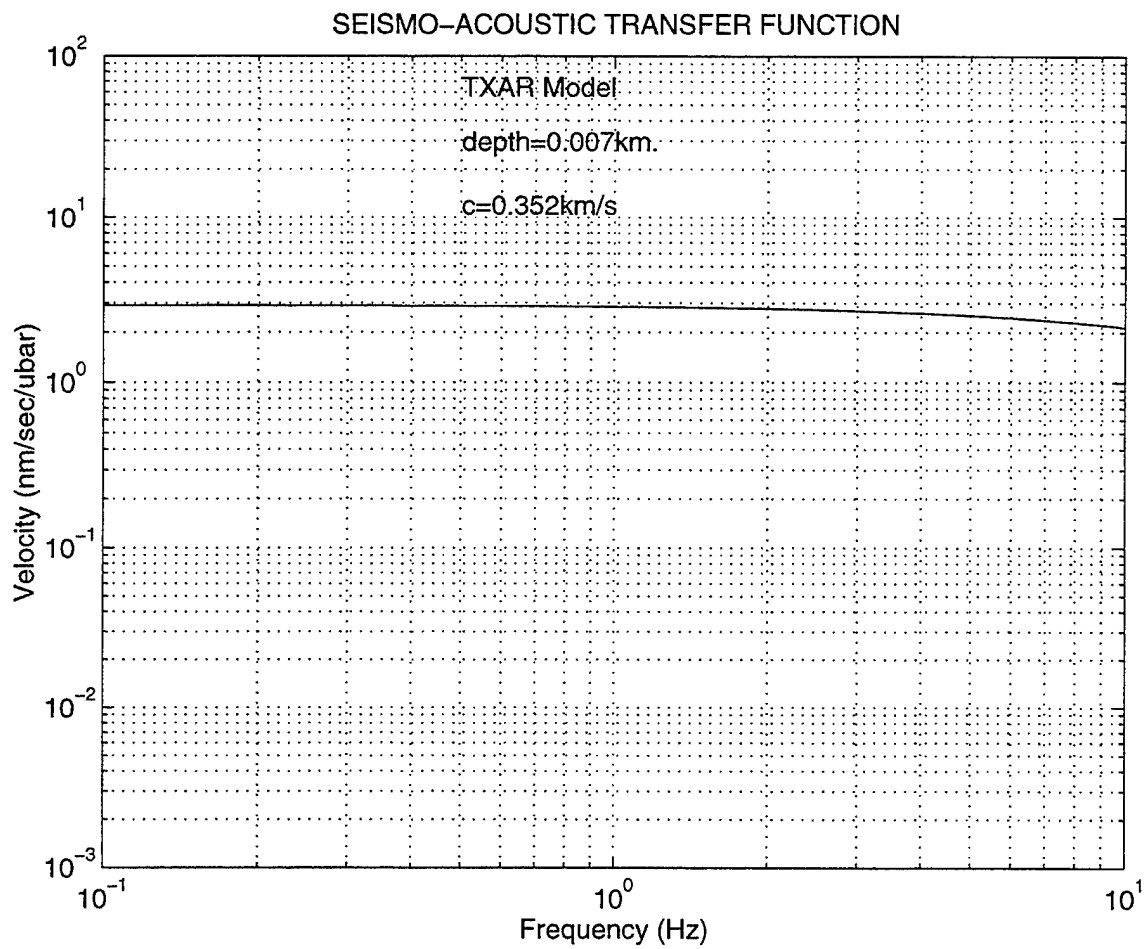


Figure 35. Seismo-acoustic transfer functions for TXAR model.

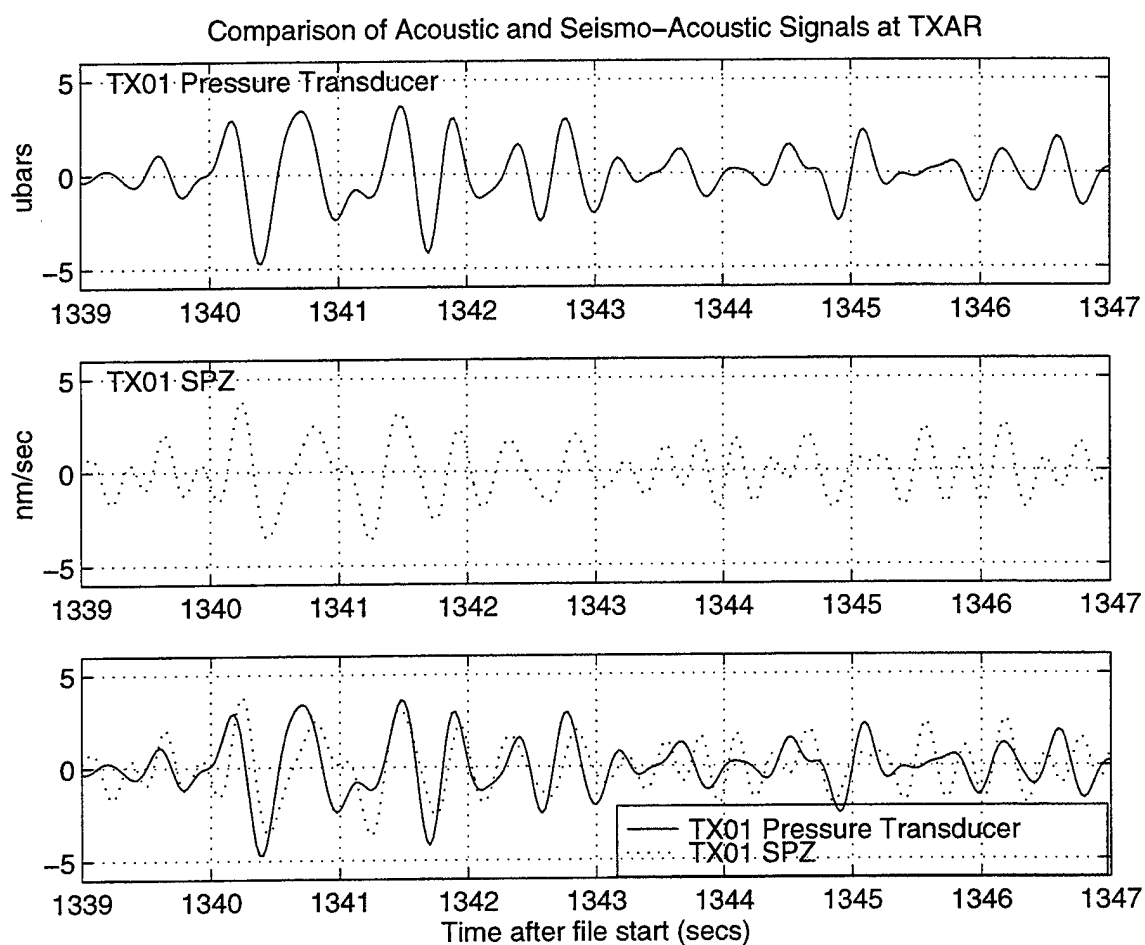


Figure 36. Comparison of acoustic and seismo-acoustic signals at TXAR. The acoustic and seismo-acoustic signals are shown individually in the upper and middle panels. The two signals are overlain in the lower panel.

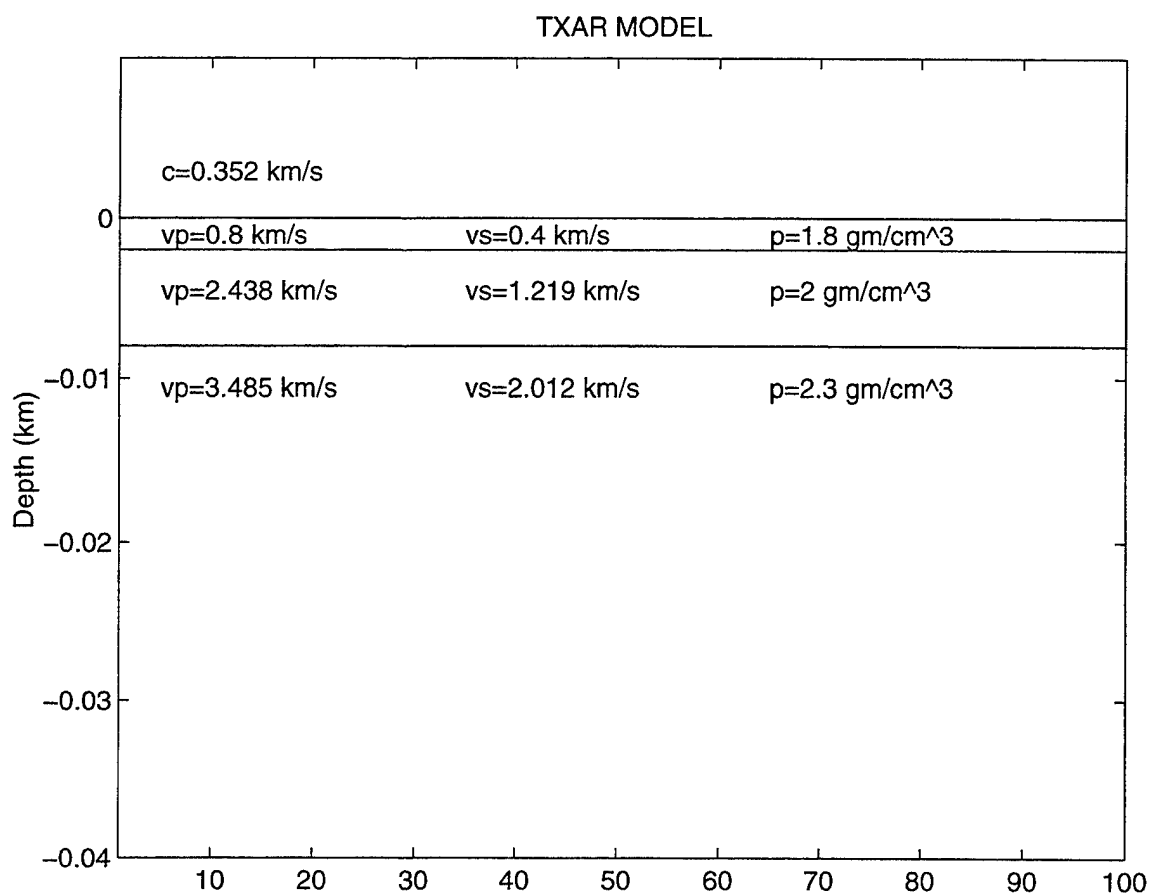


Figure 37. Model of shallow earth structure at TXAR.

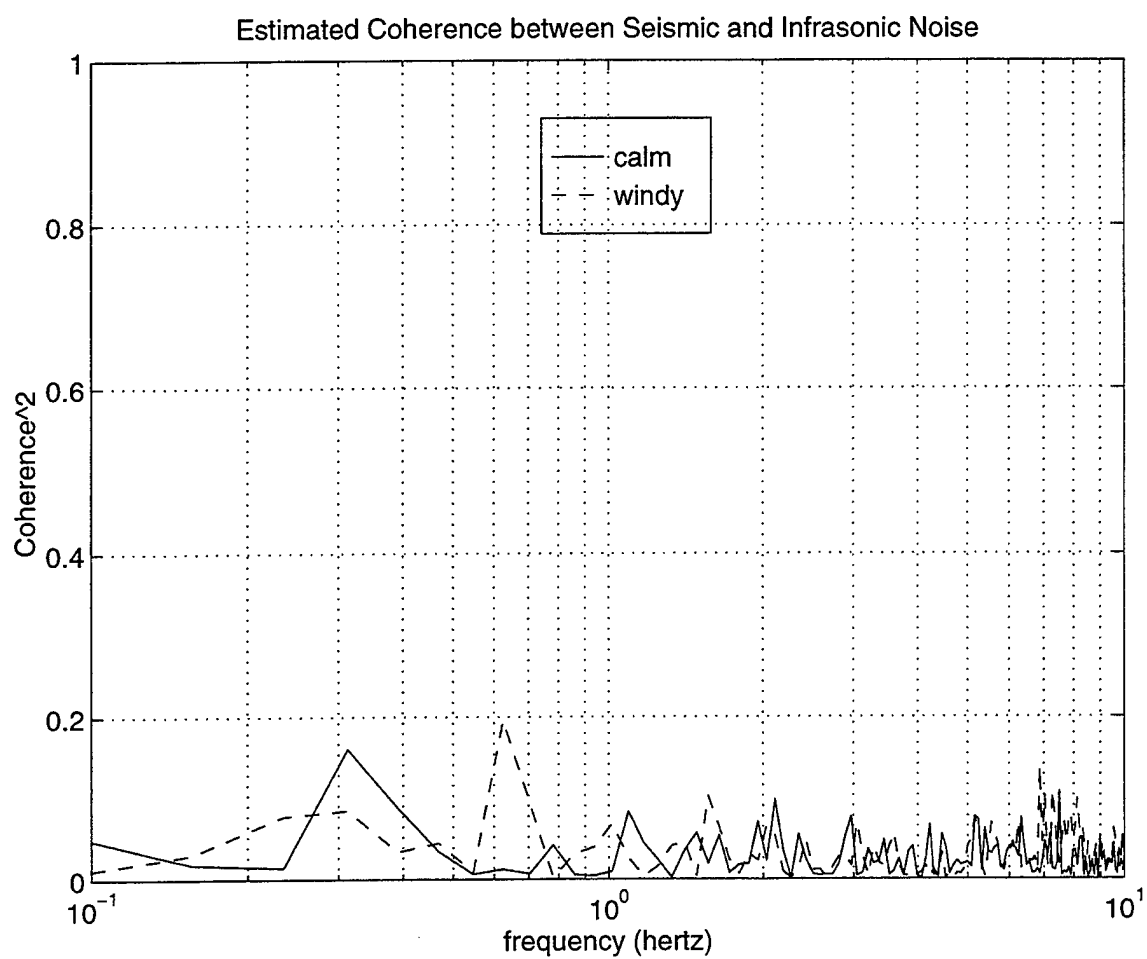


Figure 38. Estimated coherence between infrasonic and seismic data during calm and windy periods.

thus far demonstrated that acoustic signals with amplitudes of a few μ bars at frequencies greater than 1 hertz generate seismo-acoustic signals that are detectable at a "quiet" seismic site despite the discrepancy between observed and predicted scaling factors.

3.2.2 Seismo-Acoustic Correlation Detection of Short Period Acoustic Signals at TXAR

The results presented in the previous section demonstrate that short period acoustic and seismo-acoustic signals share a common waveform at TXAR. Furthermore, as indicated by the coherence estimates shown in Figure 38, short period seismic and infrasonic noise at frequencies greater than 1 hertz may be considered to be statistically independent processes under both calm and windy atmospheric conditions. Therefore, a running estimate of the normalized correlation coefficient for simultaneously acquired seismic and infrasonic data sets from collocated sensors should provide a simple and effective method for the detection of short period acoustic signals at TXAR.

A MATLAB code has been written to estimate the normalized correlation coefficient between two input data records. In its current configuration, the code accepts records of selectable lengths from the outputs of the collocated TX01 short-period vertical seismograph and pressure transducer. The records are filtered to account for differences in nominal sensor system responses and to pass data in the 2-8 hertz bandwidth. Estimates of the normalized correlation coefficient are currently made in a 5 second window which is sequentially shifted forward in one second intervals. The output of the code is a time series whose amplitudes are found in the interval [-1,1] and whose sample points are separated by 1 second in input record time. The values of this time series are expected to cluster near zero when both data records contain noise only and to be greater than zero when the records contain acoustic and seismo-acoustic signals plus noise. This configuration has been tested by using pairs of synthetically generated, statistically independent, normally distributed data records. The objective of the test was to estimate "false alarm" probability distribution characterizing this particular correlator code configuration. The histogram showing the frequency of occurrence distribution for the synthetic sample correlation coefficients is shown in

Figure 45a. Notice that the sample population is normally distributed with a near zero mean and a standard deviation of 0.112. An identical test was performed on real data acquired during intervals that were free of visible seismic signals. The resulting histogram showing the frequency of occurrence distribution for the real sample correlation coefficients is shown in Figure 39b. Observe that this sample population appears to be normally distributed with a slightly positive mean. It should also be noted that the standard deviation of the sample population drawn from the real data sets is somewhat larger than the standard deviation characterizing the synthetic population. These differences are believed to indicate that naturally occurring acoustic events make a minor but statistically significant contribution to the seismic and acoustic data recorded in the 2-8 hertz passband at TXAR.

3.2.3 Seismo-Acoustic Identification of Vented Near Regional Explosions

It was argued in the introduction to this text that the detection of an acoustic signal and its association with a prior seismic event unambiguously identifies the source of both as a vented explosion. A preliminary test was undertaken to determine if this approach could be successfully applied to the identification of vented explosions in a limited sample of the population of near regional seismic events detected at TXAR. The test was conducted during a 7 week interval extending from 7 November 1995 to 10 January 1996. During this time period, 25 work-day records of the seismic data acquired at TXAR during local daylight hours (1300-2300 GMT) were reviewed to identify the arrival times of all potentially locatable near regional seismic events. The seismo-acoustic correlator code, operating in the configuration referenced above, was used to detect acoustic events. It was applied to the outputs of the collocated seismic and infrasonic sensors at TX01 in a 45 minute time period which included the arrival time of the seismic event plus at least 25 minutes for each identified event. The correlator code detection threshold was set at 0.3. Based upon the test results identified in the previous section, the corresponding probability of a false alarm is expected to be less than 0.005. If the correlator code output was found to be equal to or in excess of 0.3 at any time in a 20 minute window starting 5 minutes after the p arrival time, a possible associated acoustic event detection was declared and the seismic array

data was analyzed to estimate the distance and azimuth to the epicenter of the seismic event and its approximate origin time. The apparent group velocity of each acoustic event detection, referenced to the epicenter and origin time of the seismic event was then determined. If the apparent group velocity of any one of the acoustic event detections was found to lie in the interval from 0.27 km/sec to 0.33 km/sec it was assumed to be associated with the seismic event and thus identifies the source of both as a probable vented explosion. During the 25 day test period the sources of 21 near regional seismic events were identified as probable vented explosions by the application of the procedures outlined above. A histogram of the occurrence times of these events is shown in Figure 40. Notice that their occurrence times tightly cluster near 1800 and 2100 hours (noon and 3 PM, local time). This observation strongly implies that the events are the result of industrial processes and is consistent with the identification of their sources as vented explosions. The approximate locations of their estimated epicenters are shown in Figure 41. These locations were derived from azimuth and distance estimates calculated from the array data for each event. The azimuth from TXAR to the epicenters were estimated from the P arrival time data. The following equation was used to estimate the approximate epicentral distance

$$D(\text{km})=6.22(dT + 6.5) \quad (2)$$

where dT is the observed difference in the p and Lg arrival times. This equation has been found to yield reliable estimates of distances to the known epicenters of selected near regional events north and northwest of TXAR. The hachured area in Figure 41 identifies a coal mining district in northern Mexico which is thought to be a likely source of the majority of near regional events located east southeast of TXAR. If it is, then the epicentral data indicate that equation 2 significantly overestimates epicentral distances for near regional sources east of the array. In this regard, it was also found that the acoustic arrivals detected by the correlator code were systematically early when referenced to the estimated epicenters east and south of the array. Thus, pending the results of calibration studies now underway at TXAR, it is tentatively concluded that:

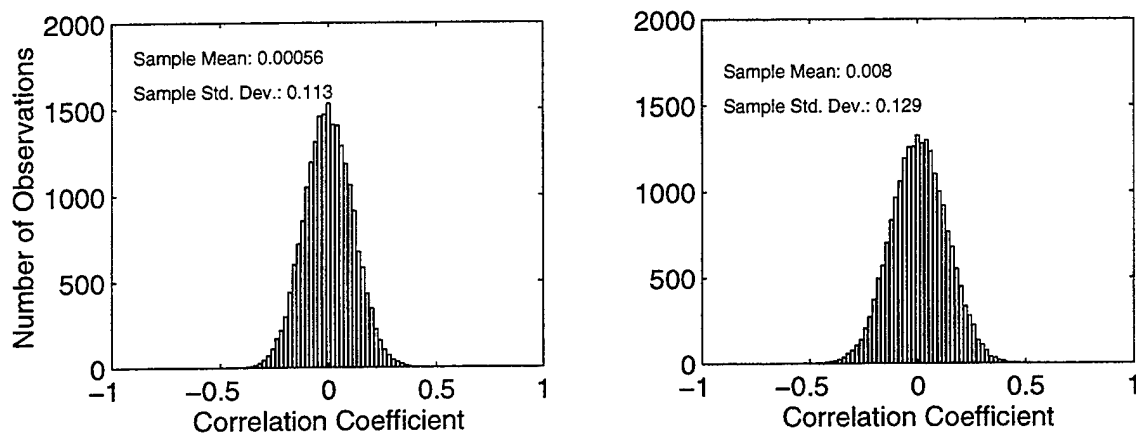


Figure 39. A) Correlation code test results with synthetic data. B) Correlation code tests results with real data.

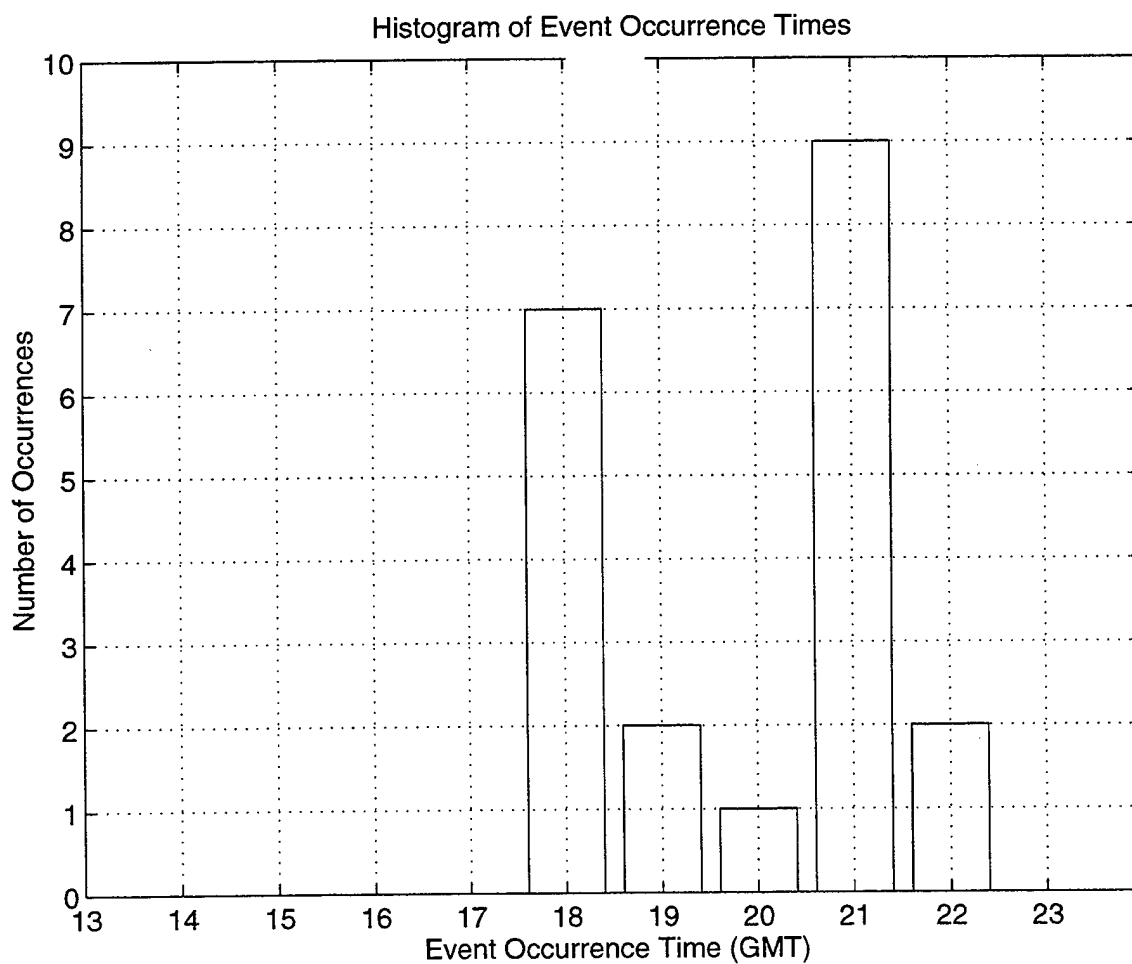


Figure 40. Histogram of occurrence times of seismic events.

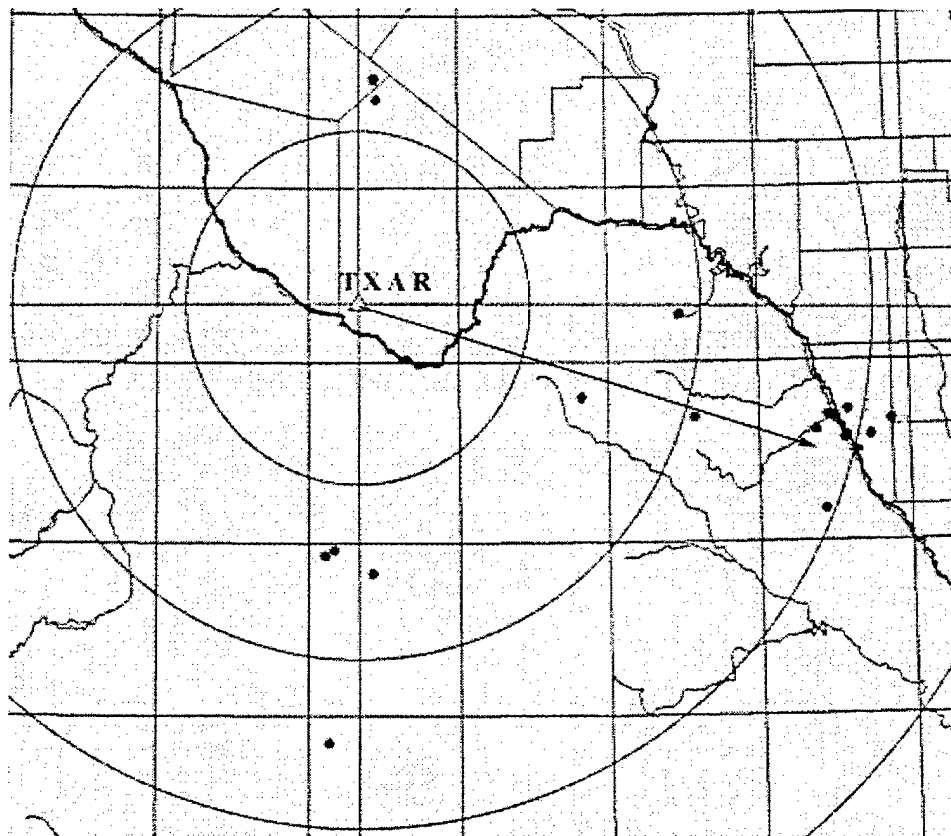


Figure 41. Location map of acoustical events recorded at TXAR.

1. At least some of the events identified as vented explosions during this test were generated in the northern Mexico coal mining district identified in Figure 41 and,
2. The use of the correlator code provides a simple but effective method for the detection of the relatively weak acoustic signals generated by near regional vented explosions.

3.3 SUMMARY AND CONCLUSIONS

The results presented above demonstrate that short period acoustic signals with pressure amplitudes of a few μ bars or less will generate seismo-acoustic signals that are detectable at a seismically "quiet" site. This observation implies that they will also be detectable at future IMS sites which are most likely to be located in quiet seismic environments. While the short period acoustic SNR will be higher at the outputs of the infrasonic monitoring system during periods of calm to light surface winds, it may be inferred from the results shown in Figures 36 and 39 that the seismo-acoustic SNR will be higher during periods of moderate to high surface winds. The results shown in Figure 39 also indicate that seismic beamforming may significantly enhance seismo-acoustic SNR's despite the fact that the seismic array is not optimally configured for short period acoustic observations. This result is attributed to the fact that unlike seismic signals, seismo-acoustic signals are not significantly affected by multi-pathing and remain spatially stable over the characteristic dimensions of a typical IMS seismic array. Thus, it may be inferred that the seismic monitoring systems installed at future IMS sites may be used as a backup infrasonic system during those periods when local atmospheric turbulence impairs the detection capability of the primary acoustic monitoring system.

The preliminary results of this study also demonstrate that the calculation of a running estimate of the normalized correlation coefficient between the outputs of colocated seismic and infrasonic sensors provides a simple but effective method for the detection of weak short period acoustic waves. The success of this approach at TXAR is attributed to the fact that while short period acoustic and seismo-acoustic signals share a common waveform, short period seismic and infrasonic noise are, for all practical purposes, statistically

uncorrelated under both calm and windy atmospheric conditions. Statistically uncorrelated short period seismic and infrasonic noise is expected to be a property of all "hard rock" geologic environments including those which are likely to be the sites of future IMS installations. However, while acoustic and seismo-acoustic signals are always linearly related, they will share a common waveform only in those environments where the seismic velocities of the formation containing the seismic observation point are uniform over a depth range that is large compared to the wavelengths of the acoustic signals. In other environments, it will be necessary to determine the frequency response characteristics of the seismo-acoustic transfer function in order to optimize the performance of the correlator code. In this regard, it has been shown that the existing model for the prediction of seismo-acoustic transfer functions suffered from serious defects when it was tested at TXAR. Until the discrepancies between the observed and predicted values of the seismo-acoustic scaling factors at TXAR can be explained, experimental measurements should be used to determine the frequency response characteristics of local seismo-acoustic transfer functions.

Finally, the results of this study infer that the detection of a short period acoustic signal and its association with an antecedent near regional seismic event is a promising method for the identification of vented explosive sources. If further research confirms this premise then it follows that the data that will be provided by the collocated seismic and infrasonic monitoring systems at future IMS sites may be used to significant advantage to eliminate the seismic signals generated by vented explosions from further consideration as possible indicators of a clandestine underground nuclear explosion.

3.4 ACKNOWLEDGMENTS

The authors would like to acknowledge the contributions of Jack Swanson who provided much of the data processing results summarized in this paper and who first demonstrated the advantages of seismo-acoustic beam forming. In addition, the experimental results presented in this paper are the result of detailed field work and could not have been acquired without the careful efforts of Paul Golden, Karl Thomason and Chris Hayward.

3.5 REFERENCES

- Bedard, A.J., R.W. Whittaker, G.E. Greene, P. Mutschlecner, R.T. Nishiyama, and M. Davidson (1992) Measurements of pressure fluctuations near the surface of the earth, Tenth Symposium on Turbulence and Diffusion 29Sept-2Oct 1992, Portland OR, *Am. Meteor. Soc.* 293-296
- Daniels, F. B. (1959) Noise reducing line microphone for frequencies below 1c/s. *Jour. acoust. soc. Am*, **31**, 529.
- Donn, W. L., I. Dalins, V. McCarty, M. Ewing and G. Kashak (1971) Air coupled seismic waves at long range from Apollo launchings. *Geophys. Jour. R. Astron. Soc.*, **26**, 161-171.
- Grover, F. H. (1971) Experimental noise reducers for an active microbarograph array. *Geophys. Jour. R. Astron. Soc.*, **26**, 41-52.
- Press, F. and M. Ewing (1951) Ground roll coupling to atmospheric compressional waves. *Geophysics* **16** 416-430.
- Sandige-Bodah, Victoria (1989) investigating the effect fractures have on seismic wave velocities at Lajitas, Texas, seismic station: Report No. GL-TR-89-0153, Geophysics Laboratory, USAF Systems Command, Hanscom AFB, MA 01731-5117, ADA215943..
- Sorrells, Gordon G. (1971) A preliminary investigation into the relationship between long-period noise and local fluctuations in the atmospheric pressure field, *Geophys. Jour. R. Astron. Soc.*, **26**, 71-82.
- Sorrells, G. G. and T. T. Goforth (1973) Low-frequency earth motion generated by slowly propagating partially organized pressure fields, *Bull. Seis. Soc. Am.*, **63**, 1583-1601.

4. ACKNOWLEDGEMENTS

Personnel contributing to this contract are: (1) Dr. Eugene Herrin, Principal Investigator, (2) Paul Golden, Director of Geophysical Laboratory, (3) Karl Thomason, Chief Engineer, (4) Nancy Cunningham, Director - Computer Laboratory, (5) David Anderson, Systems Analyst, (6) Dyann Anderson Slosar, Administration, (7) Herbert Robertson, Subcontractor, (8) Jack Swanson, Consultant, and (9) Dr. Gordon G. Sorrells, Subcontractor. Ph. D. students include: (1) Chris Hayward, (2) Relu Burlacu, (3) Zenglin Cui, (4) Jessie Bonner, and (5) Ileana Tibuleac.

4.1 PREVIOUS CONTRACTS AND PUBLICATIONS

4.1.1 Previous Contracts and Reports

4.1.1.1. ARPA Contract # MDA 972-88-K-0001

Development of an Intelligent Seismic Facility and Preparation for Participation in the Conference on Disarmament Group of Scientific Experts Technical Tests (GSETT).

Quarterly R&D Status Report, 1 Nov. 1988 through 31 Jan 1989.

Quarterly R&D Status Report, 1 Feb. through 30 Apr. 1989.

Quarterly R&D Status Report, 1 May through 31 July 1989.

Quarterly R&D Status Report, 1 Aug. through 31 Oct. 1989.

Quarterly R&D Status Report, 1 Nov. 1989 through 31 Jan. 1990.

Quarterly R&D Status Report, 1 Feb. through 30 Apr. 1990.

Quarterly R&D Status Report, 1 May through 31 July 1990.

Quarterly R&D Status Report, 1 Aug. through 31 Oct. 1990: 88-K-12.

Quarterly R&D Status Report, 1 Nov. 1990 through 31 Jan. 1991.

Quarterly R&D Status Report, 1 Feb through 30 April 1991.

Quarterly R & D Status Report, 1 May through 31 July 1991.

Quarterly R & D Status Report, 1 August through 31 October 1991.

Quarterly R & D Status Report, 1 October 1991 thru 31 January 1992.

Quarterly R & D Status Report, 31 January through 30 April 1992.

Quarterly R & D Status Report, 30 April through 31 July 1992.

Quarterly R & D Status Report, 31 July through 31 October 1992.

Semiannual Report, January 1991, SMU-R-89-226.

Semiannual Report, October 1991; SMU-R-91-252

Semiannual Report, December 1991; SMU-R-91-301

Semiannual Report, January 1992; SMU-R-92-337

Semiannual Report, November 1989; SMU-R-91-121

Semiannual Report, January 1992; SMU-R-92-373

Semiannual Report, August 1992; SMU-R-92-396

Final Report, December 1992; SMU-92-425.

4.1.1.2 ARPA Contract # MDA 972-89-C-0054

Complete and Deploy the GERESS Seismic Array in Southeast Germany, Establish Workstations Which Accept the Array Data at Bochum and at NORSAR, and Provide the Interface to the Intelligent Array System at NORSAR.

Quarterly R&D Status Report, 4 Jan. to 15 Apr. 1989.

Quarterly R&D Status Report, 15 Apr. to 15 July 1989.

Quarterly R&D Status Report, 15 July to 15 Oct. 1989.

Quarterly R&D Status Report, 15 Oct. 1989 to 15 Jan. 1990.

Quarterly R&D Status Report, 15 Jan. to 15 Apr. 1990.

Quarterly R&D Status Report, 15 Apr. to 15 July 1990.

Quarterly R&D Status Report, 15 July to 15 Oct. 1990.

Quarterly R&D Status Report, 15 Oct. 1990 to 15 Jan. 1991.

Quarterly R&D Status Report, 15 Jan. to 15 April 1991.

Quarterly R & D Status Report, 15 April to 15 July 1991.

Quarterly R & D Status Report, 15 July to 15 October 1991.

Quarterly R & D Status Report, 15 October 1991 to 15 January 1992.

Quarterly R & D Status Report, 15 January to 15 April 1992.

Quarterly R & D Status Report, 15 April to 15 July 1992.

Quarterly R & D Status Report, 15 July to 15 October 1992.

Quarterly R & D Status Report, 15 October 1992 to 15 January 1993.

Quarterly Technical Report, 4 January to 15 Apr. 1989..

Quarterly Technical Report, 15 Apr. to 15 July 1989..

Quarterly Technical Report, 15 July to 15 October 1989.

Quarterly Technical Report, 15 October 1989 to 15 Jan. 1990.

Quarterly Technical Report, 15 Jan. to 15 April 1990.

Quarterly Technical Report, 15 April to 15 July. 1990.

Quarterly Technical Report, 15 July to 15 October 1990.

Quarterly Technical Report, 15 October 1990 to 15 Jan. 1991.

Quarterly Technical Report, 15 Jan. to 15 April 1991.

Quarterly Technical Report, 15 April to 15 July 1991.

Quarterly Technical Report, 15 October 1991 to 15 January 1992.

Quarterly Technical Report, 15 January to 15 April 1992.

Quarterly Technical Report, 15 April to 15 July 1992.

Quarterly Technical Report, 15 July to 15 October 1992.

4.1.1.3 Contract # 19628-93-C-0057

Design, Evaluation, and Construction of TEXESS and LUXESS, and Research in Mini-Array Technology and Use of Data from Single Stations and Sparse Networks

Quarterly R & D Status Report, 30 April to 31 July 1993.

Quarterly R & D Status Report, 31 July to 31 October 1993.

Quarterly R & D Status Report, 31 October 1993 to 31 Januaryy 1994.

Quarterly R & D Status Report, 31 January to 30 April 1994.

Quarterly R & D Status Report, 30 April to 31 July 1994.

Quarterly R & D Status Report, 31 July to 31 October 1994.

Quarterly R & D Status Report, 31 October 1994 to 31 Januaryy 1995.

Quarterly R & D Status Report, 31 January to 30 April 1995.

Quarterly R & D Status Report, 30 April to 31 July 1995.

Quarterly R & D Status Report, 31 July to 31 October 1995.

Quarterly R & D Status Report, 31 October 1995 to 31 January 1996.

Scientific Report No. 1, October 1993, PL-TR-94-2106, ADA284580.

Scientific Report No. 2, April 1994, PL-TR-94-2258, ADA292546.

Scientific Report No. 3, October 1994, PL-TR-95-2023, ADA295787.

Scientific Report No. 4, April 1995, PL-TR-95-2091, ADA305417.

Scientific Report No. 5, October 1995, PL-TR-96-2022, ADA306407.

4.1.2 Publications

4.1.2.1 Special Reports, Papers, and Posters

- Arnett, Dick, 1992, German Experimental Seismic System (GERESS): Pamphlet, GERESS Symposium on Regional Seismic Arrays, 22-24 June 1992, Waldkirchen, Bavaria, Federal Republic of Germany.
- Bonner, Jessie, Eugene Herrin and Tom Goforth, 1995, Azimuthal variations in Rg energy in Central Texas: Appendix A, Scientific Report No. 5, 13-40, ARPA Contract # MDA 972-89-C-0054
- Golden, Paul, Eugene Herrin, and Wilbur Rinehart, 1991, The use of LTX data in preparing and compiling the final event bulletins: SMU-R-91-278, Contract # MDA 972-88-K-001
- Golden, Paul, 1992, Unconventional processing and visualization techniques: GERESS Symposium on Regional Seismic Arrays, 22-24 June 1992, Waldkirchen, Bavaria, Federal Republic of Germany.
- Herrin, Eugene, Chris Hayward, and Eugene Smart, 1991, Comparison of the Murdock and optimum seismic signal detectors: Appendix 3, SMU-R-90-121, 54-67.
- Herrin, Eugene, 1992, Construction of the GERESS array: GERESS Symposium on Regional Seismic Arrays, 22-24 June 1992, Waldkirchen, Bavaria, Federal Republic of Germany.
- Herrin, Eugene and Paul Golden, 1993, Design, evaluation and construction of two nine element experimental arrays TEXESS and LUXESS: Proceedings, 15 Annual Seismic Research Symposium 8-10 September 1993, Vail, Colorado, Sponsored by Phillips Laboratory, AFOSR & ARPA, PL-TR-93-2160, ADA271458.
- Herrin, Eugene, Paul Golden, Karl Thomason, and Chris Hayward, 1993, Seismic array technology: Poster.
- Herrin, Eugene, 1994a, Installation of posthole 54000 seismometer, Appendix 5, Scientific Report No. 2, 59-60, ARPA Contract # MDA 972-89-C-0054.

- Herrin, Eugene, 1994b, Dealing with outliers and possible evasion scenarios: Appendic A, Scientific Report No. 3, 19-35, ARPA Contract # MDA 972-89-C-0054.
- Herrin, Eugene, Paul Golden and J. Theodore Cherry, 1994, The ARPA Model 94 regional array concept: Scientific Report No. 3, 36-43, ARPA Contract # MDA 972-89-C-0054.
- Herrin, Eugene, *et al.*, 1994, Research in regional event discrimination using Ms:mb and autoregressive modeling of Lg waves: Proceedings, 16 Annual Seismic Research Symposium, 7-9 September 1994, Thornwood, New York, Sponsored by Phillips Laboratory, AFOSR, PL-TR-94-2217, ADA284667.
- Herrin, Eugene, *et al.*, 1995, Seismo-acoustic synergy: Appendix B, Scientific Report No. 5, 41-71, ARPA Contract # MDA 972-89-C-0054.
- Herrin, Eugene, G. G. Sorrells, *et al.*, 1996, Seismo-acoustic studies at TXAR: Proceedings, 18 Annual Seismic Research Symposium, Poster #39, 4-6 September 1996, Annapolis, MD, Sponsored by Phillips Laboratory, AFOSR, and AFTAC, PL-TR-96-2153, ADA313692
- Sorrells, G. G. and Eugene Herrin, 1995, Seismic detection of acoustical waves: Appendix B, Scientific Report No. 4, 33-42, ARPA Contract # MDA 972-89-C-0054.
- Sorrells, G. G., 1995, Seismo-acoustic methods for the detection of acoustic waves: Appendix C, Scientific Report No. 5, 72-86, ARPA Contract # MDA 972-89-C-0054.
- Tibuleac, Ileana and Eugene Herrin, 1996, Calibration studies at TXAR: Scientific Report No. 1, PL-TR-96-2249.

4.1.2.2 Publications

Herrin, Eugene T. and Vigdor L. Teplitz, 1996, Seismic detection of nuclearites: *Physical Review D*, 53 (12), 6762-6770.

APPENDIX 1. PRELIMINARY REPORT:

CHARACTERISTICS OF THE BROADBAND ACOUSTICAL SENSORS INSTALLED IN THE SMU LAJITAS GSE PROTOTYPE ARRAY

Seismo-acoustic studies at TXAR are discussed in Section 1 of this report. Appendix 1 is a report by Chris Hayward describing the characteristics of the acoustical sensors that were installed at TXAR.

Preliminary Report:

Characteristics of the Broadband Acoustic Sensors Installed in the SMU Lajitas GSE prototype array

Chris Hayward
Southern Methodist University

INTRODUCTION

The GSE Infrasound Expert Group¹ has recommended the installation of 60 infrasound arrays as part of the planned UN CTBT monitoring system (GSE Infrasound Experts, 1995). The infrasound system will be used to supplement other monitoring technologies to detect a 1 kiloton atmospheric explosion at distances of 2000 to 2500 km. In their report, the Group recommended studies to develop a "more detailed specification of the instrument parameters, including temperature variations, length of the noise reducing hoses, element spacing, and similar technical details." They also stated:

It would be extremely useful to begin to deploy a small number of stations in the near future, so that we could begin to gain experience with deploying and operating this type of system.

Accordingly, SMU began tests of an experimental infrasonic system at the Lajitas, Texas seismic array (TXAR) on 6-Feb-1996 recording a simple laboratory microphone connected to a pipe array of porous hoses. Results were disappointing. The microphone response (5 Hz low frequency corner) limited low frequency signals and the required power supply and signal conditioning introduced noise into both acoustic and seismic channels.

Previous work (Stachura, Siskind, and Engler, 1981) in recording quarry blast acoustic signatures near the source used a sensor based on a Validyne low pressure differential recording gauge. Rienke (1985) used a slightly different model, added a backing volume and bleed valve and then verified the calibration and response using the method of Hunt and Schomer (1979). The results reported in these documents and conversations with workers in the field suggested that a reconfigured Validyne gauge had the potential to successfully measure weak infrasonic signals in the GSE bandwidth.

Exploratory laboratory experiments were undertaken to evaluate this potential. These experiments included estimation of the self noise and response characteristics of field configured Validyne gauges as well as a preliminary investigation of the spatial response characteristics of selected porous hoses. A brief description of the Validyne gauge as configured for the TXAR field tests is found in Appendix 1. The principal results of the exploratory laboratory experiments are summarized in the following pages.

¹ Infrasound Expert Group to the Ad Hoc Committee on a Nuclear Test Ban Working Group on Verification

EXPERIMENTAL RESULTS

Self Noise Estimates

Sensor self noise levels are important for two reasons. First it is necessary to meet the GSE requirements on sensitivity. Second, it is used to determine the digitizer least significant bit (LSB) levels. There is little advantage to operating the digitizer such that more than a few bits are registering the sensor self noise.

Typically two types of noise are important, the sensor self noise under quiet conditions and that which is observed in normal signal conditions. The quiet self noise is used to determine the digitizer LSB. Non-linearities in the instrument increase the self-noise during acoustically noisy conditions. Characteristics of the signal induced noise will help determine the characteristics of any required acoustic filtering and the maximum resolution required in the digitizer.

Two experiments were done to estimate the sensor self noise. The first was a direct measurement of the system noise in a quiet environment, the second a coherence derived noise measurement in ambient laboratory noise.

Experiment 1: Direct Sensor Noise Level Measurements

To estimate sensor self-noise levels, three systems were plumbed to a common acoustic input which was then plugged. The needle valves were fully opened. The system was not completely balanced since there was still some restriction at the valve and the acoustic path to each side of the sensor was slightly different. It did however move the high frequency response corner well above the band of interest and resulted in a conservative estimate of the self-noise. In this configuration there were four obvious sources of noise; noise introduced from the electronics, ambient acoustic noise coupled through the compliant Tygon tubing, seismic vibrations that directly couple to the diaphragm, and noise that was introduced in the digital recorder.

The preamplifier gain was set high ($\times 32$) to minimize digitizer noise. There were no obvious correlations among the three sensors which were plumbed together as might be expected from ambient acoustic noise coupled through the common tubing. All sensors were run with the diaphragm vertical to minimize the effect of vertical vibration.

The results of these (Figure 1) tests indicate that the instrument self-noise is less than 0.01 μ bars rms for all sensors over any two octave band from 0.1 to 10 Hz. If the one high noise sensor is discarded as damaged then noise levels are less than 3×10^{-3} μ bars rms per two octave band.

Experiment 2: Coherence Derived Noise Estimates

To aid in the evaluation of the self-noise test results, a coherence-derived noise estimate was calculated using ambient laboratory pressure variations as the input signal. The three sensors were plumbed together into a common input which was left open to the lab. Three different 1000 second samples were recorded. Problems in the setup and sensors resulted in only one pair being usable for each sample. However, all sensors were able to be paired and tested.

The resultant spectral estimates (Figure 2, solid lines) imply a flat response from 1 to 5 Hz, and a rapid fall off at higher frequencies. Below 1 Hz the power increases at 30 dB/decade. Some of the low frequency noise may be the result of temperature fluctuations or step changes in air pressure as the air conditioning cycled. The steep fall off beyond 5 Hz is believed to be the result of the acoustic filtering effect in the sensor plumbing. The coherence for these tests was adequate for self-noise calculations for frequencies up to 6-8 Hz. Self-noise spectra derived from the coherence estimates (shown as dashed lines in Figure 2) is below that of the prior closed tube especially at the high frequencies. The self-noise has

a slope of about 30 dB/decade as might be expected considering the strong low-frequency component of the input signal. Noise at the low-frequency end above the noise of the previous closed tube experiment is believed to be caused by nonlinearity in the gauge responses or by differences in their temperature responses.

Microbarograph Calibration and Response Estimates

Three experiments were done to investigate the microbarograph response, two direct calibrations using generated pulse and sine pressure signals and one indirect calibration comparing the responses of two different gauges. During the initial tests there was no method of measuring or generating absolute pressures at the required low working pressures. Volumes in the system were unknown and thus indirect methods could not be used. However, one sensor (SN76772) had been previously calibrated by others using a step function generated by bursting a diaphragm (Hunt and Schomer, 1979) at a calibrated pressure. This unit was used as a reference in calibrating the other gauges.

Experiment 3: Step Function Calibration

A simple step function calibration test was used to initially adjust the sensors and needle valves and then to approximate the response of the system, assuming that it can be described as a simple 1 pole filter.

To compare sensitivity of each system the needle valves were completely closed. Verifying that the needle was closed was done by observing that the backing volume maintained pressure when heated slightly (by a finger tip) over a period of 10 minutes. A common 3 Hz signal from a sine wave bellows calibrator was used to drive all three systems. The amplitude of the signal was observed to be equal (within the measurement accuracy of an analog oscilloscope) at the outputs of all three gauges.

Having demonstrated that the sensors had about the same sensitivity, the needle valve on one system was then adjusted such that a step pressure pulse would fall to half its initial value in 6.7 seconds, equivalent to an RC filter with a 60 second corner. Pressure pulses were generated by alternately squeezing and releasing a small Tygon tube. Using this one system as a reference, the bellows calibrator was adjusted for a period of 10 seconds and needle valves on the other two systems adjusted such that the observed amplitude matched the reference system. Effectively, this matches the R_{back} of the gauges. It will result in matched responses if the gauge backing volumes are also the same. The backing volumes were approximately the same for these units. When the gauge responses were matched, their needle valves were cemented in place to prevent accidental movement.

Positive and negative step pulses generated by covering and uncovering a Tygon tube with a thumb were then recorded for analysis. The step response for a simple RC filter with unknown gain and time constant was fit to each recorded curve. The results (Figure 3) indicate that the high pass corner of the gauge responses varies from 1/58 to 1/66 Hz. This is more dispersion than one would prefer in matching responses, but with the small backing volumes and great sensitivity to needle valve adjustments closer response matches are difficult to achieve.

Experiment 4: Sine Wave Bellows Calibration

Following the pulse test, a calibration using a bellows calibrator salvaged from an old NBS microbarograph system was attempted. The bellows calibrator produced about a 1000 μbar peak at its maximum frequency of 1/3 Hz. The frequency of the calibrator could be crudely adjusted by adjusting the drive voltage on the DC gear-head motor. Unfortunately at frequencies lower than 1/10 Hz, friction led to small distortions in the signal and the frequency sometimes never stabilized. Calibration data were recorded at 6 different drive voltages. Each recorded segment was fitted with a tapered sine wave of arbitrary gain, phase, and frequency.

The calculated rms amplitudes derived from these tests are plotted as discrete points in Figure 4. The solid curves shown in this figure are the frequency responses derived from the step function tests. The sine and step function calibrations are clearly inconsistent. The causes for this discrepancy are currently under investigation.

Experiment 5: Open Sensor Comparison

Later experiments and observations with a spectrum analyzer suggested that either the laboratory noise spectrum or the sensor response cuts off at frequencies between 5 and 20 Hz. It is also possible that the experimental microbarograph configurations included a low-pass acoustic filter. This phenomenon was suspected to be due to the acoustic impedance of the narrow diameter bypass tube that connected the backing volume to the main input port.

To investigate this possibility, a comparison was made between the outputs of a normally configured Validyne and one with all plumbing removed from the input port.

The spectra of the two outputs (figures 5 and 6) indicates that the normal plumbing begins to affect the response at 3-4 Hz suppressing the high frequencies. The strong spike at 60 Hz in the open plumbing is assumed to be electrical rather than acoustic in this case. The transfer function between the two outputs (Figure 6) demonstrates that the low pass corner frequency caused by the tubing is about 5 Hz. This is a fortuitous result since it matches the GSE design specifications. However, for the purposes of observing industrial explosions it is preferable to increase the passband. This may be done by reconfiguring the gauges.

Porous Hose Effects

The use of porous garden hoses to do acoustic summing is widespread but poorly documented. For example, porous garden soaker hoses come in a variety of compositions, but researchers rarely remark on the type or brand of hose in use. A trip to the local hardware store procured three different types of hoses. These are:

1. a 1/4" ID laser punched soaker hose designed for low pressure drip irrigation systems (LP),
2. a high pressure low-volume woven hose designed to run in gardens (HPLV), and
3. a high-pressure high-volume hose for lawns and gardens (HPHV). This was the type installed at TXAR.

All hoses were 15.2 m (50 feet) long.

Experiment 6: Effect of an Attached Hose and Comparison of Hose Types

As a first test, the microbarograph (sensor plus backing volume) response was compared with and without a hose attached. The connected hose was coiled into a tight (50-cm diameter) circle to avoid additional spatial filtering.

The test consisted of two stages. During the first stage, the output of a microbarograph connected to a high-pressure, low-volume (HPLV) hose was compared to the outputs of open and sealed microbarographs. During the second stage the outputs of microbarographs connected to HPLV and a laser punched drip line (LP) were compared. Spectra from the results of the stage 1 test (Figure 7) illustrate that all systems converge to a common power below 10 seconds, but diverge at higher frequencies. These data indicate that the porous hose is a high cut acoustic filter. Since the hose may be regarded as a leaky transmission line, this effect should occur regardless of the number of hoses connected in parallel and should be accentuated slightly as hoses are lengthened. The low frequency noise seen in the closed system spectrum is assumed to be acoustic energy coupled through compliant tubing and thermal variations in the backing volume. If this assumption is correct, then the closed system is not fully isolated and locked at low frequencies but simply a system with a different response. Both the closed and hose system spectra have about the same noise power above 10

Hz. This is believed to represent their system noise levels. Notice, however, that the open system noise power falls below this level and continues to roll off at 30 dB/decade. This behavior suggests that the hoses and plumbing themselves may introduce additional system noise to the observed outputs. Spikes in the spectra of the open system at 20 and 30 Hz are thought to be caused by background noise from fluorescent light ballasts operating in the laboratory. Temperature fluctuations also seem to cause noise problems, perhaps as a result of unequal stresses across the diaphragm chamber.

Transfer function calculations between the hose and open system outputs (Figure 8) indicate that the porous hose introduces a low pass corner at 0.4 Hz. Coherence between the open and closed systems is essentially zero even at low frequencies suggesting that the low frequency noise is probably not directly coupled acoustically but must be related to electronic noise, seismic disturbances, or temperature fluctuations.

The stage 2 test results are shown in figures 9 and 10. Notice that the spectrum of the laser punch system (Figure 9) resembles the open system (Figure 5). In addition to a high frequency roll off seen in the stage 1 tests, the soaker hose spectrum observed during this test also includes resonance peaks at 9 and 18 Hz. These are visible although smaller in the previous test. The transfer function between the two system outputs (Figure 10) also demonstrates that the LP hose is almost equivalent to an open system in its frequency response characteristics.

Experiment 7: Effect of 5 Arm Array

In the configuration currently being evaluated at TXAR, 5 hoses are acoustically summed in a small chamber which is connected to a sensor in a borehole by a short 6 m (20 foot) hose. The sensors are operated in boreholes to stabilize temperature effect thus reducing some of the long-period noise. The radial hoses are 15.2-m (50 feet) long and connected with normal garden hose fittings.

The frequency characteristics of this configuration was investigated in the laboratory by comparing its output with hoses coiled to that of a single sensor open to the atmosphere. Ambient background noise was used as a source for one phase of the test, whereas pulses generated by closing doors and by directing a distant air jet towards the sensor for the second phase. Both of these methods may be useful as a test calibration source if it can be demonstrated that the primary energy is a propagating acoustic wave and not a turbulence cell.

Spectra of the two system outputs (Figure 11) indicate that the frequency responses of the two systems are similar from about 0.2 to 8 Hz. Differences at high frequencies are assumed to be due to the slight spatial filtering provided by the coiled hoses and a modified system response due to the effect of the greater volume and higher resistance of the hoses. As shown in Figure 12, the coherence between the two system outputs is high enough to estimate a reliable transfer function from 0.1 to 20 Hz. The transfer function indicates two corners; one at 5-6 Hz and one close to 20 Hz. After correcting for the constant delay of the 6 m hose, the phase response shown in Figure 15 seen to be nearly flat out to 20 Hz.

Hose Spatial Characteristics

The results of previously described tests have illustrated that a hose connected to the input of a microbarograph affects the overall system frequency response. The spatial filtering characteristics of porous hoses were investigated in the experiments described below.

Experiment 8: Coiled vs. Spread Hoses

A test comparing two garden soaker hoses to each other and to the LP drip line hose was done for both coiled and uncoiled configurations. The objective of this experiment was to verify that the uncoiled hose had a spatial effect as would be expected if the acoustic properties were uniform. If the response is due primarily to a leak at the connection or to a single low resistance hole, spreading the hose out should not change the response. If the

acoustic properties of the hose are nonuniform, then the coherence between two hoses laid side-by-side is reduced.

The experiment was conducted outdoors on a cold windy evening, about 4.5 m from the front of Heroy Hall (a 4 story building), with the lines laid out parallel to the face of the building. It was performed in four stages with three channels collected during each stage. During the first stage, one garden HPLV soaker was uncoiled and laid out while the other was left coiled along with the LP drip line. Fifteen minutes of ambient noise data was collected. During the second stage hose connections were to different gauges to eliminate the possibility of observed differences in outputs being attributed to a miscalibrated gauge. Another 15 minutes of data was collected. During the third stage, the LP drip line was uncoiled and laid about 8 cm from the soaker hose for 15 minutes of data acquisition. During the final stage, all hoses were uncoiled and data were acquired for an additional 15 minutes.

Spectra of the three different hoses are compared in Figure 14. It can be seen from these data that the two HPLV soaker hoses have similar responses, although the noise level is higher on one system, while the LP drip line has a significantly different response. This may be due in part to the slightly different size of the coiled LP (20 cm coil) as compared to the 50 cm coiled soaker hose. Spectra of all three hose outputs show resonance peaks at different frequencies. The drip line has one at 30 Hz. The two HPLV soaker hoses have common peaks at slightly different frequencies. In addition, the coiled hose has a peak at 8.5 Hz. It is assumed that this peak is due to the coiling. Transfer function and coherence calculations shown in Figure 15 demonstrate the expected low pass filter characteristics of the HPLV soaker hose compared to the drip irrigation hose and little coherence between the spread hose and coiled hose at even the low frequencies (0.1 Hz).

Experiment 9: Parallel Hose Coherence

Following the coiled tests, all three hoses were spread out in parallel. Maximum distance between the parallel hoses was about 30 cm, with the average about 7 cm. The stiffness and set in the hoses prevented them from laying perfectly side by side. Spectra of the three outputs are compared in Figure 16. Notice that all three spectra show resonance peaks. Comparison of the drip line hose in both the spread and coiled configuration demonstrates that it too is an effective spatial filter. Transfer functions and coherence between the three outputs as shown in Figure 17 are disturbing. The coherence is low for all pairs of hoses except at the lowest frequencies where the effects of spatial filtering are different anyway. This result suggests that either the hoses are not uniform along their length and hence each has a slightly different spatial filtering function, that the hoses were not close enough together in the experiment to sample the same space, or that there is some more complex system response that varies from hose to hose.

Experiment 10: Parallel Hose Test under Low Wind Conditions

The results of the previous parallel hose test were so puzzling that the test was rerun with the more porous LPHV hoses pegged down at 3 m intervals and positioned within 15 cm of each other along their whole length. The hoses were oriented at 90 degrees to the prevailing light wind. Wind conditions were calmer than the previous test, with breezes just stirring the leaves on occasion. It was felt that the change in hose material may have an appreciable affect on the response.

Spectra for the two outputs are compared in Figure 18. They are similar in shape but separate slightly above 0.5 Hz and have slightly different resonance response characteristics above 10 Hz. These differences are also reflected in the coherence estimates shown in Figure 19 and which is disappointingly low above 0.5 Hz.

Experiment 11: Outdoor Array Tests

As a final test, the proposed TXAR array, a five arm star with each arm 15.2 m (50 feet) in length was compared against an open microbarograph. Winds were calm (under 3 mph) during most of the test. At the center of the array an open microbarograph recorded the background noise without a pipe array. During the test a number of jet and prop planes overflights the area (we were in a takeoff and landing pattern for Love Field that day). Two data streams were recorded, one at 100 SPS and one at 500 SPS on the open system. The high frequency recording was to be used to correlate audible events with surrounding pressure pulses (such as over-flights). This turned out to be difficult to do because the bandwidth of the open system was insufficient to produce identifiable signals. If this test is repeated, a microphone should be included on one channel.

Spectra of the two outputs are compared in Figure 20. The comparison clearly illustrates the effects of spatial filtering provided by the pipe array. It should also be noted that the pipe array has introduced a strong resonance peak at about 15 Hz. The 10-dB difference in power seen at the low end is attributed to differences in sensor sensitivity. One of the sensors had been transported from the field and had not been recalibrated prior to this test. While quick checks of the system response indicated that the response had not changed appreciably, the sensitivity appears to differ. This could have been due to an overpressure event that partly damaged one of the systems. Coherence calculations between the two system outputs are not useful. Except at the lowest frequencies, 0.1 Hz, the coherence is too low to derive a useful transfer function between the two systems.

CONCLUSION

In this study a preliminary examination of the characteristics of the broadband acoustic sensors deployed at TXAR demonstrates the complexity of even a simple system and the need for careful calibration and laboratory measurements in designing such systems (as well as the large number of unknowns). The following conclusions are made based on this study:

1. Some Validyne model P305D sensors may have a low enough self-noise levels to be used as acoustic sensors although this exceeds the manufacture's specifications by nearly 2 orders of magnitude. Conservative estimates of sensor noise levels using direct measurements suggest that sensor noise is below 0.50 μ bar rms over a 0-50 Hz band. Other models are available that have greater sensitivity.
2. The small backing volume in the configured sensor system leads to a large response sensitivity to minor changes in the needle valve setting. This is difficult to set in the laboratory and susceptible to changes during transport and field installation.
3. Sensors with responses down to DC will have a DC offset that may vary with temperature. This must be included in the calculations of required system dynamic range. Sixteen bit systems are inadequate for laboratory testing.
4. Sensor calibration using simple step functions may be adequate to adjust a set of sensors to a rough match and to develop a response function assuming a simple RC system. However, results from the bellows calibrator are not consistent with those of the step function calibration. This difference has not been unexplained.
5. Coherence derived noise measurements suggest that the sensor dynamic range is limited by a nonlinear system response or by the resolution of the procedure caused by the use of a non-white signal source.
6. The acoustic characteristics of commercial soaker hoses and drip lines vary considerably with the type and manufactor and must be considered as part of the system response. Such hoses can impose and additional

high-cut filter on the system. The use of ambient laboratory background noise is not adequate to develop response of the full bandwidth of the system.

7. Spread porous hoses form a spatial filter for high frequencies but at the lengths tested are ineffective at low frequencies. Hoses have resonances that are not entirely consistent in frequency or bandwidth even with hoses of the same make. Coherence between parallel hoses is lower than expected.
8. A five arm star may reduce noise levels by as much 20 dB for frequencies above 0.3 Hz but is less effective at lower frequencies. Above 7 Hz the spectra suggest that the system response for the fielded system is different from that tested in a coiled configuration or that the system is ineffective at reducing noise.
9. Background noise during the field test falls off at 20 dB per decade frequency.
10. No theoretical design calculations were made during the present investigation. Few characteristics were available for components. The use of off-the-shelf commercial fittings with complex internal shapes makes it difficult to simplify the system to the extent that simple lumped term calculations and tables require. The current sensor/backing volume construction has an expected high cut filtering effect.

RECOMMENDATIONS

Based on this study and experience with the sensors deployed at TXAR, the following recommendations are made for additional study:

1. Other pressure sensors that might be applicable should be examined including more sensitive models from Validyne and less expensive models from Kavlico. Each sensor should be characterized by the following electrical requirements:
 - frequency response,
 - self-noise characteristics,
 - linearity,
 - temperature response,
 - signal conditioning requirements, including output levels, output impedance
 - out-of-band noise including RFI,
 - RFI susceptibility,
 - power supply requirements
2. If Validyne sensors are to be used in a field installation, the use of RFI filtering, shielding, and isolation and either a separate power supply or additional signal conditioning to permit balanced output should be investigated.
3. A different configuration for backing volume and bleed port (needle valve) should be used on future sensors. It is unknown how temperature changes may affect the current needle valve settings, or how much instruments may drift with shipping and field installation.
4. Laboratory data acquisition systems need to, at least, have the dynamic range of the anticipated field systems. Ideally the laboratory recording system should use a system similar to that required by the field installation such that signal conditioning and front end noise characteristics are the same.

5. Future studies of sensor characteristics should include either a full description of the analysis procedure or should include copies of the code and data used to produce the analysis.
6. More careful study of sensor noise levels should be done. Coherence derived noise figures may be the most useful. Because of the short wavelengths associated with some turbulence derived signals and the sensitivity of most acoustic sensors to seismic disturbances, such measurements need a great deal of planning and care.
7. Careful laboratory calibration of the sensor frequency and phase response should be done. Because measurement techniques are still being developed while sensors are being deployed, it is also essential to have a laboratory standard instrument with a known response and a standard field configured instrument with which newly assembled instruments may be matched. A standard laboratory acoustic calibration source capable of producing signals over the required bandwidth and amplitudes is also needed.
8. Coherence derived noise measurements should be done with a white or bandlimited acoustic signal source. If low frequency nonlinearities introduce additional noise and the expected noise spectrum is enriched in low frequencies (as it will be for small hose arrays), it may be advantageous to reduce the system low frequency response producing a system response that is not flat across the signal band.
9. Formal measurements of the acoustic characteristics of proposed types and models of porous hoses should be made so that it is possible to calculate the theoretical response of systems of such hoses. A calibration signal source may be needed to produce sufficient signal levels to allow measurements over the full band of interest.
10. The design of a spatial filter should consider the spatial characteristics of the noise and signal bands of interest and the spatial characteristics of the filter. Former microbarograph studies have described the characteristics of noise below 1 Hz and acoustics studies have described outdoor noise characteristics in the audible band. It is not obvious that porous hoses have a uniform consistent spatial response. More work is needed to characterize the noise.
11. The humps in the spectra of the field system should be explained. Measurement of the noise reducing capability of arrays should be made at various wind and weather conditions. This will require a semipermanent installation capable of making noise and weather measurements.
12. The affects of sensor frequency response on system dynamic range and linearity should be investigated. If background noise follows the 20 dB/decade response, then a 0.01-10 Hz system would require 60 dB of instantaneous dynamic range and linearity for a system with a flat frequency response. This may be difficult and it may be desirable to modify the system response.
13. Acoustic characteristics of sensors and sensors when coupled to backing volumes should be measured. This includes acoustic impedance and admittance for each type of sensor considered. Plumbing near the sensor needs to be carefully designed so as not to unduly affect the sensor response.

ACKNOWLEDGMENTS

The author would like to thank Bob Rienke and Al Leverette who had been using the P305D sensors in making near source measurements for some time and suggested their use for this project. Karl Thomason designed and assembled the array system and various test systems.

Mike Sorrells and Eugene Herrin provided advice and review of the study suggesting a number of fruitful ideas and pointing out problems in the early part of the study. The mistakes and problems that remain are totally those of the author and part of the natural beauty of genuine research.

This study was supported by USAF Phillips Lab Contracts #F19628-95-C-0184 and #F19628-93-C-0057 sponsored by AFTAC and ARPA.

REFERENCES

References in bold text are cited in this report. Others listed here were reviewed during the preparation of the report and test procedure.

Broch, J. T. (1971) Acoustic Noise Measurements. January 1971, 203 pp.

Burridge, R. (1971) The Acoustics of Pipe Arrays. Geophys. J. R. Astr. Soc 26:53-69.

Cook, Richard K. (1962) Strange Sounds in the Atmosphere, Part I. Sound 1:12-16.

Cook, Richard K. (1962), and Young, Jessie M. Strange Sounds in the Atmosphere, Part II. Sound 1:25-33.

Crocker, J. J. (1968) Sutherland, L. C. Instrumentation Requirements for measurement of sonic boom and blast waves --- A theoretical Study. J. Sound Vib. 7(3):351-370.

Daniels, Fred B. (1959) Noise-reducing line microphone for frequencies below 1cps. J. Acoust. Soc Am 31:529.

Group of Scientific Experts Infrasound Experts (1995), Report of the Infrasound Expert Group, December 15, 1995. [Http://www.cdadc.org/librarybox/ExpertGroup/15dec95infra.html](http://www.cdadc.org/librarybox/ExpertGroup/15dec95infra.html).

Hunt, A. (1979) Schomer, P. D. High-amplitude/low-frequency impulse calibration of microphones: A New method. J. Acoust. Soc Am 65(2):518-523

Ireland, A. T. (1942) Design of air-blast meter and calibrating equipment. BuMines Tech. Paper 635, 20 pp.

Leventhall, H. G. (1976) Kyriakides, K. Environmental Infrasound: Its occurrence and measurement. Chapter 1 in infrasound and low frequency vibration by W. Tempest. Academic Press, New York pp 1-18.

McDonald, John A. (1971) Douze, E. J., and Herrin, E. The structure of atmospheric turbulence and its application to the design of pipe arrays. Geophys. J. R. Astr. Soc 26:99-109.

Olson, J. J. (1971) Fletcher, L. R. Airblast-overpressure levels from confined underground production blasts. BuMines RI 7574, 24pp.

Reed, J. W. (1977) Atmospheric attenuation of explosion wave. J. Acoust. Soc Am 61(1):39-47.

Reinke, Bob (1985) A Digital Microbarograph System. AFWLTR 84-142.

Siskind, David E. (1974) and Summers, C. R. Blast noise standards and instrumentation. BuMines TPR 78, 18 pp.

Siskind, David E. (1976) Stachura, Virgil J.; and Radcliff, Karen S: Noise and Vibrations in Residential Structures From Quarry Production Blasting: Measurements at Six Sites in Illinois. United States Department of the Interior, Bureau of Mines, Report of Investigations 8168 xx p.

Siskind, David E. (1977) Structure Vibrations From blast produced noise: energy resource and excavation technology. Proc. 18th U.S. Symp. On Rock Mechanics, Keystone, Colo., Jun 22, 1977 pp. 1A3-1 to 1A3-4

Siskind, David E. (1977) and Stachura, V. J. Recording system for blast noise measurement. Sound and vibration, pp. 20-23.

Siskind, David E. (19Xx), Stachura, Virgil J., Stagg, Mark S., and Kopp, John W. Structure Response and Damage Produced by Airblast from Surface Mining. United States Department of the Interior, Bureau of Mines, Report of Investigations 8485 xx p.

Stachura, Virgil J. (1981) Siskind, David E.; Engeler, Alvin J.: Airblast Instrumentation and Measurement Techniques for Surface Mine Blasting. United States Department of the Interior, Bureau of Mines, Report of Investigations 8508 xx p.

Snell, C. M. (1971) and Oltmans, D. L. A revised Impersonal approach to airblast prediction. U.S. Army Waterways Experiment Sta., Explosive Excavation Res. Off., Tech. Rept. 39, Nov 1971, 108 pp.

Validyne (1987) Model P305 Operating Instructions. Validyne, 8626 Wilbur Avenue, Northridge, Calif. 91324.

Validyne(1990) P305 Differentail or absolute pressure transducer. Validyne, 8626 Wilbur Avenue, Northridge, Calif. 91324.

Whitaker, R. W. (1995) Mutschlecner, J. P. And ReVelle, Douglas O. Los Alamos Infrasonic Explosion Detection. ARPA CTBT Monitoring Technologies Conference 1995 Proceedings.

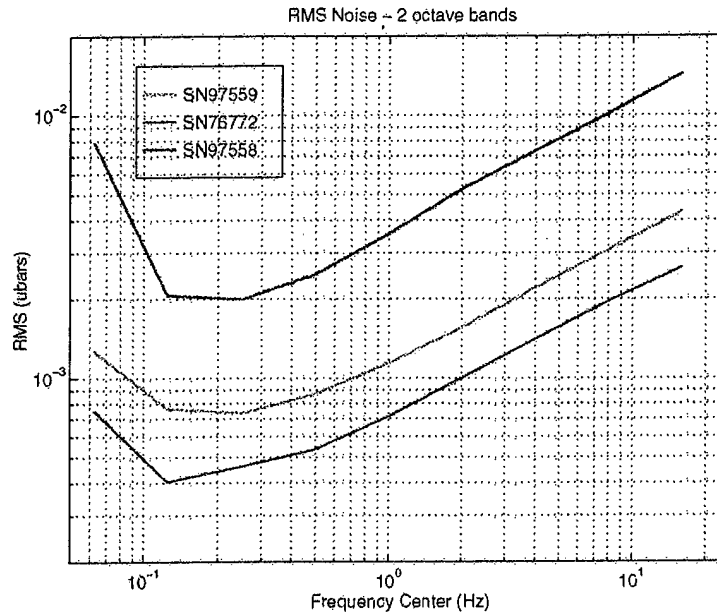


Figure 1. RMS noise levels for 2 octave bands. Points are plotted for the center frequency (bands span one octave above and below each point on the curve. Points were calculated by applying a 3 pole 2 octave Butterworth filter to each trace and then calculating the rms over a 100 second window.

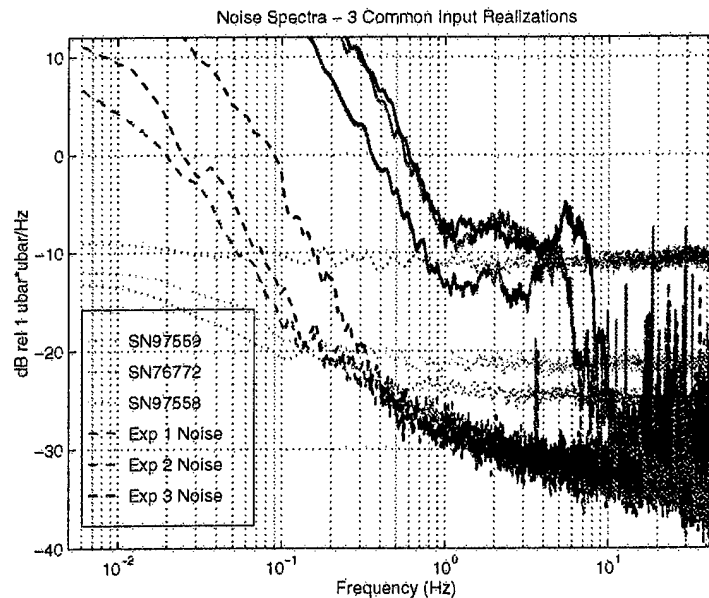


Figure 2. Coherence derived noise spectra for 3 realizations. Solid lines are the observed normalized spectra, Dotted lines are the results from the previous closed tube experiment (figure 1), and dashed lines are the coherence derived noise. The line spectra at 3.8 Hz in the coherence noise is unexplained. Lines at higher frequencies are assumed to be from transformer and lamp ballasts.

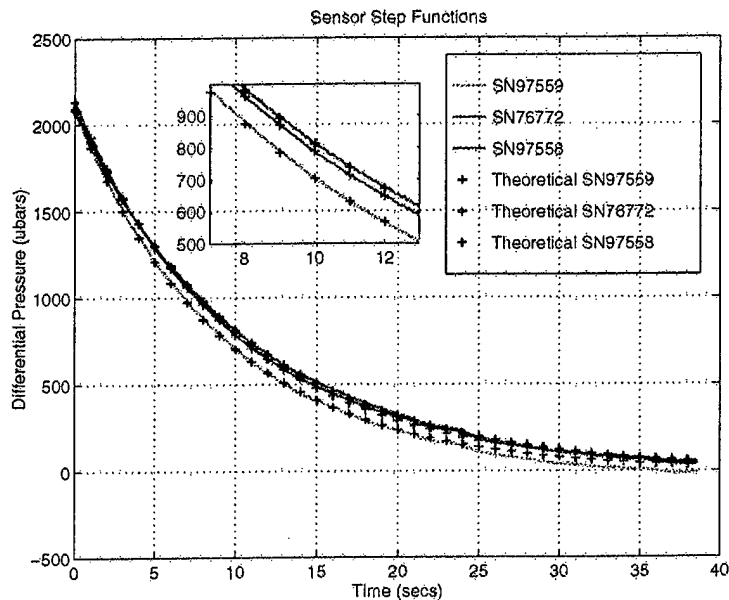


Figure 3. Sensor step functions with theoretical response overlay. Theoretical response assumes a simple RC filter where the period and gain are fitted jointly. The RC corner frequency is 57.91 seconds for SN97559, 63.17 seconds for SN76772, and 66.39 seconds for SN97558. At 25 seconds there is a small kink in the curves. This is assumed to be an external signal rather than a sudden change in the RC constant. Note that pressures are 1000 times higher than expected signals.

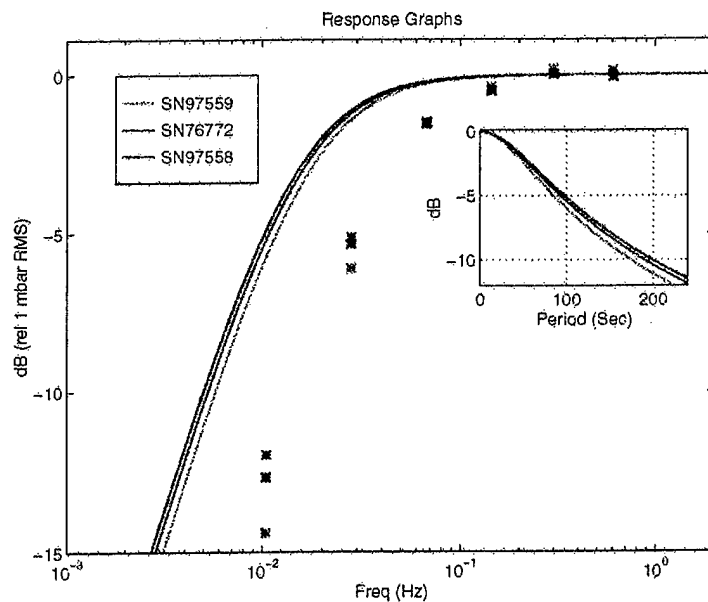


Figure 4. Results of the sine wave and pulse calibration tests. Solid lines are the frequency response derived from the pulse test. Points are the result of the sine wave test. The inset shows the response plotted as period rather than frequency. Note that -3 dB is about 60 second period. The slight divergence in the 3 responses at low frequencies is more than one would prefer in matched systems.

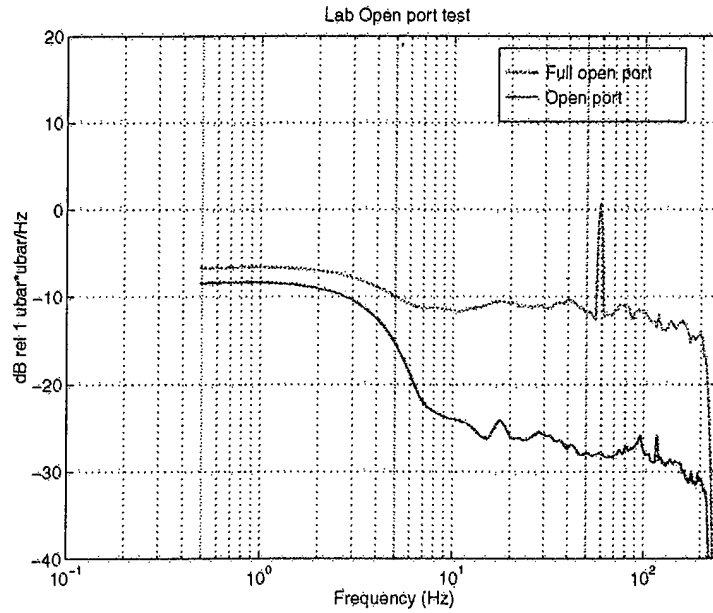


Figure 5. Spectra comparison of a normally configured and open sensor. The strong 60 Hz spike in the open system is believed to be electrical noise due to a poor ground and not acoustic. For this test, data was sampled at 500 SPS.

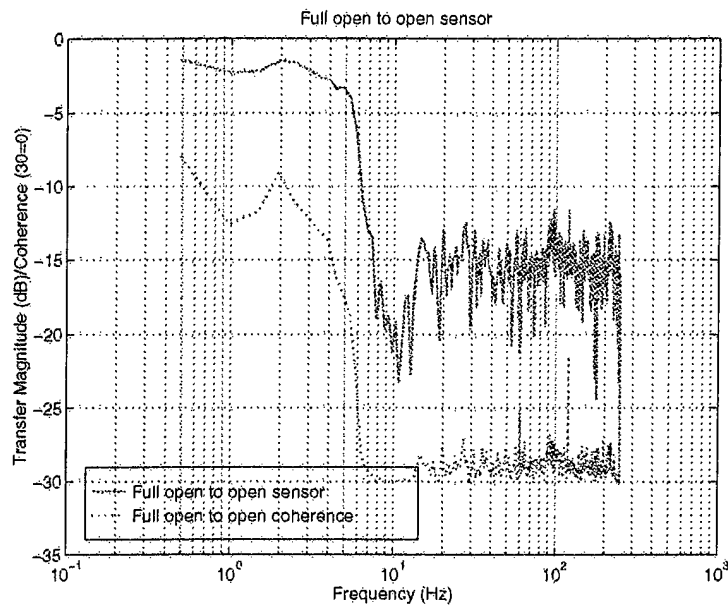


Figure 6. Transfer function and coherence between normal and open systems. The systems as installed at TXAR include this high cut response.

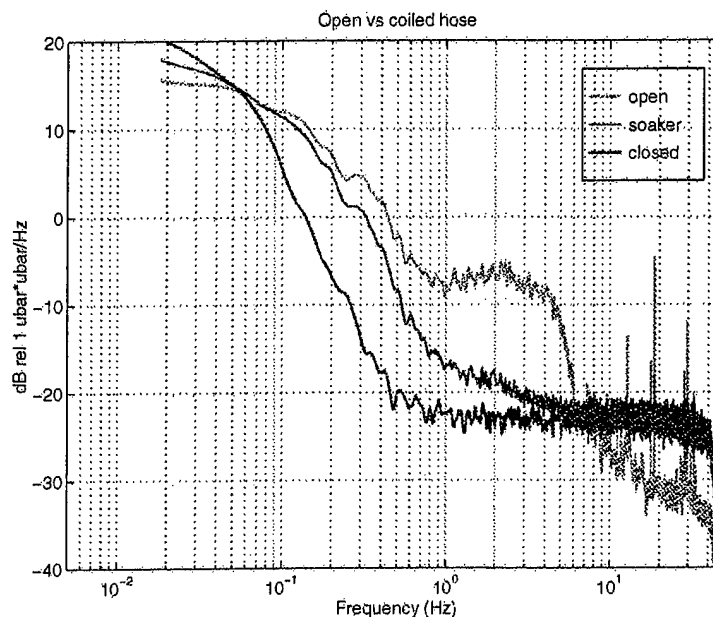


Figure 7. Spectra of the open sensor, closed tube and HPLV soaker hose. Note the high frequency roll-off of the open system compared to the other two.

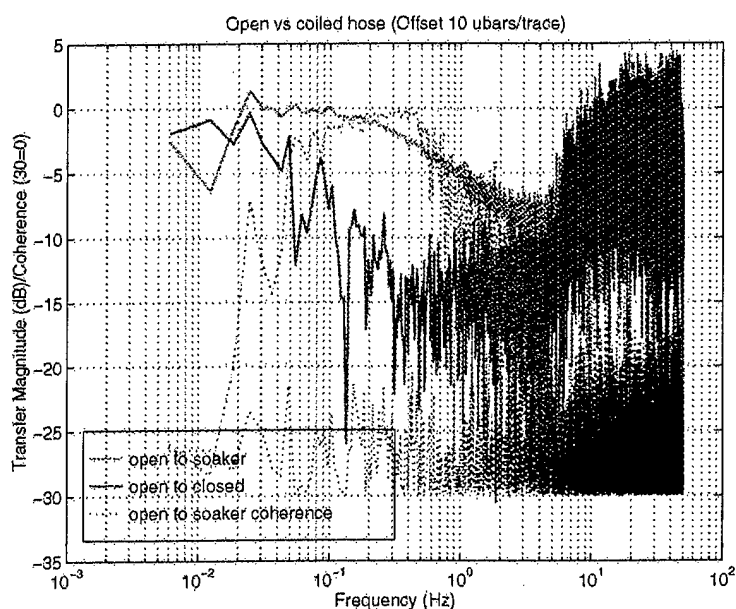


Figure 8. Transfer function and coherence between open and soaker hose and between open and closed systems. Solid lines are the transfer functions, dotted are coherence. The closed system shows little coherence (dotted red line) even at low frequencies. The HPLV hose adds a low pass filter at 0.4 Hz.

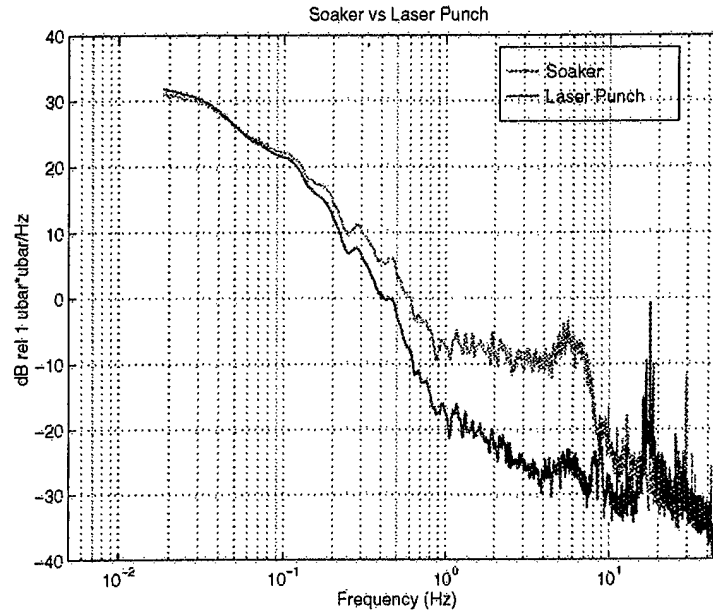


Figure 9. Spectra for the high pressure low volume soaker hose and laser punched drip line. Note the resonance peaks in the soaker hose and the 30 Hz noise peak in the drip line. Labels on this plot are reversed. Red is actually the soaker hose.

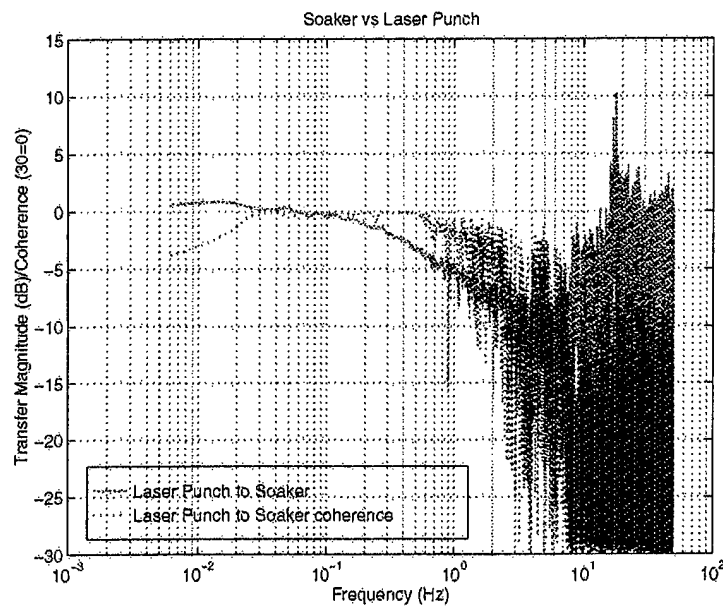


Figure 10. Transfer function between the soaker hose and laser punched system. This function is nearly identical to that between the open system and soaker hose.

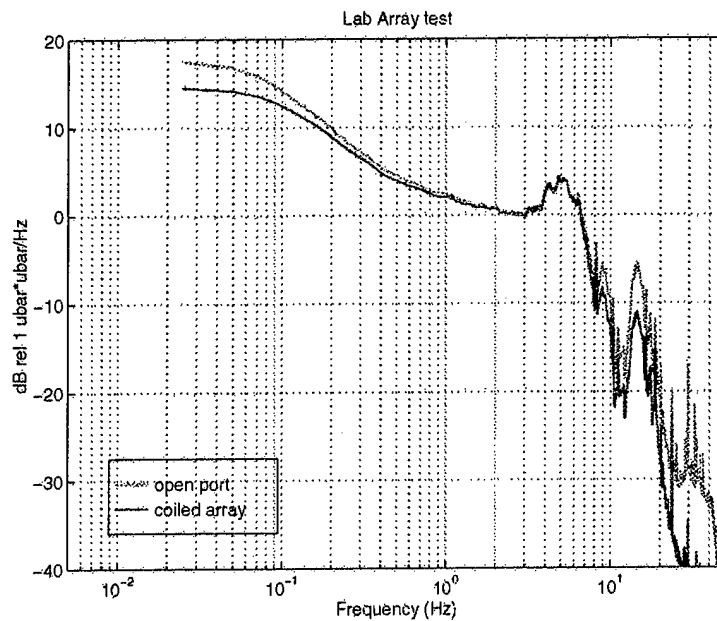


Figure 11. Spectra of coiled array and open sensor. The two are nearly identical from 0.2 to 8 Hz.

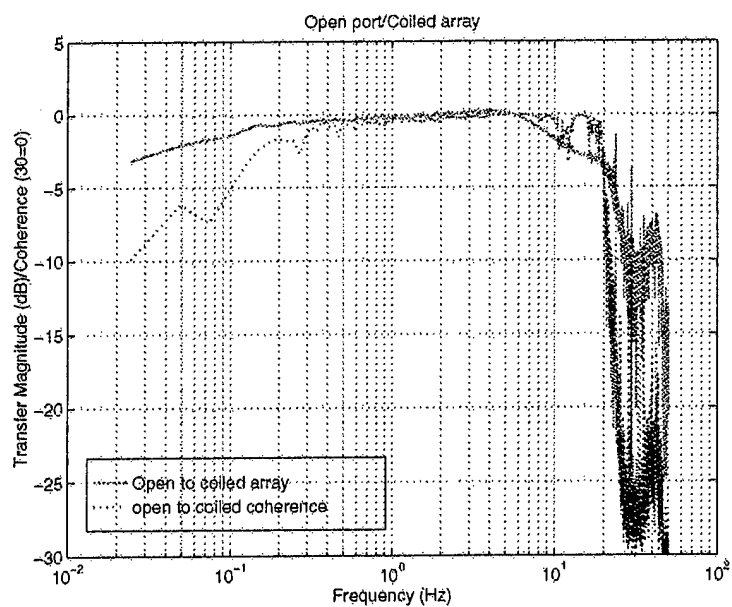


Figure 12. Transfer function/coherence between coiled array and open sensor. Dotted line is coherence.

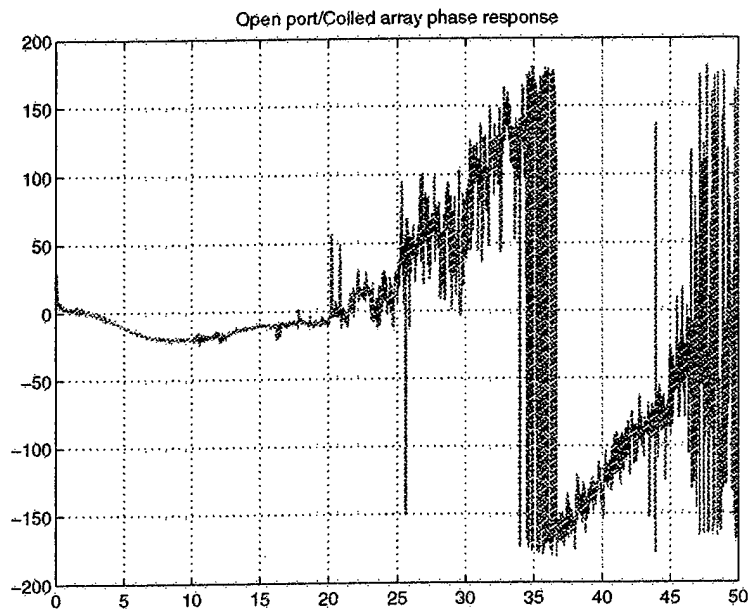


Figure 13. Phase response between coiled array and open sensor. Removed 0.027 second delay. Vertical scale is phase in degrees. Horizontal scale is frequency in Hz.

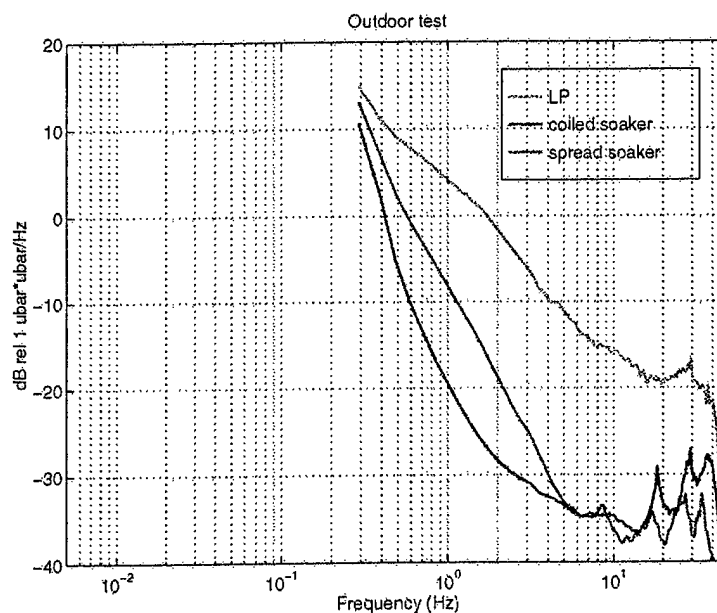


Figure 14. Spectra of coiled soaker, spread soaker, and drip line. Note the resonance peaks. Width of the peaks is about the same although the frequency is slightly different. The -10 dB difference at 1 Hz between coiled and spread hoses is due to spatial filtering.

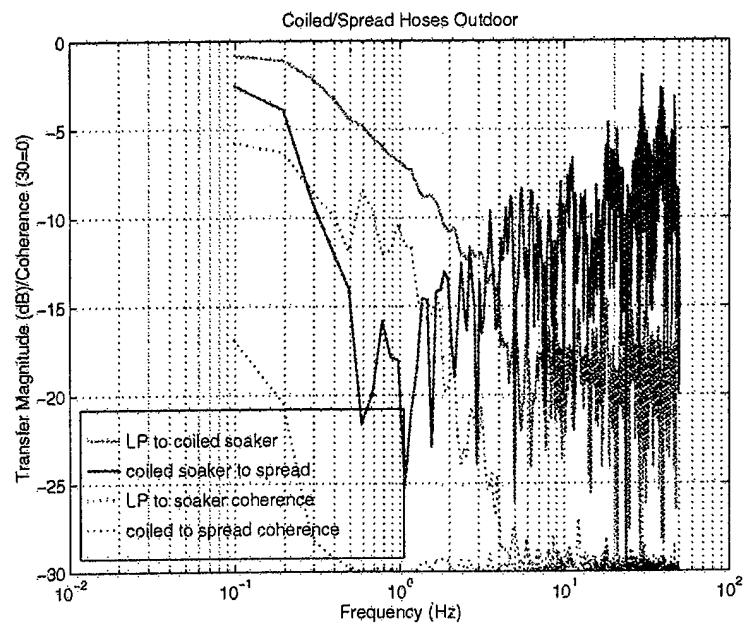


Figure 15. Transfer function and coherence plot for coiled vs. Spread soaker and coiled soaker vs. Coiled drip line. Dotted lines are coherence.

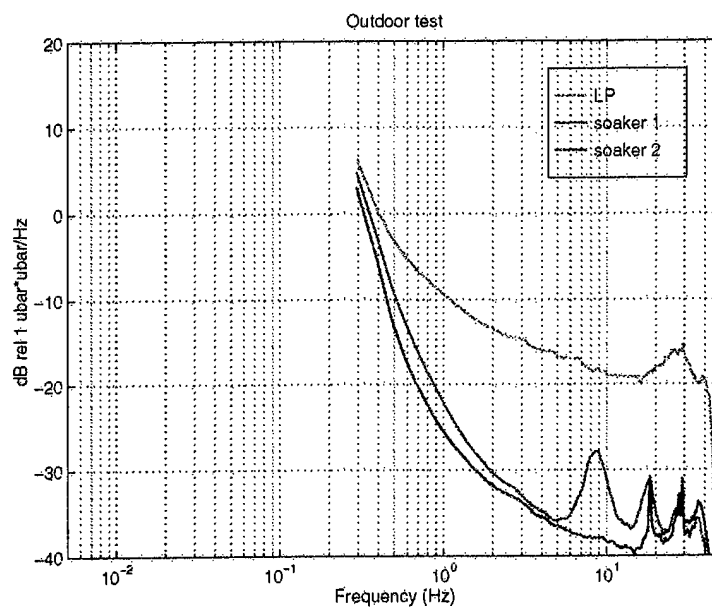


Figure 16. Spectra of the three hoses. Note that now the resonance peaks in the two spread hoses are aligned but one system has much broader peaks and more energy than the other.

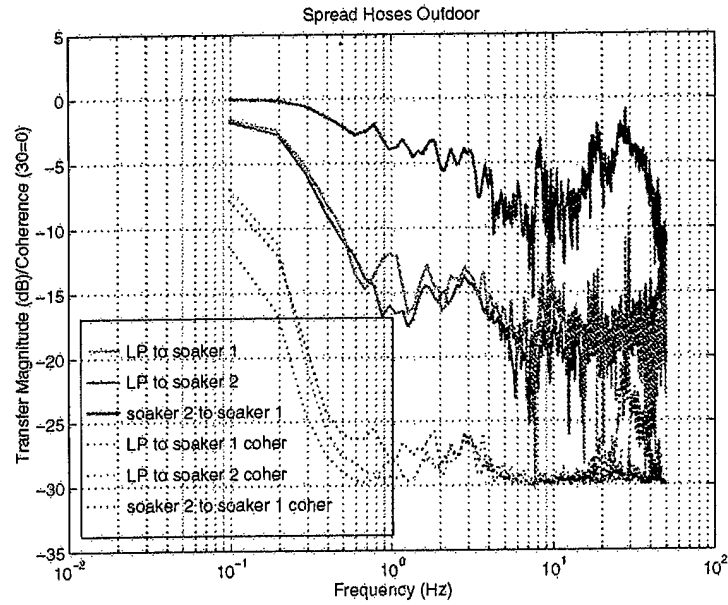


Figure 17. Transfer function and coherence among the three spread hoses. Note that the coherence is low for all paired measurements.

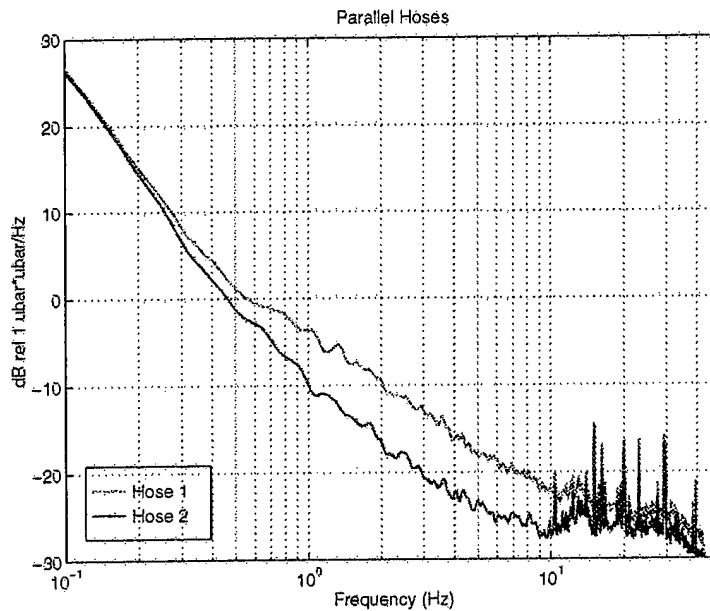


Figure 18. Spectra for the parallel hose test. Differences in the slope suggest that one hose may be non-uniform along its length.

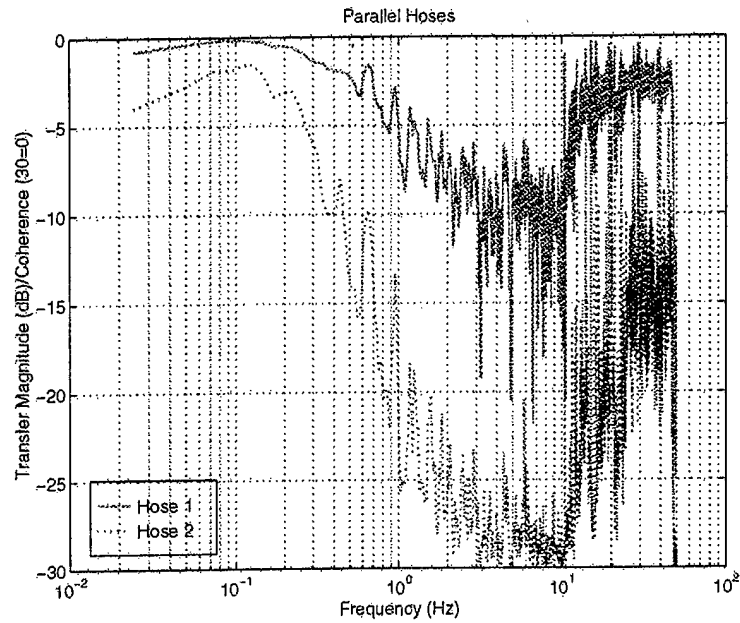


Figure 19. Coherence from parallel hose test. Coherence above 1/2 Hz is disappointingly low and similar to the previous test.

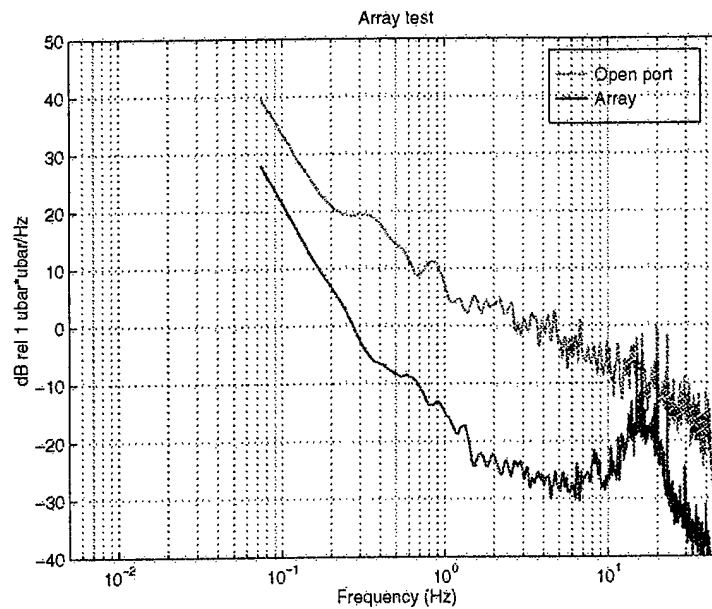


Figure 20. Spectra of the array and of a single point system. Differences at the low end are attributed to differences in sensitivity.

APPENDIX 1: DESCRIPTION OF INSTRUMENTATION

The TXAR infrasonic array is an experiment in piggy-backing an inexpensive infrasonic system onto an existing GSE Alpha array. By using existing sites and communication facilities, off-the-shelf sensors, and inexpensive pipe arrays, each acoustic channel was added for an incremental cost of \$9,000.² Since all three sites had multi-channel digitizers, this experimental cost was reduced to less than \$2,000 per site. This was done without compromising the GSE specifications (see Table 1).

The GSE requirements for a wideband microbarograph response of 1/50 to 5 Hz are significantly broader band than previous designs used during the last experimental period (McDonald, Douze, and Herrin, 1971). The requirement for a short period response requires smaller pipe arrays (8-16 m rather than 60-120 m). Even with shortened arrays, the phase response of the array may be significant and must be considered part of the instrument correction. This shortened array though may be less effective at low frequencies and historical S/N improvements may not be attainable without new technology or methods.

The system currently operating at TXAR (Figures I-1, I-2, and I-3) includes a Validyne model P305D differential pressure transducer (see Table 2). It has the advantage of being relatively inexpensive (less than \$1000), includes all signal conditioning and power supply conditioning, and is small and rugged enough for field installations. Models with greater sensitivity are available³ at additional cost and with some additional signal conditioning and power supplies.

Validyne gauges are variable reluctance devices. A coil is positioned on each side of a magnetically permeable diaphragm. These coils form two arms of an impedance bridge which is excited by a several KHz signal. Small movements of the diaphragm unbalance the bridge and produce a signal which is then demodulated, filtered, and output. The P305D includes the demodulator as part of the device.

Construction of a microbarograph from a differential gauge has been described by Burrige (1971) (Figures I-2 and I-3). Assuming that the volume of the gauge is essentially zero, the capsule equivalent capacitance can be neglected. The fore volume and backing volume in this sensor system are small relative to the volumes in older systems and hence require a high leak resistance. This is accomplished with an adjustable needle valve. A formal analysis of this system has not been done yet.

Two minor problems were encountered in interfacing the sensor to the digitizer electronics. First, the sensor produces a single ended output while the digitizer expects a balanced signal. This precludes common mode rejection and results in coupling power supply noise into the input. Second, the demodulator in the gauges also acts as an RF detector. Radio telemetry noise is easily induced on the acoustic channel. Both of these problems have been suppressed by field practices, but may need to be solved in an operational system.

Besides the sensor, the only other component of significant cost is the precision needle valve, a Whitey SS-2RF2 micrometer adjusted valve. Because the backing volume is so small (a few cm³ compared to the 3600 cm³ of older systems), adjustment of the valve⁴ is

² All cost figure here reflect the current configuration which may have to be modified for operational and maintenance purposes and cannot be used to project future costs.

³ The Validyne DP103 has roughly 30 times the sensitivity of the P305D gauge in use at TXAR.

⁴ The needle valve is shipped with a heavily greased spring loaded needle. If used without cleaning and degreasing, the needle has a tendency to creep closed over periods of a day. Disassembly and careful cleaning is essential to a reliable operation. This must be done with care since the needle is delicate and easily bent.

critical to obtaining the correct frequency response. Since even small turns of shaft a few degrees may substantially change the response and the valve has considerable mechanical hysteresis, it is essential to lock the position of the valve once the system has been calibrated. This is done by cementing the valve in place.

The entire system (see Figure I-1), minus the pipes, is small enough to fit inside the TXAR postholes and thus the sensor and backing volume are protected from rapid temperature changes. This also secures the expensive portion of the system from damage and tampering.

For this set of calibration experiments, data from three gauges was recorded on a Refraction Technology model 72 16-bit data acquisition system with programmable gain preamplifiers. The 16-bit range was a limitation because the DC offset of the system varies slightly with temperature.⁵ This was addressed during experimentation by adjusting the offset to zero prior to each experiment. However overnight temperature changes were enough to clip the digitizer during several tests. It was not possible to record data in the lab with the same resolution as is possible with the 24 bit systems at TXAR.

Lab experiments (see Table 3) examined the sensor self noise, sensitivity, system frequency response (for the sensor and backing volume system), and system response when coupled to a porous hose. Field tests at Dallas were used to verify that a stretched hose acted as linear spatial filter, compared the system response for repeatability, and compared the response of different types of hoses. Of necessity, tests were brief, and therefore they may be regarded as pilot tests demonstrating the procedures and some of the expected problems rather than formal tests of the equipment.

⁵ Reinke (personal communication) has also observed this.

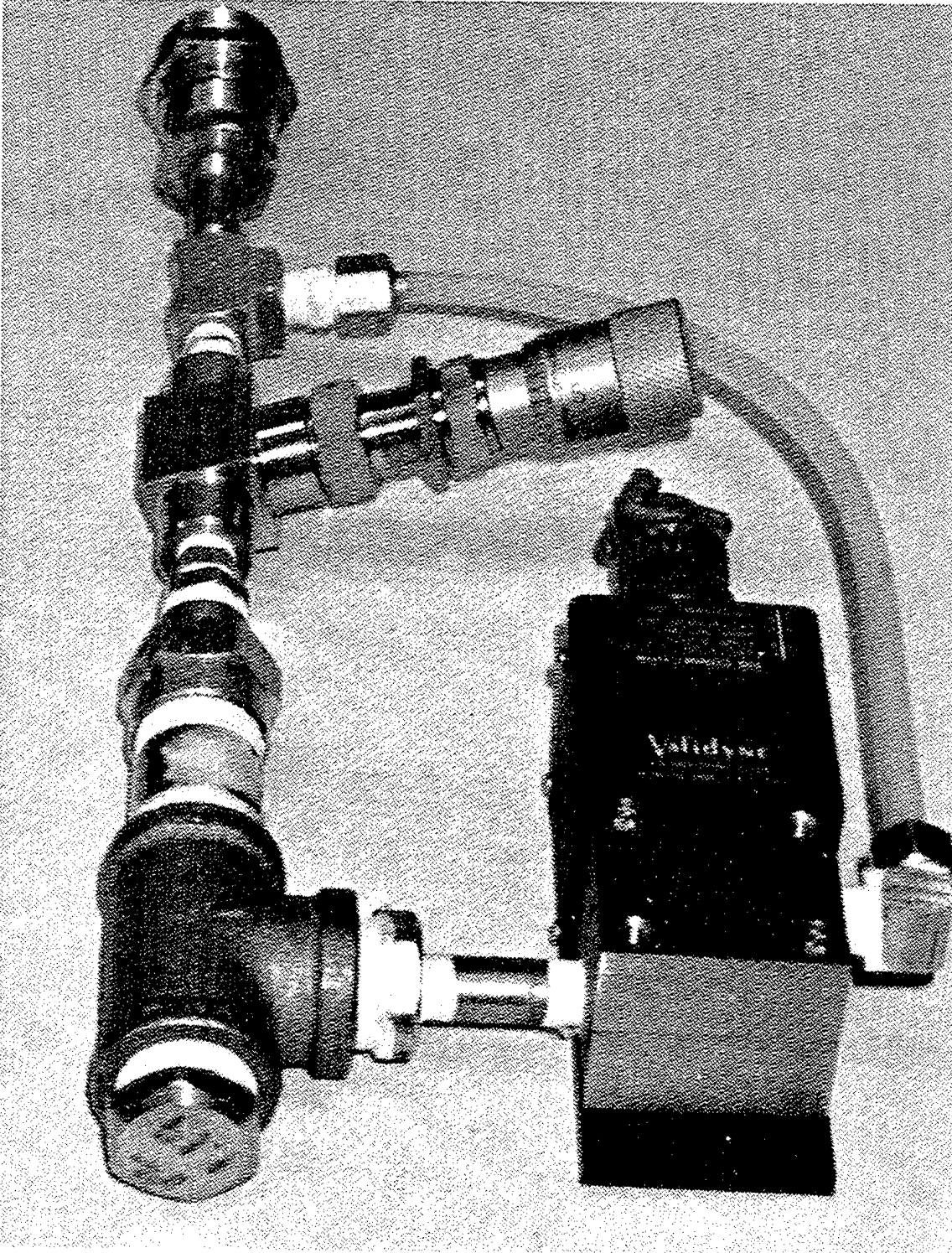


Figure 1-21. Photo of the microbarograph ready to be connected to a pipe or hose. The left port of the differential gauge is connected directly to the backing volume while the right port is connected to the input through a small bypass tube. A precision needle valve bleeds the backing volume and connects the two sides. The low frequency response may be controlled by adjusting the needle valve.

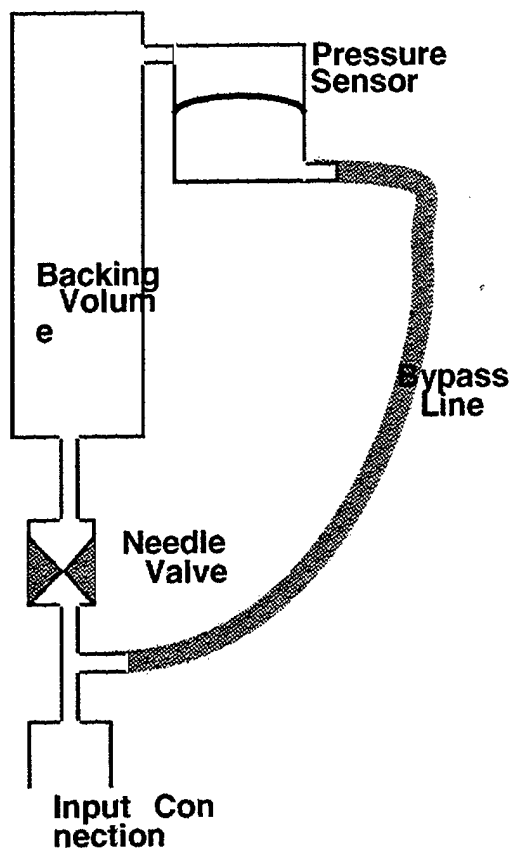


Figure I-22. Plumbing schematic of transducer assembly

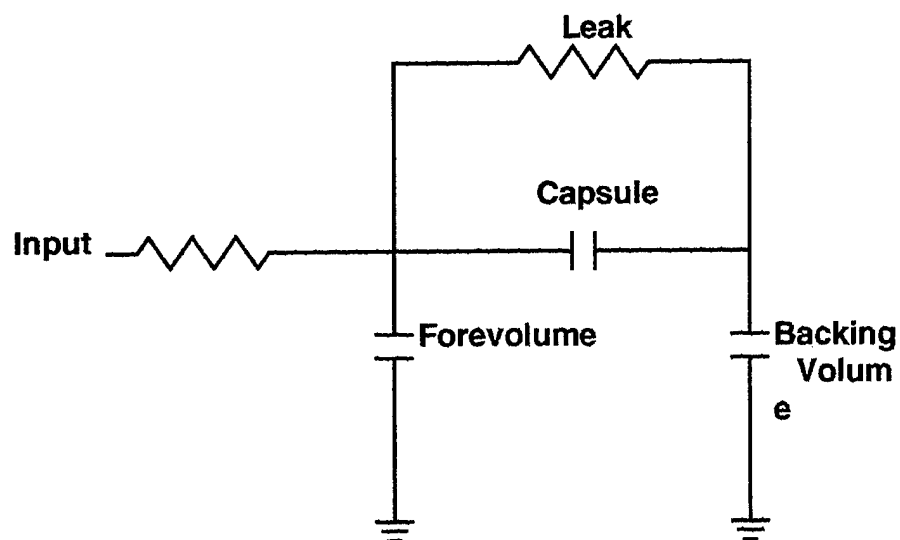


Figure I-23. Electrical analogue of the transducer assembly.

CHARACTERISTICS OF ACOUSTIC SENSORS

Table 1. Table of equipment specifications comparing GSE requirements with the TXAR equipment. Characteristics of the TXAR equipment are preliminary estimates based on manufacture's specifications, simple laboratory tests, and theoretical calculations.

Item	GSE ⁶	TXAR (Lajitas)	Comment
Sample Rate	10 SPS	40 SPS	Previous GSE report recommended 20 SPS. Current report has reduced that to 10 SPS. For TXAR 40 SPS is easier than a reduced rate and also simplifies seismo-acoustic processing. At the field site 40 SPS imposes little additional bandwidth requirement since data compression is effective in reducing the bandwidth at this high rate.
Bandwidth	0.02-5 Hz	1/60 - 16 Hz	Bandwidth has to be slightly below the nyquist. At 10 SPS a corner of 4 Hz is easily attainable with FIR antialias filters. The TXAR system low frequency starts to roll-off at 60 seconds but is usable beyond 4 minutes as has been confirmed by observing 4 minute infrasonic signals. High frequency is limited by the response of the pipe array.
Sensitivity and Noise	0.01 Pa (0.1 μ bar)	< 0.01 μ bar in a two octave band 3.4 nbar/count	Sensitivity implies an upper limit on the noise level. The level quoted is for the sensor itself. Field systems will usually be dominated by environmental and pipe array noise. TXAR systems currently drive the digitizers at a gain of 1. Higher gains (x3) could be used without clipping. The strongest observed signals at TXAR from xx-May-96 to xx-May-96 would not be clipped at gains of xx
Dynamic Range	80 dB	> 120 dB	Required dynamic range is likely to be quite high because of the extremely wide bandwidth required (8 octaves). The 80 dB range is insufficient for the sensor system used here.
Linearity	Unspecified	0.3%	Limited by the sensor. This will likely control the observed total harmonic distortion (THD). Linearity is from the manufacture's specifications and has not been measured.
Cost	\$180,000/4 element station	\$36,000/ 4 element station	The possibility of using more than 4 elements is mentioned. These would have a small incremental cost. For the TXAR system additional elements are \$9,000 each. At any one site though, two acoustic channels rather than one would only be an additional \$2,000.

Table 2. Validyne P305D manufacture's specifications as applied to the model configured for TXAR. Specification have been taken from manufacture's datasets but converted to input pressure units.

Item	Specification	Comments
------	---------------	----------

⁶ GSE equipments adapted from report xxx

CHARACTERISTICS OF ACOUSTIC SENSORS

Pressure Range	± 860 Pa	Maximum observed range at TXAR from xx-May-96 to xx-May-96 was xx Pa
Accuracy	± 2.1 Pa (0.25%) full scale including linearity hysteresis and repeatability	Refers to full scale accuracy and repeatability. For smaller than full scale signals this would be reduced.
Overpressure	1720 Pa with less than 0.5% zero shift	Easily exceeded during assembly if care is not used. Once installed in the field this is less likely to occur unless the backing volume is subjected to a rapid extreme temperature change. More sensitive units are also more rugged.
Pressure Cavity Volume	244×10^{-6} cm ³	Essentially zero.
Volumetric Displacement	18×10^{-6} cm ³ at full scale	Essentially zero.
Power	10.8 to 32 V DC @ 8 mA	Measured 8.7 mA @ 13.2 volts
Signal Output	± 5 V DC full scale @ 0.5 mA	
Zero Balance	± 0.1 V DC adjustable equivalent to ± 87 Pa	Zero balance seems to be temperature dependent. Unable to tell how much of it is electronic and how much is due to diaphragm displacement
Output Impedance	100 ohms in parallel with 2.4 ufd	
Frequency Response	0-200 Hz flat ± 1 dB for electronics	Unable to verify at this time.
output noise	less than 0.85 Pa RMS	This appears to be over the whole 0-200 Hz bandwidth.
Input/Output Isolation	Common input/output return	
Operating Temperature Range	-65 to +250 °F	
Temperature error	less than 170 μ bar /100°F	

Table 3. Table of Laboratory and Field tests of the TXAR infrasonic sensors. Dataset names are UNIX style. Datasets are SEG Y converted from RefTek recorders by PASCAL programs.

Test	Conditions	Data Set	Comments
Direct measurement of System Noise	Needle valve completely open. Input port closed to atmosphere, but all	R027.01/ open, closed	Sensors showed between 0.58, 0.36, and 1.9 ubar RMS noise over the full 0-50 Hz band as

CHARACTERISTICS OF ACOUSTIC SENSORS

	sensors plumbed together. Recorded at 100 SPS, preamp gain x32 0.006 μ bar/count		shaped by the RefTek anti-alias filters. Suspect the measurement for 1.9 ubar is wrong and that the sensor had one or more leaks in the plumbing.
Step function calibrations	Valves adjusted to give approximate response. All systems plumbed to a common input created by squeezing and releasing Tygon tube. Recorded at 100 SPS, preamp gain of x1, 0.19 μ bar /count	R028.01/ cal*	Sensors were matched to within a few percent by using a simple multimeter or storage oscilloscope. Corner frequency was adjusted to 1/60 Hz by observing the decay time of a step function. A 50% decay in 6.62 seconds is equivalent to a 60 second corner.
Sine calibrations	Sine wave bellows calibrator connected to systems. Recorded at 100 SPS preamp gain x1, 0.19 Pa/count.	R029.01/ cal*	Sensors were equally matched but calibration results do not match those of step calibration. The sine wave calibrator was salvaged from an old NBS type microbarograph.
Coherence derived self noise	Systems plumbed together with end left open to the air. Recorded at 100 SPS preamp gain x 8, 0.024 μ bar /count	R028.01/ open_tube R029.01/ open_tube	Several attempts were required. One needle valve crept closed during the night. Temperature fluctuations prevented higher gains.
Hose responses	Coiled porous and punched hoses run in comparison with open system to determine transfer function. Recorded at 100 SPS preamp gain x 1, 0.19 μ bar /count	R030.01/ noise R054.01/ shop R055.01/ opencmp	Porous hoses acted as a high cut filter. Punched hose had substantially different response. Little usable energy above 10 Hz.
Spatial Response	Coiled hose run against spread hose Recorded at 100 SPS preamp gain x 8, 0.024 μ bar /count	R030.01/ outdoor	Spatial response demonstrated
Summing tests	One system with 5 arm star array, one with open port Recorded at 100 SPS preamp gain x 32, 0.006 μ bar /count . Also	R056.01/ star* R056.02/ star*	Improvement to wind noise at frequencies above 1/5 Hz noted. Difficult to match audible observations with infrasonic events

CHARACTERISTICS OF ACOUSTIC SENSORS

	recorded at 500 SPS.		
Coherence hose tests	Two hosts side by side 15.2 m (50 feet) long less than 7 cm apart generally 90 degrees to predominant wind. Wind was very gentle. Recorded at 100 SPS preamp gain x 32, 0.006 μ bar /count	R056.01/ parallel	Coherence less than expected. Similar tests need to be performed over a variety of weather conditions and with multiple hoses and orientations.
V configuration test	Two hoses as two legs of a triangle. Base is about 4.5 m. Recorded at 100 SPS, preamp gain x 32, 0.006 μ bar /count.	R056.01/ diverge	No useful conclusions. It was hypothesized that if the parallel host test showed strong coherence, an analysis of the spectra of divergent hoses would suggest the spatial characteristics of noise and signals.
Gradient recorded	One soaker hose 15.2 m (50 feet) long connected to standard sensor. Second hose of 1/4" laser punch soaker connected in differential mode. Recorded at 100 SPS preamp gain x 32, 0.006 μ bar /count.	R76.01/ gradient	Unable to explain results. Still under consideration

THOMAS AHRENS
SEISMOLOGICAL LABORATORY 252-21
CALIFORNIA INSTITUTE OF TECHNOLOGY
PASADENA, CA 91125

SHELTON ALEXANDER
PENNSYLVANIA STATE UNIVERSITY
DEPARTMENT OF GEOSCIENCES
• 537 DEIKE BUILDING
UNIVERSITY PARK, PA 16801

• RICHARD BARDZELL
ACIS
DCI/ACIS
WASHINGTON, DC 20505

DOUGLAS BAUMGARDT
ENSCO INC.
5400 PORT ROYAL ROAD
SPRINGFIELD, VA 22151

WILLIAM BENSON
NAS/COS
ROOM HA372
2001 WISCONSIN AVE. NW
WASHINGTON, DC 20007

ROBERT BLANDFORD
AFTAC
1300 N. 17TH STREET
SUITE 1450
ARLINGTON, VA 22209-2308

RHETT BUTLER
IRIS
1200 NEW YORK AVE., NW
SUITE 800
WASHINGTON, DC 20005

CATHERINE DE GROOT-HEDLIN
UNIVERSITY OF CALIFORNIA, SAN DIEGO
INSTITUTE OF GEOPHYSICS AND PLANETARY PHYSICS
8604 LA JOLLA SHORES DRIVE
SAN DIEGO, CA 92093

• SEAN DORAN
ACIS
DCI/ACIS
• WASHINGTON, DC 20505

RICHARD J. FANTEL
BUREAU OF MINES
DEPT OF INTERIOR, BLDG 20
DENVER FEDERAL CENTER
DENVER, CO 80225

RALPH ALEWINE
NTPO
1901 N. MOORE STREET, SUITE 609
ARLINGTON, VA 22209

MUAWIA BARAZANGI
INSTITUTE FOR THE STUDY OF THE CONTINENTS
3126 SNEE HALL
CORNELL UNIVERSITY
ITHACA, NY 14853

T.G. BARKER
MAXWELL TECHNOLOGIES
P.O. BOX 23558
SAN DIEGO, CA 92123

THERON J. BENNETT
MAXWELL TECHNOLOGIES
11800 SUNRISE VALLEY DRIVE SUITE 1212
RESTON, VA 22091

JONATHAN BERGER
UNIVERSITY OF CA, SAN DIEGO
SCRIPPS INSTITUTION OF OCEANOGRAPHY IGPP, 0225
9500 GILMAN DRIVE
LA JOLLA, CA 92093-0225

STEVEN BRATT
NTPO
1901 N. MOORE STREET, SUITE 609
ARLINGTON, VA 22209

LESLIE A. CASEY
DOE
1000 INDEPENDENCE AVE. SW
NN-20
WASHINGTON, DC 20585-0420

STANLEY DICKINSON
AFOSR
110 DUNCAN AVENUE, SUITE B115
BOLLING AFB
WASHINGTON, D.C. 20332-001

DIANE I. DOSER
DEPARTMENT OF GEOLOGICAL SCIENCES
THE UNIVERSITY OF TEXAS AT EL PASO
EL PASO, TX 79968

JOHN FILSON
ACIS/TMG/NTT
ROOM 6T11 NHB
WASHINGTON, DC 20505

MARK D. FISK
MISSION RESEARCH CORPORATION
735 STATE STREET
P.O. DRAWER 719
SANTA BARBARA, CA 93102-0719

LORI GRANT
MULTIMAX, INC.
311C FOREST AVE. SUITE 3
PACIFIC GROVE, CA 93950

I. N. GUPTA
MULTIMAX, INC.
1441 MCCORMICK DRIVE
LARGO, MD 20774

JAMES HAYES
NSF
4201 WILSON BLVD., ROOM 785
ARLINGTON, VA 22230

MICHAEL HEDLIN
UNIVERSITY OF CALIFORNIA, SAN DIEGO
SCRIPPS INSTITUTION OF OCEANOGRAPHY IGPP, 0225
9500 GILMAN DRIVE
LA JOLLA, CA 92093-0225

EUGENE HERRIN
SOUTHERN METHODIST UNIVERSITY
DEPARTMENT OF GEOLOGICAL SCIENCES
DALLAS, TX 75275-0395

VINDELL HSU
HQ/AFTAC/TTR
1030 S. HIGHWAY A1A
PATRICK AFB, FL 32925-3002

RONG-SONG JIH
PHILLIPS LABORATORY
EARTH SCIENCES DIVISION
29 RANDOLPH ROAD
HANSCOM AFB, MA 01731-3010

LAWRENCE LIVERMORE NATIONAL LABORATORY
ATTN: TECHNICAL STAFF (PLS ROUTE)
PO BOX 808, MS L-200
LIVERMORE, CA 94551

LAWRENCE LIVERMORE NATIONAL LABORATORY
ATTN: TECHNICAL STAFF (PLS ROUTE)
PO BOX 808, MS L-221
LIVERMORE, CA 94551

ROBERT GEIL
DOE
PALAIS DES NATIONS, RM D615
GENEVA 10, SWITZERLAND

HENRY GRAY
SMU STATISTICS DEPARTMENT
P.O. BOX 750302
DALLAS, TX 75275-0302

DAVID HARKRIDER
PHILLIPS LABORATORY
EARTH SCIENCES DIVISION
29 RANDOLPH ROAD
HANSCOM AFB, MA 01731-3010

THOMAS HEARN
NEW MEXICO STATE UNIVERSITY
DEPARTMENT OF PHYSICS
LAS CRUCES, NM 88003

DONALD HELMBERGER
CALIFORNIA INSTITUTE OF TECHNOLOGY
DIVISION OF GEOLOGICAL & PLANETARY SCIENCES
SEISMOLOGICAL LABORATORY
PASADENA, CA 91125

ROBERT HERRMANN
ST. LOUIS UNIVERSITY
DEPARTMENT OF EARTH & ATMOSPHERIC SCIENCES
3507 LACLEDE AVENUE
ST. LOUIS, MO 63103

ANTHONY IANNACCHIONE
BUREAU OF MINES
COCHRANE MILL ROAD
PO BOX 18070
PITTSBURGH, PA 15236-9986

THOMAS JORDAN
MASSACHUSETTS INSTITUTE OF TECHNOLOGY
EARTH, ATMOSPHERIC & PLANETARY SCIENCES
77 MASSACHUSETTS AVENUE, 54-918
CAMBRIDGE, MA 02139

LAWRENCE LIVERMORE NATIONAL LABORATORY
ATTN: TECHNICAL STAFF (PLS ROUTE)
PO BOX 808, MS L-207
LIVERMORE, CA 94551

LAWRENCE LIVERMORE NATIONAL LABORATORY
ATTN: TECHNICAL STAFF (PLS ROUTE)
LLNL
PO BOX 808, MS L-175
LIVERMORE, CA 94551

LAWRENCE LIVERMORE NATIONAL LABORATORY
ATTN: TECHNICAL STAFF (PLS ROUTE)
PO BOX 808, MS L-208
LIVERMORE, CA 94551

LAWRENCE LIVERMORE NATIONAL LABORATORY
ATTN: TECHNICAL STAFF (PLS ROUTE)
PO BOX 808, MS L-195
LIVERMORE, CA 94551

• THORNE LAY
UNIVERSITY OF CALIFORNIA, SANTA CRUZ
EARTH SCIENCES DEPARTMENT
EARTH & MARINE SCIENCE BUILDING
SANTA CRUZ, CA 95064

DONALD A. LINGER
DNA
6801 TELEGRAPH ROAD
ALEXANDRIA, VA 22310

LOS ALAMOS NATIONAL LABORATORY
ATTN: TECHNICAL STAFF (PLS ROUTE)
PO BOX 1663, MS F665
LOS ALAMOS, NM 87545

LOS ALAMOS NATIONAL LABORATORY
ATTN: TECHNICAL STAFF (PLS ROUTE)
PO BOX 1663, MS C335
LOS ALAMOS, NM 87545

KEITH MCLAUGHLIN
MAXWELL TECHNOLOGIES
P.O. BOX 23558
SAN DIEGO, CA 92123

RICHARD MORROW
USACDA/TVI
320 21ST STREET, N.W.
WASHINGTON, DC 20451

• JAMES NI
NEW MEXICO STATE UNIVERSITY
• DEPARTMENT OF PHYSICS
LAS CRUCES, NM 88003

PACIFIC NORTHWEST NATIONAL LABORATORY
ATTN: TECHNICAL STAFF (PLS ROUTE)
PO BOX 999, MS K6-48
RICHLAND, WA 99352

LAWRENCE LIVERMORE NATIONAL LABORATORY
ATTN: TECHNICAL STAFF (PLS ROUTE)
PO BOX 808, MS L-202
LIVERMORE, CA 94551

LAWRENCE LIVERMORE NATIONAL LABORATORY
ATTN: TECHNICAL STAFF (PLS ROUTE)
PO BOX 808, MS L-205
LIVERMORE, CA 94551

ANATOLI L. LEVSHIN
DEPARTMENT OF PHYSICS
UNIVERSITY OF COLORADO
CAMPUS BOX 390
BOULDER, CO 80309-0309

LOS ALAMOS NATIONAL LABORATORY
ATTN: TECHNICAL STAFF (PLS ROUTE)
PO BOX 1663, MS F659
LOS ALAMOS, NM 87545

LOS ALAMOS NATIONAL LABORATORY
ATTN: TECHNICAL STAFF (PLS ROUTE)
PO BOX 1663, MS D460
LOS ALAMOS, NM 87545

GARY MCCARTOR
SOUTHERN METHODIST UNIVERSITY
DEPARTMENT OF PHYSICS
DALLAS, TX 75275-0395

BRIAN MITCHELL
DEPARTMENT OF EARTH & ATMOSPHERIC SCIENCES
ST. LOUIS UNIVERSITY
3507 LACLEDE AVENUE
ST. LOUIS, MO 63103

JOHN MURPHY
MAXWELL TECHNOLOGIES
11800 SUNRISE VALLEY DRIVE SUITE 1212
RESTON, VA 22091

JOHN ORCUTT
INSTITUTE OF GEOPHYSICS AND PLANETARY PHYSICS
UNIVERSITY OF CALIFORNIA, SAN DIEGO
LA JOLLA, CA 92093

PACIFIC NORTHWEST NATIONAL LABORATORY
ATTN: TECHNICAL STAFF (PLS ROUTE)
PO BOX 999, MS K7-34
RICHLAND, WA 99352

PACIFIC NORTHWEST NATIONAL LABORATORY
ATTN: TECHNICAL STAFF (PLS ROUTE)
PO BOX 999, MS K6-40
RICHLAND, WA 99352

PACIFIC NORTHWEST NATIONAL LABORATORY
ATTN: TECHNICAL STAFF (PLS ROUTE)
PO BOX 999, MS K6-84
RICHLAND, WA 99352

PACIFIC NORTHWEST NATIONAL LABORATORY
ATTN: TECHNICAL STAFF (PLS ROUTE)
PO BOX 999, MS K5-12
RICHLAND, WA 99352

FRANK PILOTTE
HQ/AFTAC/TT
1030 S. HIGHWAY A1A
PATRICK AFB, FL 32925-3002

KEITH PRIESTLEY
DEPARTMENT OF EARTH SCIENCES
UNIVERSITY OF CAMBRIDGE
MADINGLEY RISE, MADINGLEY ROAD
CAMBRIDGE, CB3 0EZ UK

JAY PULLI
BBN
1300 NORTH 17TH STREET
ROSSLYN, VA 22209

PAUL RICHARDS
COLUMBIA UNIVERSITY
LAMONT-DOHERTY EARTH OBSERVATORY
PALISADES, NY 10964

DAVID RUSSELL
HQ AFTAC/TTR
1030 SOUTH HIGHWAY A1A
PATRICK AFB, FL 32925-3002

CHANDAN SAIKIA
WOODWARD-CLYDE FEDERAL SERVICES
566 EL DORADO ST., SUITE 100
PASADENA, CA 91101-2560

SANDIA NATIONAL LABORATORY
ATTN: TECHNICAL STAFF (PLS ROUTE)
DEPT. 5704
MS 0979, PO BOX 5800
ALBUQUERQUE, NM 87185-0979

SANDIA NATIONAL LABORATORY
ATTN: TECHNICAL STAFF (PLS ROUTE)
DEPT. 5791
MS 0567, PO BOX 5800
ALBUQUERQUE, NM 87185-0567

SANDIA NATIONAL LABORATORY
ATTN: TECHNICAL STAFF (PLS ROUTE)
DEPT. 9311
MS 1159, PO BOX 5800
ALBUQUERQUE, NM 87185-1159

SANDIA NATIONAL LABORATORY
ATTN: TECHNICAL STAFF (PLS ROUTE)
DEPT. 5704
MS 0655, PO BOX 5800
ALBUQUERQUE, NM 87185-0655

SANDIA NATIONAL LABORATORY
ATTN: TECHNICAL STAFF (PLS ROUTE)
DEPT. 5736
MS 0655, PO BOX 5800
ALBUQUERQUE, NM 87185-0655

THOMAS SERENO JR.
SCIENCE APPLICATIONS INTERNATIONAL
CORPORATION
10260 CAMPUS POINT DRIVE
SAN DIEGO, CA 92121

AVI SHAPIRA
SEISMOLOGY DIVISION
THE INSTITUTE FOR PETROLEUM RESEARCH AND
GEOPHYSICS
P.O.B. 2286, NOLON 58122 ISRAEL

ROBERT SHUMWAY
410 MRAK HALL
DIVISION OF STATISTICS
UNIVERSITY OF CALIFORNIA
DAVIS, CA 95616-8671

MATTHEW SIBOL
ENSCO, INC.
445 PINEDA COURT
MELBOURNE, FL 32940

DAVID SIMPSON
IRIS
1200 NEW YORK AVE., NW
SUITE 800
WASHINGTON, DC 20005

JEFFRY STEVENS
MAXWELL TECHNOLOGIES
P.O. BOX 23558
SAN DIEGO, CA 92123

BRIAN SULLIVAN
BOSTON COLLEGE
INSTITUTE FOR SPACE RESEARCH
140 COMMONWEALTH AVENUE
CHESTNUT HILL, MA 02167

NAFI TOKSOZ
EARTH RESOURCES LABORATORY, M.I.T.
42 CARLTON STREET, E34-440
CAMBRIDGE, MA 02142

GREG VAN DER VINK
IRIS
1200 NEW YORK AVE., NW
SUITE 800
WASHINGTON, DC 20005

TERRY WALLACE
UNIVERSITY OF ARIZONA
DEPARTMENT OF GEOSCIENCES
BUILDING #77
TUCSON, AZ 85721

JAMES WHITCOMB
NSF
NSF/ISC OPERATIONS/EAR-785
4201 WILSON BLVD., ROOM 785
ARLINGTON, VA 22230

JIANG XIE
COLUMBIA UNIVERSITY
LAMONT DOHERTY EARTH OBSERVATORY
ROUTE 9W
PALISADES, NY 10964

OFFICE OF THE SECRETARY OF DEFENSE
DDR&E
WASHINGTON, DC 20330

TACTEC
BATTELLE MEMORIAL INSTITUTE
505 KING AVENUE
COLUMBUS, OH 43201 (FINAL REPORT)

PHILLIPS LABORATORY
ATTN: GPE
29 RANDOLPH ROAD
HANSCOM AFB, MA 01731-3010

PHILLIPS LABORATORY
ATTN: PL/SUL
3550 ABERDEEN AVE SE
KIRTLAND, NM 87117-5776 (2 COPIES)

DAVID THOMAS
ISEE
29100 AURORA ROAD
CLEVELAND, OH 44139

LAWRENCE TURNBULL
ACIS
DCI/ACIS
WASHINGTON, DC 20505

FRANK VERNON
UNIVERSITY OF CALIFORNIA, SAN DIEGO
SCRIPPS INSTITUTION OF OCEANOGRAPHY IGPP, 0225
9500 GILMAN DRIVE
LA JOLLA, CA 92093-0225

DANIEL WEILL
NSF
EAR-785
4201 WILSON BLVD., ROOM 785
ARLINGTON, VA 22230

RU SHAN WU
UNIVERSITY OF CALIFORNIA SANTA CRUZ
EARTH SCIENCES DEPT.
1156 HIGH STREET
SANTA CRUZ, CA 95064

JAMES E. ZOLLWEG
BOISE STATE UNIVERSITY
GEOSCIENCES DEPT.
1910 UNIVERSITY DRIVE
BOISE, ID 83725

DEFENSE TECHNICAL INFORMATION CENTER
8725 JOHN J. KINGMAN ROAD
FT BELVOIR, VA 22060-6218 (2 COPIES)

PHILLIPS LABORATORY
ATTN: XPG
29 RANDOLPH ROAD
HANSCOM AFB, MA 01731-3010

PHILLIPS LABORATORY
ATTN: TSML
5 WRIGHT STREET
HANSCOM AFB, MA 01731-3004